

Cover Page



Universiteit Leiden



The handle <http://hdl.handle.net/1887/38874> holds various files of this Leiden University dissertation.

Author: Martinez-Barbosa, Carmen Adriana

Title: Tracing the journey of the sun and the solar siblings through the Milky Way

Issue Date: 2016-04-13

Tracing the journey of the Sun and the Solar siblings through the Milky Way

Proefschrift

ter verkrijging van de graad van doctor
aan de Universiteit Leiden
op gezag van de rector magnificus prof. mr. C.J.J.M. Stolker,
volgens besluit van het college van decanen
in het openbaar te verdedigen op woensdag 13 april 2016
klokke 13.45 uur

door

Carmen Adriana Martínez Barbosa

geboren op 25 augustus 1984
te Bogotá, Colombia

PROMOTOR: Prof. dr. S.F. Portegies Zwart

COPROMOTOR: Dr. A.G.A. Brown

OVERIGE LEDEN: Prof. dr. L. Kaper University of Amsterdam
Prof. dr. C. Soubiran University of Bordeaux
Dr. L. Jílková
Prof. dr. H.J.A. Röttgering
Prof. dr. K.H. Kuijken

© 2016, Carmen Adriana Martínez Barbosa

Tracing the journey of the Sun and the Solar siblings through the Milky Way

Thesis, Universiteit Leiden

Illustrated; with bibliographic information and Dutch summary

ISBN: 978-94-028-0118-7

*"The most important thing is to enjoy your life
-to be happy- it's all that matters"*

Audrey Hepburn

Cover: Artistic impression of the Milky Way with one of the possible distributions of the Solar siblings at present.
Credit: Agustín Barbosa Rojas.

CONTENTS

1. Introduction	1
1.1. The constituents of the Milky Way	3
1.1.1. Orbital resonances	5
1.2. Radial migration	6
1.3. Star clusters	10
1.4. The Solar System	11
1.5. Numerical methods	13
1.5.1. The AMUSE framework	13
1.5.2. The BRIDGE integrator	14
1.6. About this thesis	15
1.7. Future perspectives	17
2. High-order hybrid N-body methods for compound systems	19
2.1. Introduction	20
2.2. Method	22
2.2.1. The Classic BRIDGE	22
2.2.2. A High-Order BRIDGE	25
2.2.3. BRIDGE in rotating frames	27
2.2.4. BRIDGE with post-Newtonian Corrections	35
2.3. Tests and Applications	37

CONTENTS

2.3.1. Implementation	37
2.3.2. High Order Bridge	38
2.3.3. Rotating bridge	41
2.4. Discussion and Conclusions	44
3. Radial Migration of the Sun in the Milky Way: a Statistical Study	47
3.1. Introduction	48
3.2. Galactic model	50
3.2.1. Central bar	51
3.2.2. Spiral arms	53
3.3. The AMUSE framework	56
3.4. Back-tracing the Sun's orbit	57
3.5. Results	60
3.5.1. Radial migration of the Sun as a function of bar parameters	62
3.5.2. Radial migration of the Sun as a function of spiral arm parameters	66
3.5.3. Radial migration of the Sun in the presence of the bar-spiral arm resonance overlap	72
3.5.4. Radial migration of the Sun with higher values of its tangential velocity	77
3.6. Discussion	78
3.7. Summary and final remarks	82
4. The evolution of the Sun's birth cluster and the search for the solar siblings with <i>Gaia</i>	87
4.1. Introduction	89
4.2. Simulation set-up	91
4.2.1. Galactic model	92
4.2.2. The Sun's birth cluster	97
4.2.3. Numerical simulations	100
4.3. Disruption of the Sun's birth cluster	100
4.4. Current distribution of Solar siblings in the Milky Way	103
4.5. The search for the solar siblings with <i>Gaia</i>	107

4.5.1. The solar siblings in the <i>Gaia</i> catalogue	107
4.5.2. Selecting solar sibling candidates from the <i>Gaia</i> catalogue	112
4.6. Discussion	115
4.6.1. Re-evaluation of existing solar sibling candidates	115
4.6.2. Applicability of the sibling selection criteria	118
4.7. Summary	119
5. The effect of Galactic stellar encounters on the outer edge of the Solar System’s parking zone	123
5.1. Introduction	124
5.2. Galaxy model and the solar orbit	128
5.2.1. Axisymmetric component	128
5.2.2. Galactic bar	131
5.2.3. Spiral arms	131
5.2.4. Solar orbits	132
5.3. Galactic stellar encounters	134
5.4. The outer limit of the parking zone	139
5.5. discussion	141
5.6. Summary and conclusions	142
Bibliography	145
Nederlandse Samenvatting	155
Resumen en Español	161
Curriculum vitæ	167
List of Publications	169
Acknowledgements	171

CHAPTER 1

INTRODUCTION

Our home, the Milky Way is an extensive barred spiral galaxy that contains hundreds of billions of stars. The majority of these objects are formed in star clusters which are continuously disrupted due to the intense gravitational force of the Galaxy. The most massive and old star clusters –often called globular clusters– populate the halo of the Galaxy every time they loose mass [e.g. Madrid et al., 2012]. The less massive and young star clusters –often called open clusters– populate the disk of the Galaxy in time-scales of order of hundreds of Myr [Portegies Zwart et al., 2010]. There are several aspects that play an important role in the dissolution of star clusters: their mass, size, Galactocentric location [Baumgardt & Makino, 2003; Madrid et al., 2012; Webb et al., 2014a] and even the shape of the Galaxy [Madrid et al., 2014]. Therefore, understanding the conditions under which star clusters dissolve in the Milky Way will lead to understand the processes involved in the formation and evolution of the Galaxy.

It is likely that the Sun has been born in an open cluster 4.6 Gyr ago. This hypothesis is supported by the products of radioactive elements found in the meteorite fossil record and by the high eccentricities of some objects in the outer Solar System. The stars that were formed together with the Sun are called solar siblings. Finding a small fraction of these stars is of great importance to constrain the environment where the Sun was born, which in

turn would provide hints on the formation of the Solar System. Additionally, reconstructing the orbits of the solar siblings in the Galaxy would lead to a more accurate determination of the location of the Sun at its birth. This information could be used to determine the correct trajectory of the Sun through the Galaxy independent of the geological record, which is important for the study of the history of the climate change and mass extinctions on Earth [Brown et al., 2010a, and references therein].

Given that open clusters are chemically homogeneous [De Silva et al., 2006, 2007], the way to identify solar siblings is by looking at stars that have the same chemical properties of the Sun. This also needs to be combined with a detailed understanding of the kinematical properties of the solar siblings, which can be obtained from self-consistent N-body simulations of the Sun's birth cluster. This thesis is focused on studying the dynamical evolution and disruption of the parental cluster of the Sun in order to predict the current location of the solar siblings. To study the evolution of the Sun's birth cluster it is necessary to investigate first the possible orbital histories of the Sun in the Milky Way. These orbits establish a set of initial phase-space coordinates where the parental cluster of the Sun was likely formed. The possible orbital histories of the Sun are also used to analyze how objects located in the outer Solar System are perturbed due to the stellar encounters experienced by the Sun along its orbit.

The main topics in this thesis are thus:

- i) The orbital history of the Sun in the Galaxy (**chapter 3**): Is it possible to know the location where the Sun was born? Did the Sun migrate from its birth place to its current position?
- ii) The study of the evolution of the Sun's birth cluster (**chapter 4**): Was the Sun's birth cluster affected by the non-axisymmetries of the Milky Way potential? What are the regions in the Galaxy where it is more likely to search for solar siblings?
- iii) The effect of the environment in which the Solar System evolved on the Oort cloud (**chapter 5**): How did stellar encounters affect the objects in the outer Solar System? Is it possible that some of these objects have never been perturbed by close stellar encounters?

1.1 THE CONSTITUENTS OF THE MILKY WAY

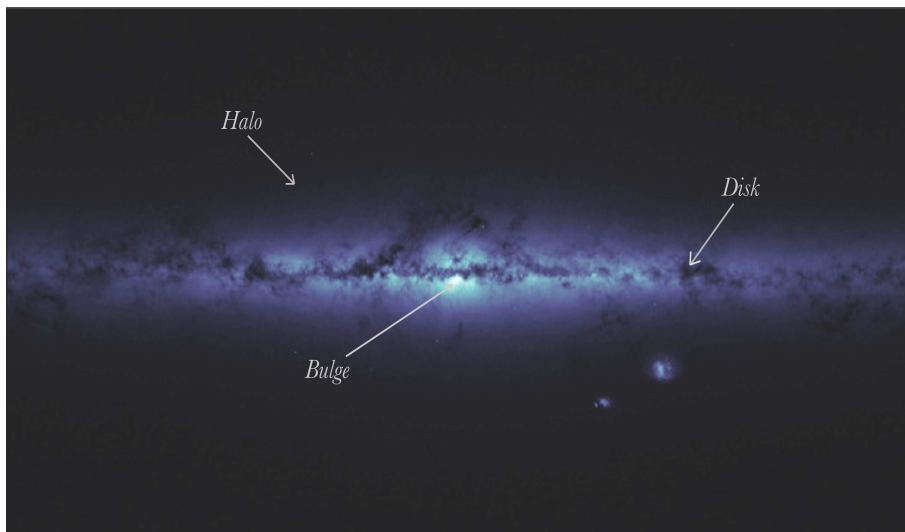


FIGURE 1.1: Picture of the Milky Way built from the *Gaia* housekeeping data (see http://www.cosmos.esa.int/web/gaia/iow_20150703). Credits: ESA/Gaia and E. Serpell.

The above questions are tackled by means of numerical simulations, which are explained briefly in Sect. 1.5 and in a deeper detail in **chapter 2**. In the upcoming subsections I present a general picture of the Milky Way and its constituents that will serve to contextualize the content of the next chapters of this thesis.

1.1. The constituents of the Milky Way

The luminous part of the Milky Way contains a stellar halo, a central bulge and a disk, as illustrated schematically in Fig. 1.1. These three Galactic components have different chemical and kinematical properties, suggesting that different mechanisms might have played an important role in the formation and evolution of the Galaxy.

The stellar halo of the Galaxy is a vast structure that surrounds the Galactic disk. This structure is thought to harbor the remnants of hundreds of dwarf galaxies and globular clusters that have been or are in the process of being disrupted due to the intense gravitational field of the Galaxy. As a consequence,

the stellar population of the halo comprises very old stars, with ages of $\sim 10 - 15$ Gyr [Kalirai, 2012]. Several studies over the last few decades have shown that the stellar halo might have two components [Carollo et al., 2007]: An inner halo, which extends over distances up to $10 - 15$ kpc from the Galactic centre and an outer halo, which dominates the region beyond $15 - 20$ kpc from the Galactic centre. The stellar population of the inner halo has a metallicity distribution which peaks at $[\text{Fe}/\text{H}] = -1.6$ dex, while in the outer halo the peak is at $[\text{Fe}/\text{H}] = -2.2$ dex [Carollo et al., 2010]. The stars in the halo are characterized by spanning a broad range of orbital eccentricities. Additionally, some studies have suggested different rotational motion for these stars according to their metallicity [Carollo et al., 2007, 2010]. However, these claims are still under debate in the literature [see e.g. Fermani & Schönrich, 2013].

The bulge is the central component of the Milky Way. It contains about 15% of the the total luminosity of the Galaxy [Portail et al., 2015] and a stellar population with mean metallicity of $\langle [\text{Fe}/\text{H}] \rangle \simeq -0.23$ dex [Johnson et al., 2013]. The mass of the bulge is about $2 \times 10^{10} M_{\odot}$ [Sofue et al., 2009]. Measurements of the density distribution of the bulge reveal that it hosts a triaxial bar which resembles a flattened ellipse with semi-major axis of ~ 3 kpc [Freudenreich, 1998], a vertical semi-major axis of 1 kpc [Monari et al., 2013] and inclination of $20^{\circ} - 30^{\circ}$ with respect to the Sun-Galactic center line [Romero-Gómez et al., 2011, and references therein]. The bar is considered to move as a solid body with pattern speed of $50 - 60 \text{ km s}^{-1} \text{ kpc}^{-1}$ [Dehnen, 2000; Bissantz & Gerhard, 2002]. This motion originates regions in the Galactic disk where stars are in orbital resonance with the bar. This effect will be discussed in more detail in Sect. 1.1.1.

The disk of the Milky Way is a flattened structure supported by rotational motion which contains a total mass of $\sim 6 \times 10^{10} M_{\odot}$ [Sofue et al., 2009]. Based on observations, Gilmore & Reid [1983] found that the Galactic disk is better described by two components: a thick and a thin disk¹. The thick disk is mainly composed of stars older than ~ 9 Gyr [Fuhrmann, 2008; Haywood et al., 2013; Bergemann et al., 2014], which span a metallicity range of $-2.2 \lesssim$

¹Bovy et al. [2012b] however, found that the scale-height of the Milky Way's disk can be described as a smoothly decreasing function, calling into question the existence of the thick disk.

1.1 THE CONSTITUENTS OF THE MILKY WAY

$[\text{Fe}/\text{H}] \lesssim 0.0$ dex with a peak at $[\text{Fe}/\text{H}] \sim -0.5$ dex [Bensby et al., 2007]. Measurements of the azimuthal velocities of these stars show that they are lagging with respect to the thin disk stars by $30 - 90 \text{ km s}^{-1}$ [Chiba & Beers, 2000]. In the local Standard of rest (LSR), the stars in the thick disk have a spatial velocity in the range of $70 \lesssim v_{\text{LSR}} \lesssim 180 \text{ km s}^{-1}$ [Bensby et al., 2014]. The thin disk on the other hand, is a flattened stellar distribution which extends radially up to 15 kpc from the Galactic centre [Ruphy et al., 1996]. The scale height of the thin disk is three times smaller than that of the thick disk, being 0.3 kpc [Jurić et al., 2008]. The stars belonging to the thin disk are younger than $\sim 8 - 10$ Gyr and they cover a range of metallicities in the range of $-1 \lesssim [\text{Fe}/\text{H}] \lesssim 0.4$ dex [Ivezić et al., 2008] which peaks at $[\text{Fe}/\text{H}] \sim -0.1$ dex [Kordopatis et al., 2013]. At solar radius, the circular velocity of the thin disk is $\sim 220 \text{ km s}^{-1}$ [McMillan & Binney, 2010; Bovy et al., 2012a]. Additionally, the thin disk stars are characterized to have a low peculiar velocity of up to $v_{\text{LSR}} = 50 \text{ km s}^{-1}$ [Bensby et al., 2014].

The disk of the Milky Way contains spiral arms, which are non-axisymmetric structures where the stellar density is about 10 – 20% larger than in other parts of the Galactic disk. The current structure of the spiral arms is rather uncertain. While some studies argue that our galaxy contains two spiral arms [Drimmel, 2000], other studies suggest that the Milky Way is best characterized with a four-armed spiral pattern [Vallée, 2002]. More complicated models even propose the existence of multiple spiral arms moving with different patterns speeds [Lépine et al., 2011a]. Like the Galactic bar, the spiral arms rotate as solid bodies, with a pattern speed of $15 - 30 \text{ km s}^{-1} \text{ kpc}^{-1}$ [Antoja et al., 2011, and references therein]. As a consequence, some stars in the disk will be in resonance with these non-axisymmetric structures, as is explained below.

1.1.1. Orbital resonances

The bar and spiral arms of the Galaxy rotate as rigid bodies with constant pattern speed. This motion however, is not the same as that of the disk which rotates differentially. As a consequence, disk stars located at different radii will experience different forcing due to the bar and/or the spiral arms. In particular, some of the disk stars will be in resonance with some of these non-axisymmetric structures. The resonances generated by the bar and spiral arms are:

- 1) The corotation resonance (CR), where the angular rotation of disk stars equals that of the perturber. Therefore, the CR is given by: $\Omega_s = \Omega_p$, where Ω_s is the stellar angular frequency and Ω_p is the pattern speed of either the bar or the spiral arms. Hereafter, we refer to the corotation resonance of the spiral arms as CR_{sp} and to the corotation resonance of the bar as CR_{bar} .

- 2) The Lindblad resonances (LR), where disk stars feel the force of the perturber at a frequency equal to their epicyclic frequency, k . As one moves inward or outward from the corotation circle, the relative frequency at which a star encounters the perturber increases or decreases. There are two radii for which this relative frequency is the same as k . These radii define the inner and outer Lindblad resonances (ILR/OLR). The Lindblad resonances occur when: $\Omega_p = \Omega_s \pm k/m$, where m is the multiplicity of the perturbation. The negative sign corresponds to the ILR and the positive sign to the OLR. For the case of an $m = 2$ pattern, the ILR/OLR are referred to as the 2:1 resonances (or first-order resonances). Similarly, for an $m = 4$ pattern the ILR/OLR are quoted as the 4:1 resonances (or second-order resonances) [see e.g. Minchev & Famaey, 2010]. Hereafter, we refer to the first order LR of the bar as ILR_{bar} and OLR_{bar} . The first order LR of the spiral arms are referred to as ILR_{sp} and OLR_{sp} respectively. For spiral structures containing four arms, the second-order LR are quoted as 4:1 $\text{ILR}_{\text{sp}}/\text{OLR}_{\text{sp}}$.

An important consequence of the resonances generated by the bar and spiral arms is stellar radial migration [Sellwood & Binney, 2002; Roškar et al., 2008a,b; Minchev & Famaey, 2010; Roškar et al., 2012; Roškar & Debattista, 2014] which is the process by which disk stars move from their birth radii due to a change in their angular momentum. Radial migration has been successful at explaining the flattening of the age-metallicity relation (AMR) in the solar neighborhood [Nordström et al., 2004; Holmberg et al., 2009; Casagrande et al., 2011] and the metallicity gradient observed in the Milky Way [Casagrande et al., 2011] and in other spiral galaxies [Bakos et al., 2008]. In the next section the stellar radial migration process is explained in more detail.

1.2. Radial migration

Many models of the chemical evolution of the Milky Way have assumed that stars remain near their Galactocentric birth radii [e.g. Matteucci & Francois, 1989; Boissier & Prantzos, 2000; Chiappini et al., 2001]. However, this assumption has been called into question because of the measurements of the metallicity gradient in the Milky Way [Casagrande et al., 2011] and other galaxies [Bakos et al., 2008] and due to the discovery that stellar radial migration is possible [e.g. Sellwood & Binney, 2002].

The idea that stars may not remain near their birth radii is not new. Wielen [1977] suggested that the diffusion of stellar orbits in the velocity space induces a drift in the galactocentric radius of an ensemble of stars. In this manner, a disk star may change its space velocity by more than 10 km s^{-1} per Galactic revolution, provoking a change in position of about 1.5 kpc after 200 Myr ². The diffusion of stellar orbits is a relatively slow process, driven by random scattering by giant molecular clouds.

Later on, Sellwood & Binney [2002] studied the stellar motion in self-gravitating disks. They showed that the diffusion processes explained by Wielen [1977] are insufficient to explain stellar radial migration. Sellwood & Binney [2002] showed that resonant interaction with spiral arms, in particular the corotation resonance, alter the angular momentum of disk stars (L_z) on a very short timescale. At the Lindblad resonances, the change of angular momentum is much smaller. Given that in these interactions the Jacobi energy is conserved, changes in the energy and angular momentum of stars are just related by the pattern speed of the spiral arms (i.e. $\Delta E = \Omega_{\text{sp}} \Delta L_z$).

Sellwood & Binney [2002] also determined the change in radial action of migrating stars, ΔJ_R . The radial action can be interpreted as a measurement of the change in the circularity of a stellar orbit. At corotation, $\Delta J_R = 0$, which means that the angular momentum and energy are exchanged without causing additional heating to the stellar orbits. At the Lindblad resonances on the other hand, $\Delta J_R = \pm \frac{\Delta L_z}{m}$. Therefore, changes in L_z produce a very

²This change in position is comparable to the epicyclic motion of the stars due to an axisymmetric Galaxy model. Consequently, it is not larger than the migration produced by spiral arms.

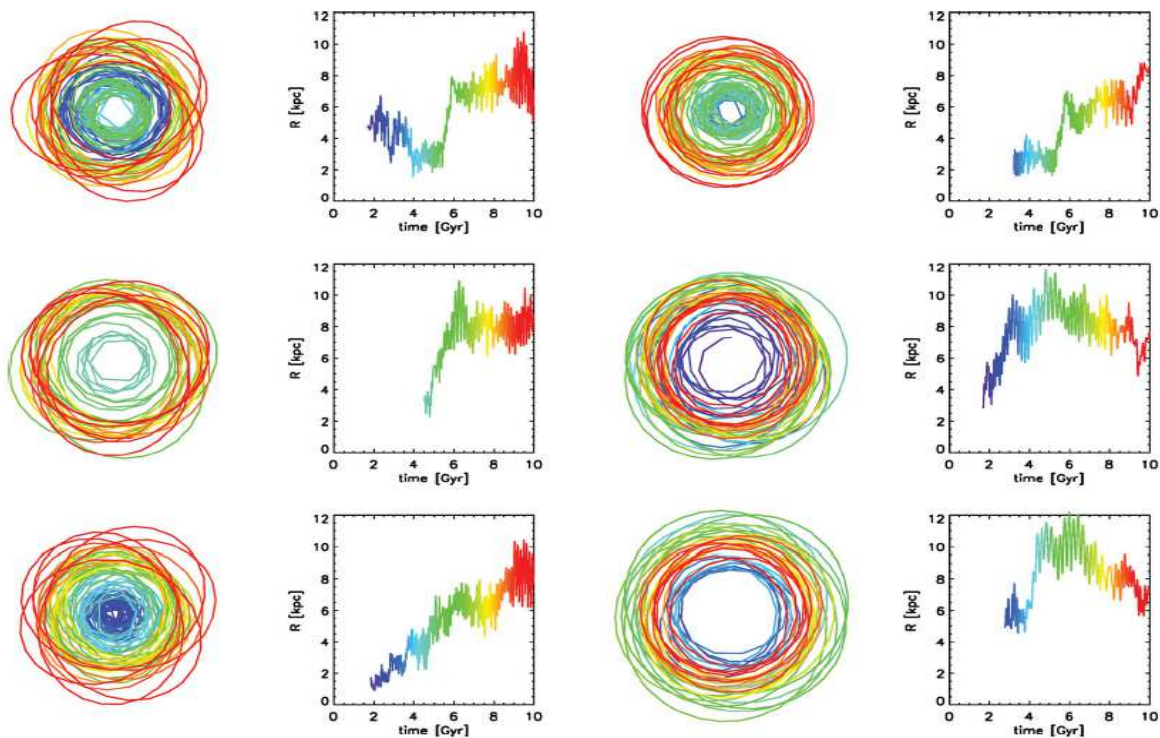


FIGURE 1.2: Some examples of orbits from the simulations of Roškar et al. [2012]. Orbits are colored according to time to make the temporal evolution more apparent, with blue corresponding to early and red to late times. Stars can migrate inwards and outwards very rapidly without substantially increasing their eccentricities. These orbits were selected such that the stars at the end of the simulation are between 7 – 9 kpc from the Galactic centre.

efficient heating in the orbits of the stars.

The ability of the CR_{sp} to redistribute stars substantially without heating, is a critical aspect of the mixing process in the Galaxy. However, the spiral arms need to be transient structures for this mechanism to work. If the spiral arms are steady, the corotation resonance results simply in orbit trapping. In this case, a star inside of corotation gains angular momentum so that it moves to a region outside of the corotation radius. Here, the star is now leading the spiral arm where it is pulled back by the overdensity losing the previously gained angular momentum [Roškar & Debattista, 2014]. This trapping results in a horseshoe orbit which remains at a constant L_z when the spiral structure is steady. Therefore, the spiral arms need to be transient, surviving just one half the orbital period of the horseshoe orbit to deposit the star on the other side of the resonance before it gets pulled back in the other direction [Sellwood & Binney, 2002].

Roškar et al. [2012] explored the causes of the radial migration in disks with self-propagating spiral structure. They found that stars may migrate rapidly while retaining a nearly circular orbit (see e.g. Fig. 1.2), confirming the findings of Sellwood & Binney [2002]. Roškar et al. [2012] also found that stars may radially migrate distances of up to 5 kpc on a timescale of 500 Myr (see e.g. top row Fig. 1.2). They argued that this rapid stellar migration is a consequence of the interaction with two successive corotation resonances corresponding to different spiral patterns. However, they emphasize that this extreme radial migration is not the norm. In the case of the solar neighborhood, they argue that $\sim 65\%$ of the stars might have come from elsewhere, while 35% might have formed in-situ.

Other authors have studied the complexities that radial mixing introduces for stellar population studies. Lépine et al. [2003] argue that the interaction of the stars with the CR_{sp} leads to a bimodal distribution in the metallicity gradient of the Galaxy. Additionally, Roškar et al. [2008b] found that more than 50% of stars on mostly circular orbits in the solar neighborhood of their model have come from elsewhere and that migration flattens the age-metallicity relation (AMR) and the metallicity distribution function (MDF) in the Milky Way. Additionally, Roškar et al. [2008a] showed that radial migration could drastically alter the stellar population properties of outer disks. They predicted

that galactic disks with broken exponential profiles should show an inflection in the mean age profile corresponding to the break radius. This has been confirmed indirectly by surface photometry [Bakos et al., 2008] and directly by integral field spectroscopy [Yoachim et al., 2010, 2012], providing further evidence that radial mixing occurs in other galaxies.

The previous studies have shown the effect of radial mixing caused by galactic spiral structure. What is the effect generated by bars? When fully formed, bars mostly heat the disk through the ILR_{bar} and the OLR_{bar} . Since bars are not transient, efficient exchange of angular momentum is not expected at the corotation resonance, because stars are trapped in horseshoe orbits [Roškar & Debattista, 2014]. However, Minchev & Famaey [2010] argued that in presence of overlapping of resonances from other disk structure, the horseshoe orbits can be disrupted and stars may efficiently gain or lose angular momentum in a similar fashion to the transient spiral mechanism proposed by Sellwood & Binney [2002].

If disk stars radially migrate during their lifetimes, it is likely that the Sun has also migrated from its birth place to its current position in the Galaxy. Wielen et al. [1996] found that the Sun has a metallicity which is larger by $+0.17 \pm 0.04$ dex than the average metallicity of nearby stars at solar age. This would imply that the Sun was born closer to the Galactic centre, at ~ 6 kpc. Recent theoretical studies further support this hypothesis [see e.g. Minchev et al., 2013]. However, improved measurements of the stellar metallicity show that the metallicity distribution function (MDF) in the solar neighborhood, peaks closer to the Sun's metallicity, at about 0.1 dex. This means that the Sun is a completely average star and therefore, it might have not migrated [Casagrande et al., 2011]. Some theoretical studies also suggest that our star has not migrated considerably during its journey through the Milky Way [see e.g. Mishurov, 2006; Klačka et al., 2012]. In **chapter 3** we address the question of the radial migration of the Sun and the Galactic conditions that would allow considerable radial migration of this star within a Galaxy model with non-transient spiral structure.

1.3. Star clusters

Most of the stars in the Galaxy are born in star clusters [Lada & Lada, 2003; Allen et al., 2007]. Many stars located in the halo are born in globular clusters, while the stars located in the disk are born in open clusters or associations.

The Milky Way contains approximately 150 globular clusters located in the halo, with mass estimates ranging from $\sim 10^3 M_\odot$ to $2.2 \times 10^6 M_\odot$ [Portegies Zwart et al., 2010]. These systems have sizes of ~ 10 pc and they consist of very old (population II) stars, with ages higher than 10 Gyr. Most of the globular clusters are probably formed through the merging of dwarf galaxies with the Milky Way [Miholics et al., 2015]. Direct evidence of this theory is provided by the Sagittarius dwarf galaxy, which is in process of merging with the Galaxy [Ibata et al., 1994].

Open clusters on the other hand, are confined to the Galactic disk, specially within the spiral arms. They span a broad range of masses, sizes and ages. The young open clusters for instance, have masses of the order of $10^3 M_\odot$. These systems harbor a stellar population not older than 1 Gyr which is compressed in a size of ~ 1 pc [Portegies Zwart et al., 2010]. Old open clusters have ages of 1 – 8 Gyr [Magrini et al., 2015; Scholz et al., 2015; Yakut et al., 2015], and typical masses of $10^3 - 10^4 M_\odot$ [Friel, 1995, and references therein]. Therefore, old open clusters are expected to be dynamically relaxed and mass segregated. In general, open clusters are important tools in the study of the Galactic disk. They serve to determine the spiral arm structure [Carraro, 2014; Bobylev & Bajkova, 2014], to investigate the mechanism of star formation and its recent history [Friel, 1995], and to study the shape and temporal evolution of the metallicity gradient of the Milky Way [Magrini et al., 2009, 2015].

The high eccentricities and inclinations of objects located in the outer Solar System as well as the decay products of ^{60}Fe and ^{26}Al found in the meteorite fossil record suggest that the Sun was born in an open cluster 4.6 Gyr ago [Adams, 2010]. All the stars that were born with the Sun in the same open cluster are called solar siblings. Finding a small fraction of these stars is important to understand the environment and the position in the Galaxy where the Solar System was born. The trajectory of the Sun through the Galactic disk affects the evolution of the Solar System, in particular the Oort cloud, which is

sensitive to the environment the Sun passes through along its orbit [Portegies Zwart & Jílková, 2015]. In **chapter 4** we study the evolution of the open cluster where the sun was born 4.6 Gyr ago and we make predictions on the region in the space of parallaxes, proper motions and radial velocities where it is more likely to find solar siblings. Selecting stars from this region in combination with a detailed study of their age, metallicity and chemical properties will increase the success rate in identifying solar siblings in the future.

1.4. The Solar System

At smaller Galactic scales we find the Solar System, with a size of order of $\sim 10^5$ AU (about half a parsec) from the Sun. Beyond the domain of the planets, at around of 40 AU, the Solar System harbors thousands of planetesimals or comets which are suspended in a region called the Oort cloud [Oort, 1950], as illustrated in Fig. 1.3. There are two scenarios that explain the formation of the Oort cloud. In the first scenario, the planetesimals are scattered by a distant planet beyond Neptune, yielding to the increment in their semi-major axes and eccentricities. In the second scenario, the planetesimals are scattered and even ejected from the Solar System due to the passage of a single star [Schwamb, 2014, and references therein]. This star could be a solar sibling that, during the interaction with the Sun, transferred material to the Solar System and in turn captured planetesimals from the Sun. In this respect, Jílková et al. [2015] argue that the planetesimals located in the inner Oort cloud such as Sedna [Brown et al., 2004] and 2012VP₁₁₃ [Trujillo & Sheppard, 2014] were captured from the planetesimal disk of another star with mass of $1.8 M_{\odot}$ that impacted the Sun at $\simeq 340$ AU.

In the Solar System, planetesimals with large aphelion distances (> 1000 AU) are affected by external forces generated by the perturbation from passing stars and by spiral arms and giant molecular clouds [Dones et al., 2004]. Another perturbation comes from the vertical component of the tidal force from the Galactic disk (referred to as Galactic tide) [Heisler & Tremaine, 1986]. The Galactic tide can efficiently increase or decrease the perihelion distances of planetesimals with large semi-major axes and eccentricities and randomize their inclination [Higuchi et al., 2007]. Passing stars also randomize the orbital parameters and

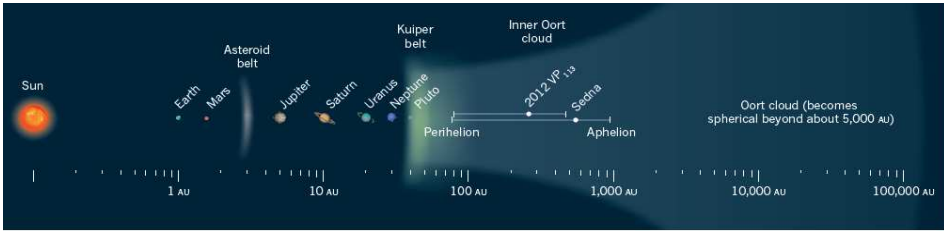


FIGURE 1.3: Artistic impression of the Solar System taken from Schwamb [2014]. The planets are located within 30 AU from the Sun. The region between ~ 40 AU and 1000 AU from the Sun is known as the inner Oort cloud. In this region, Sedna and 2012VP₁₁₃ reside. Beyond 1000 AU, the Oort cloud becomes spherical. This region is where the observed long-period comets come from.

even eject planetesimals from the Solar System by giving velocity kicks. Due to their random nature, the perturbations from passing stars may play an important role in the production of the nearly isotropic inclination of planetesimals [Higuchi & Kokubo, 2015]. An important aspect of the Galactic tide and the stellar encounters is that they change the angular momentum of planetesimals in the Oort cloud. Eventually, when their angular momentum or perihelion is small enough, planetesimals can enter the planetary region, triggering what is known as comet showers. Some terrestrial impact craters and extinction events on Earth [Hut et al., 1987; Shoemaker & Wolfe, 1986] may be related to these cometary showers [Melott et al., 2012].

The perturbations in the Oort cloud due to stellar encounters were larger in the past, when the Sun was still in its birth cluster. Once the cluster was dissolved, the perturbations were caused by disk stars located along the orbit of the Sun. The probability of an encounter with a disk star is much smaller than of a close encounter in the star cluster, but the lower encounter rate is compensated in part by the longer time spent in the relatively low-density environment of the Galaxy compared to the time spent in the star cluster [Portegies Zwart & Jílková, 2015]. Because of this, stellar encounters in the cluster likely affected the orbits of the objects in the inner Oort cloud [e.g. Brassier & Schwamb, 2015], more than the stellar encounters due to disk stars. The region in the space of eccentricity versus semi-major axis where planetesimals have been only perturbed by encounters with solar siblings is known as the parking zone

[Portegies Zwart & Jílková, 2015]. The orbits of planetesimals located in the parking zone maintain a record of the interaction of the Solar System with stars belonging to the Sun’s birth cluster. Therefore, these orbits carry information that can constrain the natal environment of the Sun. Portegies Zwart & Jílková [2015] determined the outer edge of the parking zone being at $2 - 4 \times 10^4$ AU, meaning that the planetesimals with semi-major axes down to this range have not been perturbed by encounters with disk stars. In **chapter 5** we improve the determination of the outer edge of the Solar System’s parking zone by using possible solar orbits that were computed in a Galaxy potential including bar and spiral arms. This result has implications for the role of stellar encounters on the formation of the Oort cloud.

1.5. Numerical methods

1.5.1. The amuse framework

This thesis makes use of numerical simulations through the AMUSE framework to study the motion of the Sun and the dynamical evolution of the Sun’s birth cluster in the Galaxy. AMUSE or Astrophysical MULTipurpose Software Environment [Portegies Zwart et al., 2013; Pelupessy et al., 2013] is a Python-based framework where different simulation codes (or solvers) can be coupled to simulate realistic systems. The physical processes (or domains) that can be modelled in AMUSE are: gravitational dynamics, stellar evolution, hydrodynamics and radiative transfer. There are two advantages that make AMUSE a powerful tool to simulate astrophysical systems. First, it is possible to include different domains in a simulation by just adding a few lines of code in a Python script. For instance, stellar evolution effects can be easily added into a N-body code. Without AMUSE, these two simulation codes would have to be merged by hand, which would need time and a deep knowledge of such codes. Second, it is possible to simulate the same set of initial conditions by using two different solvers of the same domain. For instance, a star cluster can be evolved by using two different N-body codes, just by changing two lines of code in the Python script. This allows to test and verify in a very easy way the results.

We use the AMUSE framework to tackle three main problems: i) The orbital

history of the Sun in the Galaxy (**chapter 3**), ii) The dynamical evolution of the already extinct parental cluster of the Sun (**chapter 4**) and iii) The effect of the environment in which the Solar System evolved on the Oort cloud (**chapter 5**).

1.5.2. The bridge integrator

To solve the aforementioned questions, it is necessary to make numerical simulations in which the Galaxy model accounts for the non-axisymmetric structures of the Milky Way. We thus insert to the AMUSE framework an analytic model of the Galaxy that includes a rotating bar and spiral arms. In order to use this Galaxy model, it is necessary to develop a code to integrate the stellar motion in rotating frames. This code is an improvement of the existing BRIDGE algorithm [Fujii et al., 2007], which is a code to perform fully self-consistent N-body simulations of star clusters and their parent galaxies. BRIDGE uses a direct code to compute accurately the motion of the particles in star clusters, and a faster scheme to evolve the parent galaxy. One of the characteristics of the BRIDGE integrator is that it uses a second-order Leapfrog scheme to compute the force of the stars in the cluster due to the parent galaxy; however, the Leapfrog scheme does not provide a good energy conservation and enough accuracy in the orbit integration, specially in chaotic regions generated by the resonances of the bar and spiral arms. In **chapter 2** we present a BRIDGE integrator of higher order and a BRIDGE which is applicable to rotating coordinate systems. With these generalizations of the BRIDGE integrator it is possible to study the motion of stars that are under the influence of the bar and spiral arms of the Galaxy.

1.6. About this thesis

This thesis is focused on the orbital history of the Sun and the dynamical evolution of the Sun's birth cluster through the Milky Way. Below, the questions related to these topics are introduced in more detail.

In **chapter 2** we present different generalizations of the BRIDGE integrator. We developed a high-order BRIDGE and a BRIDGE which is applicable to rotating coordinate systems. We show that these two integrators combined are suitable

to perform open cluster simulations in analytic Galaxy models containing a rotating bar and spiral arms. We also discuss the formulation of BRIDGE for cases where part of a stellar system evolves in the post-newtonian regime. Given that the high-order and rotating BRIDGE are implemented in AMUSE, it is also possible to include other physical processes such as stellar evolution effects in star cluster simulations. We used the high-order and rotating BRIDGE to study the orbital history (and radial migration) of the Sun in the Galaxy and the evolution and disruption of the Sun’s birth cluster in the Milky Way.

In **chapter 3** we present a statistical study of the radial migration of the Sun in the Galaxy. We aim to study the orbital motion of the Sun during the last 4.6 Gyr in order to find its birth radius. The methodology employed was to integrate the orbit of the Sun backwards in time, using different parameters of the bar and spiral arms and different present-day phase-space coordinates according to the observed uncertainties. We found that in general, the Sun has not migrated from its birth place to its current position in the Galaxy (R_{\odot}). However, considerable radial migration of the Sun is possible when: 1) The 2 : 1 Outer Lindblad resonance of the bar is separated from the corotation resonance of spiral arms by a distance around of 1 kpc. 2) When these two resonances are at the same Galactocentric position and further out than the solar radius. In these two cases the migration of the Sun is from outer regions of the Galactic disk to R_{\odot} , placing the Sun’s birth radius at around 11 kpc. The orbit integrations carried out in this study also show that it is unlikely that the Sun has migrated significantly from the inner regions of the Galactic disk to R_{\odot} . The former results are limited to Galactic potentials where the spiral structure is non-transient. Therefore, we might underestimate the true migration that the Sun might have experienced.

The results presented in **chapter 3** provide the initial phase-space coordinates where the Sun’s birth cluster was formed in the Galaxy and therefore, they are the first step to study the evolution and disruption of the parental cluster of the Sun in the Milky Way.

In **chapter 4** we present the results concerning to the evolution and disruption of the Sun’s birth cluster in the Galaxy. We aim to understand how simulations in combination with *Gaia* data can be used to pre-select solar siblings candidates. For this, we performed self-consistent numerical simulations of

the parental cluster of the Sun including the gravitational N-body forces within the cluster, the gravitational forces due to the Galaxy potential and the effects of stellar evolution on the cluster population. We found that the disruption time-scale of the cluster is insensitive to the details of the non-axisymmetric components of the Milky Way model. The final distribution of solar siblings, which is model-dependent, was used to make predictions about the number of solar siblings that should appear in the *Gaia* and *GALAH* surveys. We also demonstrate that it is possible to find a region in the space of parallaxes (ϖ), proper motions (μ) and radial velocities (V_r) where it is likely to find solar siblings. This probability can be computed by calculating the ratio of the number of simulated solar siblings to that of the number of stars in a model Galactic disk, which we refer to as the sibling fraction (f_{sib}). We found that $f_{\text{sib}} \geq 0.5$ in the region given by: $\varpi \geq 5$ mas, $4 \leq \mu \leq 6$ mas yr $^{-1}$, and $-2 \leq V_r \leq 0$ kms $^{-1}$. Selecting stars from this region in combination with a detailed examination of their ages, metallicities and chemical abundances, will increase the success rate of searches for solar siblings in the future.

Finally, in **chapter 5** we present the improvement in the estimate of the number of encounters experienced by the Sun in the past, in order to determine more accurately the outer edge of the Solar System’s parking zone. Following the methodology described in **chapter 3**, we integrated the orbit of the Sun backwards in time, using different present-day Galactocentric phase-space coordinates, according to the measured uncertainties. The resulting orbits were inserted in the largest simulation of the Galaxy up to date [51 billion particles, Bédorf et al., 2014], where the stellar velocity dispersion is estimated at each position. We use three different solar orbits to compute the Galactic stellar encounters. We found that the strongest stellar encounters have been with stars with $M = 0.1 M_{\odot}$ at distances of 741 – 1320 AU. These encounters set the outer edge of the Solar System’s parking zone at semi-major axes of 300 – 1300 AU, which is one order of magnitude smaller than the previous determination made by Portegies Zwart & Jílková [2015]. This result suggest that objects in the Solar System with semi-major axis smaller than 300 AU have not been perturbed by encounters with field disk stars.

1.7. Future perspectives

Launched in 1989 and operated until 1993, *Hipparcos* was the first satellite to measure accurately the astrometric properties of about 120000 stars brighter than 12.4 mag. The impact of *Hipparcos* on astrophysics was extremely valuable and diverse. It provided important data to investigate the stellar kinematics and the dynamical structure of the solar neighborhood, ranging from the evolution of star clusters, associations and moving groups [Perryman et al., 1998], improvement on the determination of the Oort constants [Olling & Merrifield, 1998], evidence of a galaxy merger in the early formation history of the Milky Way [Helmi et al., 1999] and the measurement of the solar motion [Dehnen & Binney, 1998]. However, the accuracy of *Hipparcos*, which was around of 1 mas, allowed to map mainly disk stars at a distance limit of 1 kpc from the Sun. More accurate parallaxes, proper motions and radial velocities for larger samples of stars belonging to the bulge, halo and disk are needed to constrain current theories on formation and evolution of the Milky Way.

Being the successor of *Hipparcos*, *Gaia* is a mission that will measure the astrometric properties of more than one billion stars brighter than 20 mag [Lindegren et al., 2008]. For stars brighter than 15 mag, *Gaia* will measure their parallaxes and proper motions with accuracies ranging from 10 to 30 μas . For sources at 20 mag, the accuracy of *Gaia* will be up to 600 μas . *Gaia* is mostly oriented to study the structure and formation history of our Galaxy; but this survey will also have a significant impact on asteroid studies, stellar astronomy, fundamental physics and on future searches of solar siblings. In **chapter 4** we give predictions on the regions in the space of parallaxes, proper motions and radial velocities where is more likely to find solar siblings. A large fraction of solar siblings might be found in the upcoming *Gaia* catalogue just by looking at such a regions in the kinematical phase-space. However, a complete determination of their ages, metallicity and chemical composition needs to be done in order to establish the true solar sibling candidates. The upcoming data from the *GALAH* survey will be extremely valuable in this respect, since this observing program will determine the chemical composition of one million of stars in the Galaxy with high accuracy. Complementary data from the Gaia-ESO survey, WEAVE and 4MOST will also be crucial to future searches of

solar siblings.

At smaller scales on the other hand, the upcoming *Gaia* catalogue will also be extremely useful, since it will provide data to understand the stability of the Solar System. The completeness of the *Gaia* data will permit a robust identification of the probability of recent stellar encounters as a function of perihelion time [see e.g. García-Sánchez et al., 2001, for a previous estimation by using *Hipparcos*]. Although is not straightforward to connect individual stellar encounters with specific impact craters on Earth [Bailer-Jones, 2015], *Gaia* will allow to investigate the link between stellar encounters and impacts in a statistical sense [Feng & Bailer-Jones, 2014].

CHAPTER 2

HIGH-ORDER HYBRID N-BODY METHODS FOR COMPOUND SYSTEMS

F.I. Pelupessy, C.A. Martínez-Barbosa, G. Gonçalves Ferrari
and S.F. Portegies Zwart

Journal of Computational Astrophysics and Cosmology, in revision

Abstract

The BRIDGE integrator [Fujii et al., 2007] presents an efficient method to calculate the combined evolution of a small system embedded in larger systems, the typical application being the collisional dynamics of star clusters in the large scale environment of their parent galaxies. Here, we present generalizations of the principles of BRIDGE to a wider set of applications: we generalize the second order coupling of BRIDGE to higher order and we present a formulation for a rotating frame of reference. We also discuss the formulation of BRIDGE for cases where part of the system evolves

in the post-Newtonian regime. We present example applications for these cases and discuss the conditions under which our integrators can be applied.

keywords: Stellar dynamics; Methods: N -body simulations; Methods: numerical

2.1. Introduction

Over the past five decades astrophysical simulations have been an indispensable tool to understand large observational datasets and gain knowledge about the formation and evolution of astrophysical systems. The demand for such simulations has increased accordingly and, in close relationship with the development of computer hardware, it is likely to continue to grow in the coming years due to the recent introduction of multi-core architectures such as Graphic Processing Units (GPUs) as general purpose performance boosters.

The main bottleneck in gravitational N -body codes is often attributed to the amount of computational work needed to accurately compute the orbits of the particles in the system on a star-by-star basis. For the direct summation method, which is the simplest and more accurate method for calculating forces, the computational cost scales as $\mathcal{O}(N^2)$. A way to alleviate the computational requirements for N -body simulations emerged with the development of tree-based algorithms which approximates the forces by means of a multipole expansion, where interactions with a subset of distant particles are only included via multipole terms. This in practice reduces the computational costs to $\mathcal{O}(N \log(N))$ at the expenses of a more complex algorithmic implementation and a decreased precision in the force calculation. In addition, the development of a momentum-conserving fast multi-pole method (FMM) lowered the computational complexity of N -body simulations to $\mathcal{O}(N \log(\log(N))) \approx \mathcal{O}(N)$ [Dehnen, 2014]. Each one of these methods have its own range of applicability. For example, direct summation methods are more appropriate for simulations of collisional systems such as planetary systems, star-clusters, galactic nuclei and black-hole (BH) dynamics. Tree- and FMM-based codes are better suitable for studies of collisionless systems such as galactic dynamics and cosmological

simulations. In addition to this, with the introduction of parallel architectures, GRAvity PipE (GRAPE) dedicated boards, and more recently, GPUs, a big boost (typically one to two orders of magnitude) in computational speed was accomplished and today's simulation codes have greatly improved their nominal dynamic range and numerical precision [see e.g. Portegies Zwart & Bédorf, 2014; Belleman et al., 2014].

On the other hand, gravitational N -body simulations require both, a fast way to calculate the forces and an accurate integration method to evolve the particles in time. Tree- and FMM-based codes typically adopt a simple leap-frog scheme, whereas in direct summation codes, symplectic schemes (for long term integrations of planetary systems) and high-order Hermite schemes (for integrations of star-clusters or galactic nuclei with BHs) have been systematically adopted. Symplectic schemes with hierarchical splitting have been recently developed and they could be an alternative to non-symplectic Hermite schemes. Other techniques such as the use of an individual or block-time-step algorithm [Makino et al., 2006], Ahmad-Cohen neighbour scheme [Ahmad & Cohen, 1973] and more exotic hybrids [Wisdom & Holman, 1991; McMillan & Aarseth, 1993; Pelupessy et al., 2012] reduce the computational costs associated with the force calculation. The block-time-step scheme is specially helpful in this sense, because in this case only a subset or block of particles need to be evolved per time-step, which in practice reduces the total calculation cost considerably in simulations which cover a wide range in time-scales. Nevertheless, an additional layer of efficiency can be gained by tailoring the integration method to the specific problem at hand. For example, a hybrid method named BRIDGE and firstly introduced by Fujii et al. [2007], was developed as a way to combine two different gravitational solvers. BRIDGE was developed to study the evolution of a star-cluster orbiting a parent galaxy.

The BRIDGE method is based on an second order extension of the mixed variable symplectic (MVS) scheme developed in the context of long term integrations of planetary systems. In its classic version [Fujii et al., 2007], BRIDGE couples a highly accurate direct code with a fast tree-code in a single compound solver, making the co-evolution of collisionless and collisional systems self-consistent. This BRIDGE method is quite powerful, both for the elegant principle it embodies as well as for the efficiency it allows, combining different

specialized solvers without the necessity to modify each one of the solvers individually. In Saitoh & Makino [2010]; Pelupessy et al. [2013] the BRIDGE method has been extended for coupling a gravitational solver and a SPH-based hydrodynamical solver, using a fully asynchronous time-stepping scheme, where the gravity and hydro solvers are allowed to use different time-step sizes to optimize performance.

The aim of this chapter is to present different generalizations of the classical BRIDGE method, which allows for the coupling between an arbitrary number of specialized solvers. In Sect. 2.2 we present a brief review of the classical BRIDGE method. We also introduce generalizations of this integrator, such as a high-order BRIDGE, a BRIDGE which includes post-Newtonian corrections and a BRIDGE to be used in rotating coordinates. In Sect. 2.3 we show the validation and applications of each generalized BRIDGE integrator. We discuss the advantages and limitations in Sect 2.4 and conclude in Sect. 2.4.

2.2. Method

2.2.1. The Classic Bridge

In the classic BRIDGE scheme a hybrid integrator combining two different gravitational solvers is constructed in order to study the evolution of a system comprised of two interacting systems, the canonical example being a star-cluster orbiting a parent galaxy. For this example the cluster is integrated using a 4-th Hermite direct summation code. Interactions between stars in the galaxy, and between the cluster and the galactic stars are resolved using a hierarchical tree-code. In this section we briefly revise the BRIDGE method, as a preparation for the discussion on its high-order generalization and extensions.

The BRIDGE integrator can be formulated from a Hamiltonian splitting argument, in a way similar to the derivation of symplectic integrators used in planetary dynamics. The Hamiltonian of a N -body system with sub-systems A and B under gravitational interaction is given by the expression:

$$H = \sum_{i \in A \cup B}^N \frac{\|\mathbf{p}_i\|^2}{2m_i} - \sum_{i \neq j \in A \cup B}^N \frac{Gm_i m_j}{\|\mathbf{r}_i - \mathbf{r}_j\|}. \quad (2.1)$$

The systems A and B may represent a star cluster and its parent Galaxy respectively. Following Fujii et al. [2007], the Hamiltonian shown in Eq. 2.1 can be separated in the following way:

$$H = H_{A+B} + H_{int} = H_A + H_B + H_{int}, \quad (2.2)$$

where:

$$\begin{aligned} H_A &= \sum_{i \in A}^N \frac{\|\mathbf{p}_i\|^2}{2m_i} - \sum_{i \neq j \in A}^N \frac{Gm_i m_j}{\|\mathbf{r}_i - \mathbf{r}_j\|} \\ H_B &= \sum_{i \in B}^N \frac{\|\mathbf{p}_i\|^2}{2m_i} - \sum_{i \neq j \in B}^N \frac{Gm_i m_j}{\|\mathbf{r}_i - \mathbf{r}_j\|} \\ H_{int} &= - \sum_{i \in A, j \in B}^N \frac{Gm_i m_j}{\|\mathbf{r}_i - \mathbf{r}_j\|} \end{aligned} \quad (2.3)$$

The time evolution of the whole system can be written, for a second order approximation, as follows:

$$\begin{aligned} e^{\tau H} &= e^{\frac{\tau}{2} H_{A+B}} e^{\tau H_{int}} e^{\frac{\tau}{2} H_{A+B}} \quad \text{or} \\ e^{\tau H} &= e^{\frac{\tau}{2} H_{int}} e^{\tau H_{A+B}} e^{\frac{\tau}{2} H_{int}}. \end{aligned} \quad (2.4)$$

The operator $e^{\tau H_{int}}$ represents pure momentum kicks, since H_{int} only depends on the positions. During this process, the velocity of the stars in the cluster are updated due to the external force generated by the galaxy. The velocity of the stars in the galaxy are also updated after computing the acceleration due to their self-gravity by means of a tree code.

Since H_A and H_B are completely independent the evolution operator $e^{\tau H_{A+B}} = e^{\tau H_A} e^{\tau H_B}$ consists of the separate evolution of the the two subsystems. For the example of a cluster in a galaxy, a direct code is used to evolve accurately the stellar cluster while a tree code is used in parallel to follow the evolution of the galaxy system. A full time-step in BRIDGE integrator then consists of i) mutually kicking the sub-systems A and B for $\frac{\tau}{2}$, ii) evolving the two sub-systems A

and B in isolation for τ using suitable codes together with an update of their positions, and iii) mutually kicking the sub-systems A and B for another $\frac{\tau}{2}$.

In the classical BRIDGE scheme a fully self-consistent treatment of the whole system is achieved using Eq. 2.4. The bridge integrator can allow a more efficient calculation of the evolution of the joined system under the following conditions: the first requirement (which is a necessary requirement) is that the timestep allowed by the interaction terms H_{int} is longer than one or both of the internal timesteps of the H_A and H_B systems (this can happen, but not exclusively so, if the two subsystems are spatially and temporally well separated). Secondly, and this is optional, it may be that the two systems are evolving in a different regime, such that different integrators, geared towards their respective dynamics, can be used. For the cluster-galaxy example both conditions contribute: the internal dynamical timescale of a cluster is much shorter than the interaction timescale of the cluster-galaxy interactions, and the cluster is governed by collisional dynamics while the galaxy experiences collisionless dynamics.

Thus the coupling of codes in BRIDGE works well when the interacting sub-systems stays relatively well separated in spatial and/or temporal scales during a simulation. It is not difficult to find a counter example where the BRIDGE integrator degenerates: take e.g. a star cluster where the stars are assigned to system A and B at random. In this case the formal splitting is still valid, but the timestep required reduces to the global minimum timestep. Note that in the approach above, the coupling strategy is defined manually at the beginning of a simulation and therefore the coupling remains static throughout the time evolution of the system. If a merger of the two clusters occurs during the simulation, the BRIDGE scheme evolves into the degenerate case and one has to monitor the simulation carefully. In principle, the use of a self-adaptive time-stepping in BRIDGE would alleviate this issue. However, ultimately, the problem would still exist since the coupling strategy still remains static throughout the simulation, therefore, demanding the use of unnecessarily small time-steps for the coupling. A dynamic approach where the system is merged and/or split as necessary would provide a more robust solution in this case. A similar method like this was adopted by Iwasawa et al. [2015], but then coded directly in C.

The above formulation provides fully symplectic time evolution. However, in practice, each of the codes being bridged may not be symplectic, in which case the compound solver is not symplectic. Note that the above formulation is not limited to only two sub-systems. Indeed, multiple sub-systems being integrated by different specialized solvers can be bridged either by a Hamiltonian splitting technique (see section 2.2.2) or by applying the above split scheme recursively [Pelupessy et al., 2012].

2.2.2. A High-Order Bridge

For systems in which the spatial and/or temporal scale of interaction of two or more sub-systems are not well separated, the BRIDGE scheme may have numerical difficulties. Additionally, the coupling of two integrators of high order (fourth and higher order are often used in the context of cluster problems) still occurs with a second order method, which ultimately determines the global order of the compound method. In order to address these issues, it is necessary to increase the order of the BRIDGE scheme. We present here a generalization of the classical BRIDGE to a high-order coupling scheme. First, we show how BRIDGE can be extended to a higher order, also taking into account multiple subsystems. Then we describe how the order of the coupling scheme can be decided based on the integrators being bridged.

We begin by assuming a system of particles, $S = \bigcup_k S_k$, composed by a number Q of sub-systems S_k . In this case the total Hamiltonian of the system,

$$H = \sum_{i \in S} \frac{\|\mathbf{p}_i\|^2}{2m_i} - \sum_{i \neq j \in S} \frac{Gm_i m_j}{\|\mathbf{r}_i - \mathbf{r}_j\|}, \quad (2.5)$$

can be split such that we obtain:

$$H = \sum_k H_{S_k} + \sum_{k \neq l} H_{S_k S_l}^{int}. \quad (2.6)$$

The terms in Eq. 2.6 are given by the following relations:

$$\begin{aligned}
 H_{S_k} &= \sum_{i \in S_k} \frac{\|\mathbf{p}_i\|^2}{2m_i} - \sum_{i \neq j \in S_k} \frac{Gm_i m_j}{\|\mathbf{r}_i - \mathbf{r}_j\|} \\
 H_{S_k S_l}^{int} &= \sum_{i \in S_k, j \in S_l} \frac{Gm_i m_j}{\|\mathbf{r}_i - \mathbf{r}_j\|}.
 \end{aligned} \tag{2.7}$$

Based on this splitting, a general, multi sub-system, second order time evolution operator can be constructed as follows:

$$\begin{aligned}
 \text{Bridge}_2(\tau) &= \prod_k^Q e^{\frac{\tau}{2} H_{S_k}} \prod_{k \neq l}^Q e^{\tau H_{S_k S_l}^{int}} \prod_k^Q e^{\frac{\tau}{2} H_{S_k}} \quad \text{or} \\
 \text{Bridge}_2(\tau) &= \prod_{k \neq l}^Q e^{\frac{\tau}{2} H_{S_k S_l}^{int}} \prod_k^Q e^{\tau H_{S_k}} \prod_{k \neq l}^Q e^{\frac{\tau}{2} H_{S_k S_l}^{int}}.
 \end{aligned} \tag{2.8}$$

Similarly to the classical BRIDGE, operators $e^{\tau H_{S_k}}$ independently evolves each of the sub-systems S_k in isolation. Operators $e^{\tau H_{S_k S_l}^{int}}$ represents the pure momentum kicks due to the interaction between sub-systems S_k and S_l . In the case of the Hamiltonian in eq. 2.6, the forces due to the interaction terms do not depend on velocities, therefore, the operators $e^{\tau H_{S_k S_l}^{int}}$ commute amongst themselves. We note, however, that commutability is not possible for velocity dependent forces and therefore, a special treatment is required (see section 2.2.4). Since each of the operators $e^{\tau H_{S_k}}$ and $e^{\tau H_{S_k S_l}^{int}}$ can, in principle, be associated to different solvers running concurrently, a highly efficient parallel implementation can be achieved for the generalized BRIDGE scheme in eq. 2.8.

A high-order BRIDGE scheme can be constructed in a similar way as in a symplectic integrator. By defining the drift and kick operators as:

$$D(\tau) = \prod_k^Q e^{\tau H_{S_k}}, \tag{2.9}$$

and

$$K(\tau) = \prod_{k \neq l}^Q e^{\tau H_{S_k S_l}^{int}}, \tag{2.10}$$

eq. 2.8 can be extended to a higher order by composition of $D(\tau)$ and $K(\tau)$ operators [Heirer et al., 2006]. For a 4th symmetric composition with 4 stages, the high-order BRIDGE takes the form:

$$\begin{aligned} \mathbf{Bridge}_4(\tau) = & D(u_0\tau)K(u_0\tau)D(u_1\tau)K(v_1\tau) \\ & D(u_2\tau)K(v_1\tau)D(u_1\tau)K(v_0\tau)D(u_0\tau), \end{aligned} \quad (2.11)$$

[e.g. Yoshida, 1990; Heirer et al., 2006, also for the coefficients u_i, v_i]. For a sixth and higher order symmetric compositions of the symmetric method, $D(\tau/2)K(\tau)D(\tau/2)$ leads to

$$\begin{aligned} \mathbf{Bridge}_6(\tau) = & D(w_0/2\tau)K(w_0\tau)D((w_0 + w_1)/2\tau) \dots \\ & \dots D((w_{s-1} + w_s)/2\tau)K(w_s\tau)D(w_s/2\tau), \end{aligned} \quad (2.12)$$

with coefficients w_i given in Sofroniou & Spaletta [2005] and Heirer et al. [2006]. We notice that the self-adjoint methods associated to eqs. 2.11 and 2.12 are also equally possible. The formulation above provides a fully symplectic time evolution if the codes being bridged are symplectic as well.

Using this scheme, codes/integrators of different orders can be coupled in order to construct a formally high-order scheme by matching the order of the BRIDGE to be used during the coupling. For example, when coupling a sixth order to a fourth order method, it is appropriate to choose $\mathbf{Bridge}_4(\tau)$ in order to have a fourth order convergent compound method. If on the other hand $\mathbf{Bridge}_6(\tau)$ would have been chosen, the method would be still be only fourth order (constrained by the fourth order sub-integrator). On the other hand, the logic of selecting an appropriate BRIDGE order may not always be straightforward: for example: if a second, fourth and sixth order were coupled in the classical BRIDGE ($\mathbf{Bridge}_2(\tau)$), resulting in an second order convergent compound method. This, however, can be improved by adopting the notion of a hierarchical coupling strategy: the fourth and sixth order codes being bridged with $\mathbf{Bridge}_4(\tau)$, and then this compound method being bridged with the remaining second order code using $\mathbf{Bridge}_2(\tau)$. In this hierarchical coupling strategy, while formally the overall order of convergence of the compound solver is still second order, locally, sub-systems being evolved with the more precise codes are still being coupled at higher order than the rest of the system,

and this can be advantageous if this subsystem dominates in the overall error or requires higher precision, for example because of the requirement to resolve close encounters. We note then, that, while the methods presented here are highly flexible, the choice of integrators is highly problem dependent.

2.2.3. Bridge in rotating frames

It is often expedient to consider a system in a non-inertial, rotating frame of reference. An example of this being the evolution of one or more (potentially interacting) stellar system in an analytic galaxy potential, with contributions from a galactic halo component, stellar disc, central bar and galactic spiral arms. In general, the bar and spiral arms of galaxies rotate as rigid bodies with certain pattern speed [Minchev & Famaey, 2010]. This means that the potential associated with these galactic components will depend on time in an inertial frame. In this case choosing a frame corotating with either bar and/ or spiral arms will make the potential contribution of these time independent and integrating in this frame will allow for larger timesteps and/or better energy conservation behavior. For these cases we can formulate a BRIDGE for a rotating frame of reference, such that the interactions between the stellar systems and the terms in the equations of motion arising from the non-inertial terms are bridged (the latter is convenient since it, as we will see, it allows the use of 'normal' integrators, formulated for an inertial frame, without changes).

First, we consider a particle of mass m located in a frame that rotates around the z -axis with constant angular speed Ω . The Hamiltonian of this particle is given by the relation:

$$\begin{aligned}
 H &= \frac{\|\mathbf{p}\|^2}{2m} + U_{\text{gen}}(\mathbf{r}, \mathbf{p}), \\
 H &= \frac{\|\mathbf{p}\|^2}{2m} + U_{\text{ext}}(\mathbf{r}) - (\Omega \times \mathbf{r}) \cdot \mathbf{p} - \frac{1}{2}m\|\Omega \times \mathbf{r}\|^2.
 \end{aligned}
 \tag{2.13}$$

Here \mathbf{r} and \mathbf{p} are the position and momentum vectors of the particle in the rotating frame. The term $U_{\text{ext}}(\mathbf{r})$ is the potential energy due to an external force, which depends only on the position of the particle. In particular, $U_{\text{ext}}(\mathbf{r})$ represents the galactic potential. The last two terms in Eq. 2.13 correspond to a potential energy which accounts for the centrifugal and Coriolis forces. The

energy associated to the centrifugal and Coriolis forces together with $U_{\text{ext}}(\mathbf{r})$, represents the total generalized potential energy of the particle, $U_{\text{gen}}(\mathbf{r}, \mathbf{p})$.

Note that $U_{\text{gen}}(\mathbf{r}, \mathbf{p})$ depends on the momentum of the particle. Therefore, it is not possible to split the above hamiltonian to obtain the drift and kick operators as in Eqs. 2.9 and 2.10. Thus, the way to construct a rotating BRIDGE integrator is by splitting the equations of motion of a test particle that satisfies Eq. 2.13.

There are two approaches to generate a rotating BRIDGE namely the canonical and non-canonical approximations [see also e.g. Pfenniger & Friedli, 1993]. In Sects. 2.2.3 and 2.2.3 we explain these approaches in more detail. We also generalize the rotating BRIDGE integrator to be used in systems of self-interacting particles.

Canonical approximation

In this approach, the equations of motion of a particle moving in a rotating frame, are defined in terms of the canonical coordinates (\mathbf{Q}, \mathbf{P}) . The canonical momentum (\mathbf{P}) is defined as

$$\mathbf{P} = \frac{\partial \mathcal{L}}{\partial \dot{\mathbf{Q}}} = \frac{\partial \mathcal{L}}{\partial \dot{\mathbf{r}}} = \mathbf{p} + m(\boldsymbol{\Omega} \times \mathbf{r}). \quad (2.14)$$

Here \mathcal{L} is the Lagrangian $\mathcal{L} = \dot{\mathbf{Q}}\mathbf{P} - H$. The canonical momentum can be interpreted as the velocity of the particle seen in the inertial reference frame which is coaxial to the rotating one. By using Eq. 2.14 we can obtain the canonical momenta in cartesian components:

$$\begin{aligned} P_x &= p_x - m\Omega y \\ P_y &= p_y + m\Omega x \\ P_z &= p_z. \end{aligned} \quad (2.15)$$

The equations of motion of a particle that satisfies Eq. 2.13 can then be written in terms of the canonical moment as follows:

$$\begin{aligned}
 \dot{x} &= p_x/m + \Omega y; & \dot{p}_x &= F_x + \Omega P_y \\
 \dot{y} &= p_y/m - \Omega x; & \dot{p}_y &= F_y - \Omega P_x \\
 \dot{z} &= p_z/m; & \dot{p}_z &= F_z.
 \end{aligned} \tag{2.16}$$

Here \mathbf{F} is the external force associated to $U_{\text{ext}}(\mathbf{r})$. We proceed to split Eqs. 2.16 to build the kick and drift operators. The set of equations that represent the kick operator $K(\tau)$ is the following:

$$\begin{aligned}
 \dot{x} &= \dot{y} = \dot{z} = 0, \\
 \dot{p}_x &= F_x + \Omega P_y, \\
 \dot{p}_y &= F_y - \Omega P_x, \\
 \dot{p}_z &= F_z.
 \end{aligned} \tag{2.17}$$

The solution of these equations is :

$$\begin{aligned}
 v_x(t + \tau) &= \left[v_x(t) - \left(\frac{a_y + \Omega^2 y}{\Omega} \right) \right] \cos(\Omega\tau) \\
 &+ \left[v_y(t) + \left(\frac{a_x + \Omega^2 x}{\Omega} \right) \right] \sin(\Omega\tau) \\
 &+ \frac{a_y + \Omega^2 y}{\Omega},
 \end{aligned} \tag{2.18a}$$

$$\begin{aligned}
 v_y(t + \tau) &= - \left[v_x(t) - \left(\frac{a_y + \Omega^2 y}{\Omega} \right) \right] \sin(\Omega\tau) \\
 &+ \left[v_y(t) + \left(\frac{a_x + \Omega^2 x}{\Omega} \right) \right] \cos(\Omega\tau) \\
 &- \frac{a_x + \Omega^2 x}{\Omega},
 \end{aligned} \tag{2.18b}$$

$$v_z(t + \tau) = v_z(t) + a_z \tau. \tag{2.18c}$$

Here τ corresponds to the rotating BRIDGE timestep.

The drift operator $D(\tau)$ in the canonical approximation is represented by the following set of equations:

$$\begin{aligned}
\dot{p}_x &= \dot{p}_y = \dot{p}_z = 0, \\
\dot{x} &= p_x/m + \Omega y, \\
\dot{y} &= p_y/m - \Omega x, \\
\dot{z} &= p_z/m.
\end{aligned} \tag{2.19}$$

The solution of these equations is

$$\begin{aligned}
x(t + \tau) &= \left[x(t) - \frac{v_y}{\Omega} \right] \cos(\Omega\tau) \\
&\quad + \left[y(t) + \frac{v_x}{\Omega} \right] \sin(\Omega\tau) + \frac{v_y}{\Omega},
\end{aligned} \tag{2.20a}$$

$$\begin{aligned}
y(t + \tau) &= - \left[x(t) - \frac{v_y}{\Omega} \right] \sin(\Omega\tau) \\
&\quad + \left[y(t) + \frac{v_x}{\Omega} \right] \cos(\Omega\tau) - \frac{v_x}{\Omega},
\end{aligned} \tag{2.20b}$$

$$z(t + \tau) = z(t) + v_z\tau. \tag{2.20c}$$

The canonical formulation has two advantages: it generates a stable algorithm and this approximation is symplectic (see Fig. 2.1). However, for systems with interacting particles we will see that it is convenient to have a drift operator that is independent of Ω , which is not the case for the canonical formulation (although this can be remedied by introducing a further splitting).

Non-canonical approximation

In the non-canonical approximation, the motion of a particle is defined in terms of its position and velocity coordinates (\mathbf{r} , \mathbf{v}). Given the generalized force $\mathbf{F}_{\text{gen}} = m\mathbf{a} - m\Omega \times (\Omega \times \mathbf{r}) - 2m(\Omega \times \mathbf{v})$, the equations of motion of a particle in a rotating frame can be written as:

$$\begin{aligned}
\dot{x} &= v_x; & \dot{v}_x &= a_x + \Omega^2 x + 2\Omega v_y, \\
\dot{y} &= v_y; & \dot{v}_y &= a_y + \Omega^2 y - 2\Omega v_x, \\
\dot{z} &= v_z; & \dot{v}_z &= a_z.
\end{aligned} \tag{2.21}$$

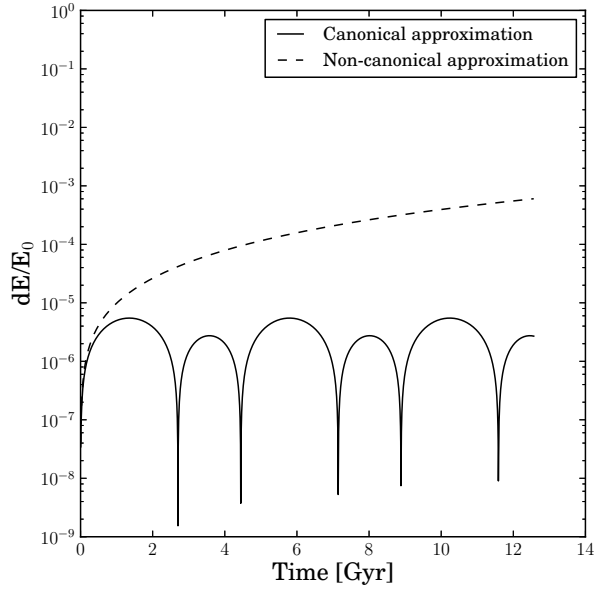


FIGURE 2.1: Energy error as a function of time of a particle in a rotating frame. Here we use a second order rotating BRIDGE with a timestep of 1 Myr.

We split Eqs. 2.21 to build the kick and drift operators. The set of equations that represent the kick operator $K(\tau)$ is the following:

$$\begin{aligned}
 \dot{x} &= \dot{y} = \dot{z} = 0, \\
 \dot{v}_x &= a_x + \Omega^2 x + 2\Omega v_y, \\
 \dot{v}_y &= a_y + \Omega^2 y - 2\Omega v_x, \\
 \dot{v}_z &= a_z.
 \end{aligned}
 \tag{2.22}$$

The solution of these equations is

$$\begin{aligned}
v_x(t + \tau) = & \left[v_x(t) - \left(\frac{a_y + \Omega^2 y}{2\Omega} \right) \right] \cos(2\Omega\tau) \\
& + \left[v_y(t) + \left(\frac{a_x + \Omega^2 x}{2\Omega} \right) \right] \sin(2\Omega\tau) \\
& + \frac{a_y + \Omega^2 y}{2\Omega},
\end{aligned} \tag{2.23a}$$

$$\begin{aligned}
v_y(t + \tau) = & \left[v_x(t) - \left(\frac{a_y + \Omega^2 y}{2\Omega} \right) \right] \sin(2\Omega\tau) \\
& + \left[v_y(t) + \left(\frac{a_x + \Omega^2 x}{2\Omega} \right) \right] \cos(2\Omega\tau) \\
& - \frac{a_x + \Omega^2 x}{2\Omega},
\end{aligned} \tag{2.23b}$$

$$v_z(t + \tau) = v_z(t) + a_z\tau. \tag{2.23c}$$

Here the vector \mathbf{a} corresponds to the acceleration of the particle due to the external galactic potential $U_{\text{ext}}(\mathbf{r})$, and τ is the Rotating BRIDGE timestep.

The drift operator $D(\tau)$ on the other hand, is represented by the following set of equations:

$$\begin{aligned}
\dot{v}_x = \dot{v}_y = \dot{v}_z &= 0, \\
\dot{x} &= v_x, \\
\dot{y} &= v_y, \\
\dot{z} &= v_z.
\end{aligned} \tag{2.24}$$

The solution of these equations is

$$x(t + \tau) = x(t) + v_x(t + \tau)\tau, \tag{2.25a}$$

$$y(t + \tau) = y(t) + v_y(t + \tau)\tau, \tag{2.25b}$$

$$z(t + \tau) = z(t) + v_z(t + \tau)\tau. \tag{2.25c}$$

By using the non-canonical approximation, a second order rotating BRIDGE can be constructed in the following way:

$$\text{RBridge}_2(\tau) = K(\tau/2) \cdot D(\tau) \cdot K(\tau/2), \quad (2.26)$$

where the operators $K(\tau)$ and $D(\tau)$ are described by Eqs. 2.23 and 2.25 respectively. Consequently, every $\tau/2$ a star receives a velocity kick due to the external galactic potential and every τ the position of the star is updated.

The Rotating BRIDGE can be easily generalized to a system of self interacting particles. The hamiltonian of a stellar system A which is located in a frame that rotates around the z -axis with constant angular speed Ω is given by:

$$H = H_A + H_{\text{int}}, \quad (2.27)$$

where

$$H_A = \sum_{i \in A}^N \frac{\|\mathbf{p}_i\|^2}{2m_i} - \sum_{i \neq j \in A}^N \frac{Gm_i m_j}{\|\mathbf{r}_i - \mathbf{r}_j\|},$$

$$H_{\text{int}} = \sum_{i \in A}^N \left[U_{\text{ext}}(\mathbf{r}_i) - (\Omega \times \mathbf{r}_i) \cdot \mathbf{p}_i - \frac{1}{2} m_i \|\Omega \times \mathbf{r}_i\|^2 \right]. \quad (2.28)$$

The temporal evolution of the system in a second order approximation is given by Eq. 2.26, which can also be written as:

$$e^{H_{\text{int}} \frac{\tau}{2}} e^{H_A \tau} e^{H_{\text{int}} \frac{\tau}{2}}. \quad (2.29)$$

Here the term $e^{H_{\text{int}} \tau}$ represents the kick operator $K(\tau)$ while the term $e^{H_A \tau}$ corresponds to the drift operator $D(\tau)$. For a system of self-interacting particles the drift operator is given by:

$$\mathbf{x}(t + \tau) = \mathbf{x}(t) + \mathbf{v}(t + \tau/2)\tau, \quad (2.30)$$

$$\mathbf{v}'(t + \tau/2) = \mathbf{v}(t + \tau/2) + \mathbf{a}_{cc}\tau/2. \quad (2.31)$$

Thus, the evolution of system A during a rotating BRIDGE timestep τ is given by the following steps:

- i) At $\tau/2$ the system receives a velocity kick due to the external potential of its parent galaxy (Eqs. 2.23). This velocity is referred to as $\mathbf{v}(t + \tau/2)$.

- ii) The positions of the stars are updated for a time step τ (Eq. 2.30). Additionally, the velocities of the stars are updated once more after evolving system A through a direct N-body code (Eq. 2.31).
- iii) The system receives a velocity kick for another $\tau/2$ (Eqs. 2.23). This kick is computed by using the previous velocity $\mathbf{v}'(t + \tau/2)$. Note that the only difference between the rotating and classical BRIDGE is in the kick operator. In particular, the code evolution operator $e^{H\Delta\tau}$ does not have to be changed.

The above procedure can also be applied to a more generalized case in which there are several self-gravitating systems.

The precision of the Rotating BRIDGE can be increased by applying the drift and kick operators in accordance with Eqs. 2.11 and 2.12. In this case a higher order rotating BRIDGE can be generated.

2.2.4. Bridge with post-Newtonian Corrections

In order to extend BRIDGE to include post-Newtonian (PN) corrections a special treatment is needed so that the velocity dependency in the PN terms can be handled correctly. Here we adopt the recipe developed in Hellström & Mikkola [2010], where an auxiliary velocity, $\mathbf{w}_i(t)$ with $\mathbf{w}_i(t = 0) = \mathbf{v}_i(t = 0)$, is introduced in order to make the time evolution operators separable, thus allowing the use of an explicit leapfrog-like algorithm for implement the PN corrections.

In BRIDGE, the operators $e^{\tau H_{S_k}}$ and $e^{\tau H_{S_k S_l}^{int}}$ in eqs. 2.9 and 2.10 can be associated to different solvers, which evolve the different sub-systems in a simulation. If, for example, the j -th sub-system requires PN corrections and we assume that interactions with others sub-systems can be treated without PN corrections, then only the operator $e^{\tau H_{S_k}}|_{k=j}$ in eq. 2.9 needs to be modified, which consists of a simple substitution of a regular Newtonian solver by a PN one for this particular j -th sub-system.

In the more complex case where several interacting sub-systems require PN corrections, both operators $D(\tau)$ and $K(\tau)$ in eqs. 2.9 and 2.10 have to be modified accordingly. In the following, we will assume that from a total number Q of sub-systems being bridged, a number Q^N are “Newtonian”, and

a number Q^{PN} require PN corrections, so that $Q = Q^N + Q^{PN}$. Moreover, we define S^N as the set of ‘‘Newtonian’’ sub-systems and S^{PN} as the set of ‘‘post-Newtonian’’ sub-systems, so that $S = S^N \cup S^{PN}$. In this way, operator $D(\tau)$ in eq. 2.9 can be extended into the following expression

$$\tilde{D}(\tau) = \prod_{k \in S^N}^{Q^N} e^{\tau H_{S_k^N}} \prod_{k \in S^{PN}}^{Q^{PN}} e^{\tau H_{S_k^{PN}}}. \quad (2.32)$$

Here $e^{\tau H_{S_k^N}}$ represents a Newtonian solver for the k -th sub-system in S^N and $e^{\tau H_{S_k^{PN}}}$ represents a PN solver for the k -th sub-system in S^{PN} . We clarify here that by PN solver we mean a code that evolve the particles under the total acceleration $\mathbf{a} = \mathbf{a}^N + \mathbf{a}^{PN}$, not just \mathbf{a}^{PN} as might be implied by our notation.

The operator $K(\tau)$ in eq. 2.10 can be extended as follows. We first define some auxiliary kick operators,

$$K^{N \leftrightarrow N}(\tau) = \prod_{k \neq l}^{Q^N} e^{\tau H_{S_k^N S_l^N}^{int}}, \quad (2.33)$$

$$K^{N \leftrightarrow PN}(\tau) = \prod_{k \in S^N}^{Q^N} \prod_{l \in S^{PN}}^{Q^{PN}} e^{\tau H_{S_k^N S_l^{PN}}^{int}}, \quad (2.34)$$

$$K^{PN \leftrightarrow PN}(\tau) = \prod_{k \neq l}^{Q^{PN}} e^{\tau H_{S_k^{PN} S_l^{PN}}^{int}}, \quad (2.35)$$

from which follows that the extended kick operator for BRIDGE with PN corrections can be written as:

$$\begin{aligned} \tilde{K}(\tau) &= K^{N \leftrightarrow N}(\tau/2) \cdot K^{N \leftrightarrow PN}(\tau/2) \cdot K^{PN \leftrightarrow PN}(\tau) \cdot \\ &\quad \cdot K^{PN \leftrightarrow N}(\tau/2) \cdot K^{N \leftrightarrow N}(\tau/2) \\ &= K^{PN \leftrightarrow PN}(\tau/2) \cdot K^{PN \leftrightarrow N}(\tau/2) \cdot K^{N \leftrightarrow N}(\tau) \cdot \\ &\quad \cdot K^{N \leftrightarrow PN}(\tau/2) \cdot K^{PN \leftrightarrow PN}(\tau/2). \end{aligned} \quad (2.36)$$

Eq. 2.33 represents the Newtonian kick due to the interaction between ‘‘Newtonian’’ sub-systems, and is identical to the original definition in eq. 2.10.

Eq. 2.34 represents the kick due to the interaction between “Newtonian” and “post-Newtonian” sub-systems. In this particular case, a choice has to be made on whether PN corrections should be included or not. Such decision could be based, for example on the distance between the two interacting sub-systems. Eq. 2.35 represents the PN kick due to the interaction between “post-Newtonian” sub-systems. Finally, eq. 2.36 represents the extended kick operator to be used in BRIDGE with PN corrections.

2.3. Tests and Applications

2.3.1. Implementation

The above new BRIDGE integrators can be implemented in a number of different ways. For the tests here we will use the Astrophysical Multipurpose Software Environment (AMUSE) [Pelupessy et al., 2013; Portegies Zwart et al., 2013]. AMUSE is a python software environment for astrophysical simulations. AMUSE presents a wide variety of astrophysical codes using homogeneous interfaces, simplifying their use. AMUSE contains codes from different domains, amongst which a number of gravitational dynamics codes.

For the BRIDGE integrators here, it is important to note that the gravitational dynamics codes in AMUSE provide convenient implementations of the evolution operator $e^{\tau H}$ in the form of an `evolve_model` method on the interface. This can then be combined with simple force evaluations (evaluated by other component codes or implemented on the interface level) to provide $e^{\tau H_{int}}$, the interaction type operators. Thus the integrators presented above can be quickly formulated using ready made ‘building blocks,’ selecting the appropriate integrators from the ones available, balancing the needs for the precision in the calculations with the performance or special features of a given code.

To illustrate this, in Fig. 2.2 we show the usage of the BRIDGE integrator through the AMUSE framework. In this example, we present the steps needed to evolve a star cluster (contained in the cluster particle set) in its parent galaxy (the galaxy set). The initial realization can be constructed within AMUSE using e.g. a Plummer sphere model. Other realizations are implemented in AMUSE such as king profiles [King, 1966] and fractal distributions [Goodwin

```

(1) code1=Hermite()
(2) code1.particles.add_particles(cluster)
(3) code2=BHTree()
(4) code2.particles.add_particles(galaxy)
(5) sys=Bridge(timestep=0.1 | units.Myr)
(6) sys.add_system(code1, (code2,))
(7) sys.add_system(code2, (code1,))
(8) sys.evolve_model( 10 | units.Myr )

```

FIGURE 2.2: Example usage of the BRIDGE integrator through the AMUSE framework.

& Whitworth, 2004]. At (1) we initialize the N-body integrator to calculate the internal evolution of the star cluster. In this case, we use the Hermite integrator [Hut et al., 1995]. For a list of gravity codes implemented in AMUSE, we refer the reader to Pelupessy et al. [2013]. (2) We send the particle data to the N-body code. (3) and (4) similarly a code appropriate for the galaxy model (in this case a tree-code) is started and initialized. (5) We instantiate the BRIDGE integrator, setting a timestep for the coupling timescale. For a BRIDGE in rotating coordinates, the initialization is made by typing: `sys=Rotating_Bridge()`. (6) and (7) We couple the gravity code and the galaxy into the BRIDGE integrator. The method `add_system` has two arguments: the *system* and a set with *interaction partners*. The *interaction partners* indicate which systems will kick the *system*. Therefore, in line (6) the galaxy will kick the particles in the gravity code. In line (7) the particles in the gravity code will kick the galaxy. In this way we ensure that both cluster and parent galaxy will be evolved self-consistently. (8) We evolve the compound system for a set amount of time.

2.3.2. High Order Bridge

To evaluate the high-order formulation of bridge and show that we indeed can construct high-order compound methods this way, we first calculate the evolution of a very simple system, namely a stable hierarchical quadruple system consisting of two binary systems orbiting each other. The total system comprises of 4 equal mass bodies [for a total mass of 1 in N-body units, Heggie

2.3 TESTS AND APPLICATIONS

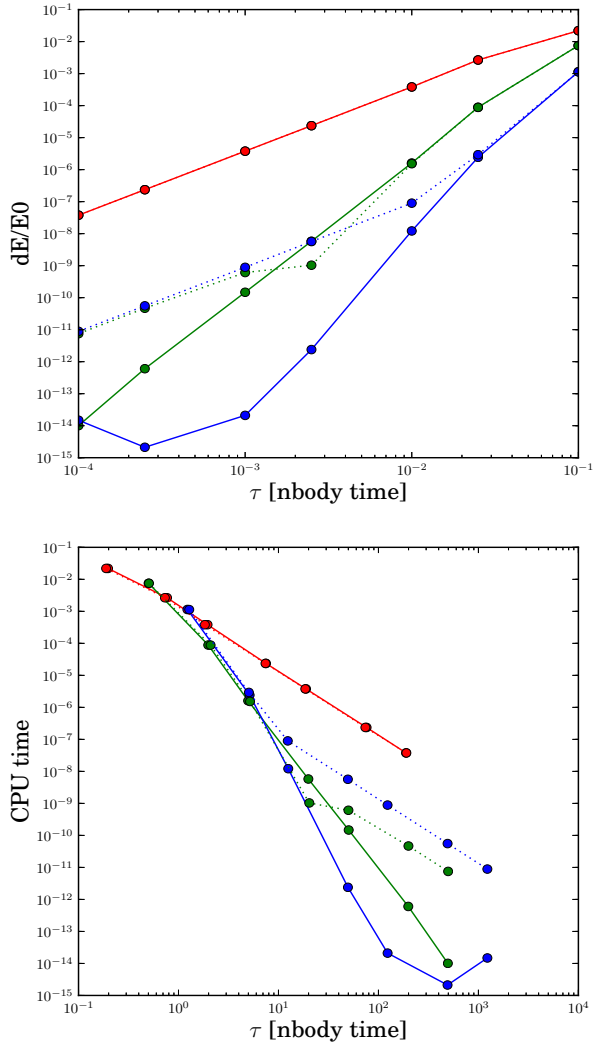


FIGURE 2.3: *Left:* Energy error for quadruple system test. Drawn lines: second, fourth and sixth order bridge coupling results (left to right, red green and blue) and Kepler solver subsystem. Dotted lines: same with leapfrog subsystem. *Right:* CPU time for the quadrupole test. Note the CPU time is indicative of the scaling only, because for such a small problem the overhead of the bridging method is large.

& Mathieu, 1986], and the orbits are coplanar with the two binary orbits having a semi-major axis $a = 1/8$ and moderate eccentricity ($\epsilon = 0.5$). The two

CHAPTER 2 : HIGH-ORDER HYBRID N-BODY METHODS FOR COMPOUND SYSTEMS

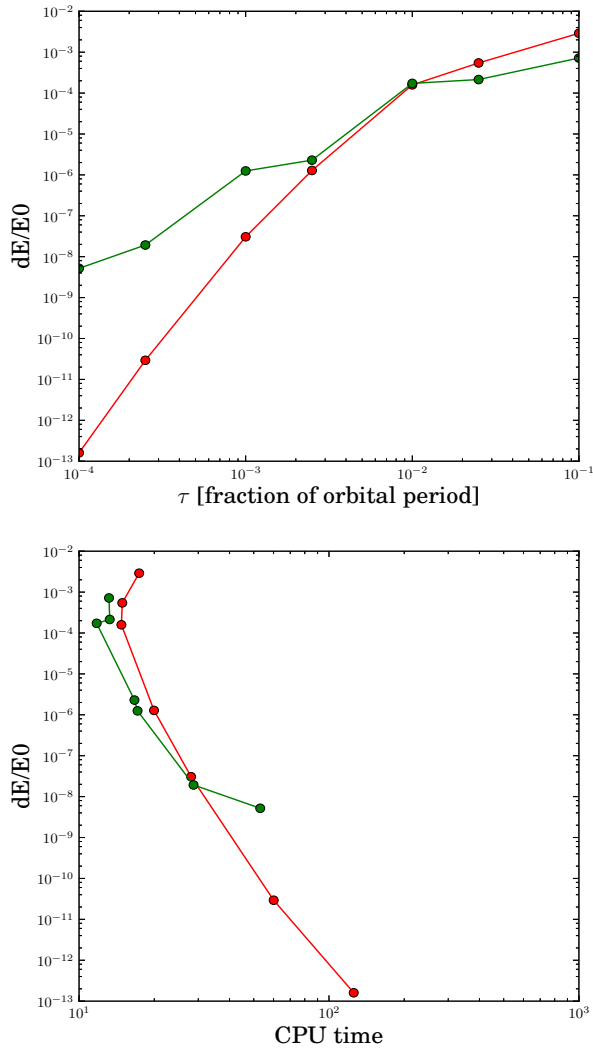


FIGURE 2.4: *Left:* Energy error for orbiting King clusters test. Plotted is the energy error as function of the BRIDGETimestep (given as fraction of the orbital period). Green: integration using $\text{Bridge}_2(\tau)$, red: results for $\text{Bridge}_4(\tau)$ *Right:* CPU times. Note the CPU time is indicative of the scaling only, because for such a small problem the overhead of the bridging method is large.

binaries in turn are set-up in an orbit with $a = 1.$ and $\epsilon = 0.5.$ The two binary systems are integrated in separate codes, and their interaction is bridged using

the standard leapfrog bridge, and a fourth order and sixth order method. The binaries can be evolved using a Kepler solver, which calculates the evolution of the subsystems exact to machine precision, or a leapfrog integrator, which is second order.

If we investigate the results for the bridged Kepler solvers in figure 2.3, where we have plotted the relative energy error as function of the bridge timestep, we see that the BRIDGE schemes show the expected error behavior, appropriate for their respective order (note that the sixth order integrator shows saturation at machine precision as expected). If we change the integrator of the subsystems to a leapfrog integrator (dotted lines), at small time steps ($< 10^{-3}$) the energy error is ~ 3 orders of magnitude higher with respect to the integration with the Kepler solver. This energy error is caused by the integration of the subsystems, which show the expected second order behavior (we keep the ratio of the timestep in the subsystem to the bridge timestep constant). This tests shows that the high-order BRIDGE schemes can be effectively applied in cases where the compound integrators allow for the extra precision.

Improved precision beyond the common ~ 16 decimal places and $\sim 10^{-12}$ energy conservation per step is hard, and requires special treatment of the force evaluation and timestepping. Recently, Boekholt & Portegies Zwart [2015] designed a gravitational N -body method in which the precision can be tuned to arbitrary precision.

In figure 2.4 we show the energy error behavior for a similar test where we put two clusters in orbit around each other. The models consist of King models with 64 particles, put on circular orbits with a separation of 8 N -body length units. We integrate for half an orbital period (which is 284 N -body time units). The two models are integrated using a high precision sixth order method, and bridged using either $\text{Bridge}_2(\tau)$ or $\text{Bridge}_4(\tau)$. As we can see in figure 2.4 the energy error shows the expected order behavior in the two cases.

2.3.3. Rotating bridge

To evaluate the accuracy of the Rotating BRIDGE, we show in Fig. 2.5 the maximum fractional energy error as a function of bridge timestep of a star moving in different galactic potentials representing the Milky Way. In this plot, the Galaxy is represented by: a pure axisymmetric potential (top panel);

CHAPTER 2 : HIGH-ORDER HYBRID N-BODY METHODS FOR COMPOUND SYSTEMS

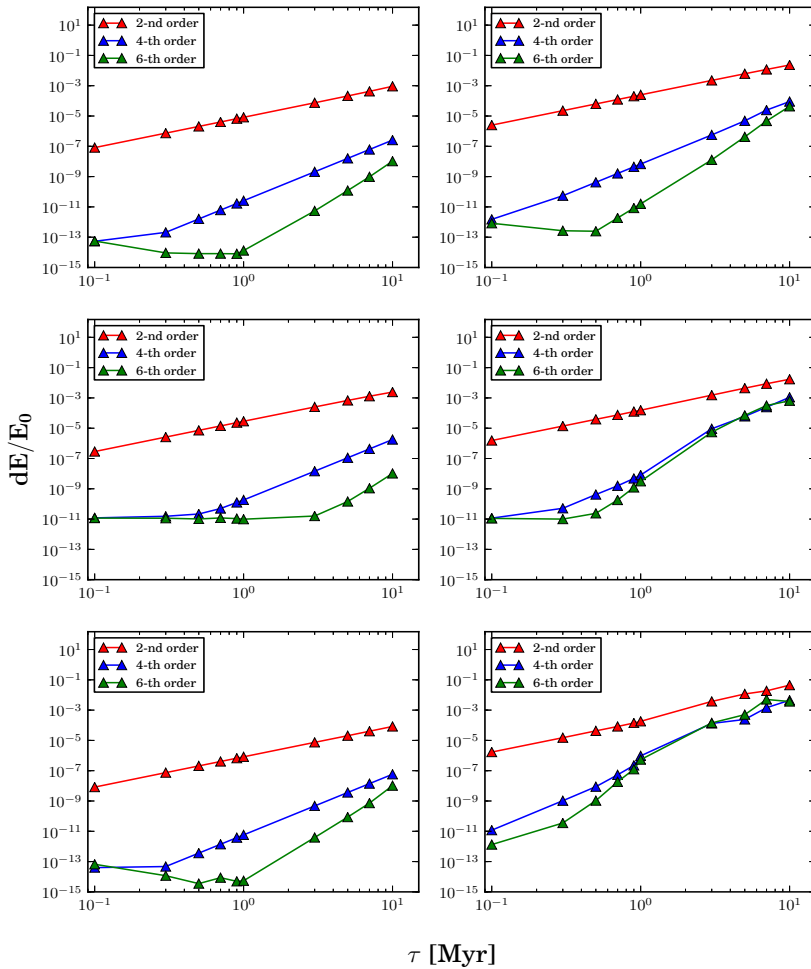


FIGURE 2.5: Maximum fractional energy error as a function of Bridge timestep of a star moving with: *Left*: a nearly circular orbit ($\epsilon = 0.01$). *Right*: An eccentric orbit ($\epsilon = 0.5$). The red lines correspond to the normal second order rotating BRIDGE. The blue and green lines correspond to the rotating BRIDGE in a fourth and sixth order approximation respectively. For more details, see the text.

an axisymmetric + bar potential (middle panel); and an axisymmetric + spiral arms potential (bottom panel).

The axisymmetric potential was modelled by taking into account the parameters of Allen & Santillán [1991]. The central bar was modelled with a Ferrers

2.3 TESTS AND APPLICATIONS

potential [Ferrers, 1877] and the spiral arms were modelled as perturbations of the axisymmetric Galactic potential following the tight winding approximation [Antoja et al., 2011]. Both bar and spiral arms rotate as rigid bodies with different pattern speeds. For further details on the Galactic model, we refer the reader to Martínez-Barbosa et al. [2015]. Contrary to Fig. 2.3, in this example we use physical units, i.e. the BRIDGE timestep is in Myr.

We also show two different stellar motions. On the left panel, a single star moves through the Galaxy in a nearly circular orbit with $\epsilon = 0.01$. On the right panel, the star moves in an eccentric orbit with $\epsilon = 0.5$. We computed both orbits during ten orbital periods. The circular and eccentric orbits have orbital periods corresponding to 224 and 471 Myr respectively.

By analyzing the figure, we can observe that the fourth and sixth order integrators generate a better energy conservation compared to the normal (second order) rotating BRIDGE scheme. Additionally, note that the energy error is smaller in circular than in more eccentric orbits for a given Galaxy model and BRIDGE timestep. This is expected, because the external tidal field is constant in circular orbits. However, note that even in eccentric orbits, a high-order rotating BRIDGE can allow a good energy conservation at small timesteps ($dE/E_0 < 10^{-7}$ at $\tau \leq 1$ Myr). We computed the energy error of a star in the eccentric orbit for 100 orbital periods (more than a Hubble time) and for each of the Galaxy models explained above. We found that the fractional energy error is of the order of 10^{-7} when using $\tau \leq 1$ Myr. Therefore, the high-order Rotating BRIDGE is a suitable scheme to compute the stellar motion in analytical Galaxy models.

In Fig. 2.6 we show the evolution of a star cluster in the Milky Way by using a high-order rotating BRIDGE. The cluster is modelled with a Plummer sphere of 1700 stars. The Galaxy is modelled with an analytic prescription that contains an axisymmetric potential (bulge, disk and a dark matter halo) together with a bar and spiral arms. We evolved the star cluster during 4.6 Gyr. We use the HUAYNO code [Pelupessy et al., 2012] to resolve the gravitational effects among the stars and a sixth order rotating BRIDGE to couple the N-body code with the Galaxy model. Given that we use the AMUSE framework to perform the simulation, we added the SEBA population synthesis code [Portegies Zwart & Verbunt, 1996; Toonen et al., 2012] to model stellar evolution effects in the

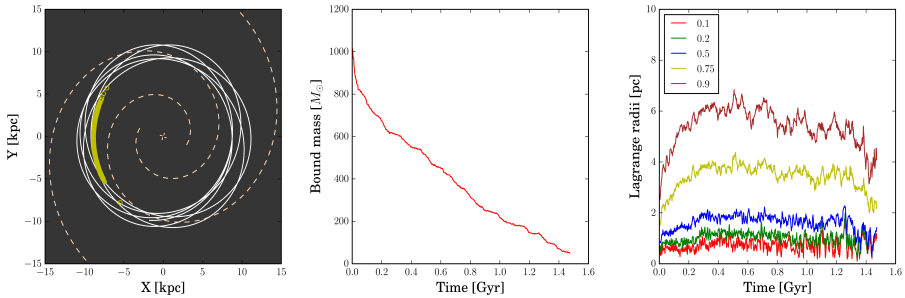


FIGURE 2.6: Evolution of a star cluster in the Milky Way using a rotating BRIDGE integrator to a sixth order. *Left*: Distribution of the stars (yellow points) in the Galactic disk after 4.6 Gyr of evolution. The white line corresponds to the orbit of the cluster before dissolution. The pink dashed lines represent the present-day potential of the spiral arms. *Middle*: Bound mass of the star cluster as a function of time. *Right*: Lagrange radii of the star cluster as a function of time.

cluster. The BRIDGE timestep used was such that the maximum energy error in the simulation was of the order of 10^{-7} .

During 4.6 Gyr of evolution, the star cluster moves in an orbit with $\epsilon = 0.1$, its pericenter being at 8.6 kpc with respect to the Galactic center (e.g solid white line, left panel Fig. 2.6). During the first 0.1 Gyr of evolution, the star cluster loses mass due to stellar evolution (see middle panel Fig. 2.6). After ~ 0.1 Gyr, two-body relaxation effects and the external tidal field of the Galaxy are the main mechanisms that dissolve the star cluster. Both stellar evolution and two-body relaxation effects make the cluster expands (see right panel Fig. 2.6). This phenomenon is called expansion phase [Gieles et al., 2011] and it has been observed by several authors previously [i.e Madrid et al., 2012, and references therein]. After ~ 0.6 Gyr, the effect of the tidal field becomes more important. This produces a gradual evaporation of the star cluster (see right panel Fig. 2.6) which contributes with its completely disruption in the Galaxy at ~ 1.5 Gyr (middle panel Fig. 2.6). After 4.6 Gyr, the stars are spread in the second and third quadrants of the Galaxy, with galacto-centric distances of around 8 kpc. (see left panel Fig. 2.6).

2.4. Discussion and Conclusions

The classical BRIDGE scheme [Fujii et al., 2007] provides an elegant and convenient integrator under the conditions discussed in section 2.2.1, namely that there are multiple subsystems where there is a separation in timescales of the interactions, and/or there are different regimes of gravitational dynamics at play.

We have shown that this coupling can be extended to higher orders, as well as multiple interacting systems and deeper hierarchies of subsystems. We name this **suspension-bridge**. Suspension-bridge provides a high-order hierarchical symplectic coupling between two or more subsystems. The formulation is relatively independent of the actual implementation of the needed evolution operators and we have implemented them within the AMUSE framework. Here the different numerical integrators available provide ready-made building blocks to combine in different type of integrators that can be tailored towards the specific application and precision required. We tested the method on gravitational systems in which we coupled Newtonian gravitational dynamics with Newtonian forces via a direct N-body codes, confirming the energy conservation has the right order for the second, fourth and sixth order coupling strategies, up to machine precision ($dE/E \simeq 10^{-15}$), if the requirements on the component integrators are met. Within AMUSE up to tenth order methods are available. The method is hierarchical and the same expansion can be repeated to construct more complicated suspension schemes.

We have also presented a variant of BRIDGE for a rotating frame of reference. The formulation follows a similar splitting argument, where a formally symplectic scheme follows if we use canonical coordinates. A non-canonical formulation is somewhat easier to combine with self-interacting systems. The only difference with the classical BRIDGE is that the kick operator effecting the interactions between the different subsystems must be adapted. Note that the evolution in between the kicks has not changed form (and can use the same integrators as before). In the non-canonical case the resulting integrator is not formally symplectic (and this manifests itself as a small drift in energy), but for practical applications (e.g. a stellar cluster in a galaxy potential) the resulting drift is neglectable (due to the relative low number of orbits) especially

if combined with a higher order integration scheme.

Acknowledgements

We thank Tjarda Boekholt, Adrian Hamers and Arjen van Elteren for enriching discussions. This work was supported by the Interuniversity Attraction Poles Programme initiated by the Belgian Science Policy Office (IAP P7/08 CHARM) and by the Netherlands Research Council NWO (grants #643.200.503, #639.073.803 and #614.061.608) and by the Netherlands Research School for Astronomy (NOVA). The numerical computations were carried out using the Little Green Machine at Leiden University.

CHAPTER 3

RADIAL MIGRATION OF THE SUN IN THE MILKY WAY: A STATISTICAL STUDY

C.A. Martínez-Barbosa, A.G.A. Brown and S. Portegies Zwart

2015, MNRAS, 446, 823-841

Abstract

The determination of the birth radius of the Sun is important to understand the evolution and consequent disruption of the Sun's birth cluster in the Galaxy. Motivated by this fact, we study the motion of the Sun in the Milky Way during the last 4.6 Gyr in order to find its birth radius. We carried out orbit integrations backward in time using an analytical model of the Galaxy which includes the contribution of spiral arms and a central bar. We took into account the uncertainty in the parameters of the Milky Way potential as well as the uncertainty in the present day position and velocity of the Sun. We find that in general the Sun has not migrated from

its birth place to its current position in the Galaxy (R_{\odot}). However, significant radial migration of the Sun is possible when: 1) The 2 : 1 Outer Lindblad resonance of the bar is separated from the corotation resonance of spiral arms by a distance ~ 1 kpc. 2) When these two resonances are at the same Galactocentric position and further than the solar radius. In both cases the migration of the Sun is from outer regions of the Galactic disk to R_{\odot} , placing the Sun's birth radius at around 11 kpc. We find that in general it is unlikely that the Sun has migrated significantly from the inner regions of the Galactic disk to R_{\odot} .

Keywords: Galaxy: kinematics and dynamics; open clusters and associations: general; Sun: general

3.1. Introduction

The study of the history of the Sun's motion within the Milky Way gravitational field is of great interest to the understanding of the origins and evolution of the solar system [Adams, 2010] and the study of past climate change and extinction of species on the earth [Feng & Bailer-Jones, 2013]. The determination of the birth radius of the Sun is of particular interest in the context of radial migration and in the quest for the siblings of the Sun [Brown et al., 2010a; Portegies Zwart, 2009]. The work in this chapter is motivated by the possibility in the near future of combining large amounts of phase space data collected by the *Gaia* mission [Lindegren et al., 2008] with data on the chemical compositions of stars (such as collected by the Gaia-ESO survey [Gilmore et al., 2012]) in order to search for the remnants of the Sun's birth cluster. Our approach is to guide the search for the Sun's siblings by understanding in detail the process of cluster disruption in the Galactic potential, using state of the art simulations. One of the initial conditions of such simulations is the birth location, in practice the birth radius, of the Sun's parent cluster. In this chapter we present a parameter study of the Sun's past orbit in a set of fully analytical Galactic potentials and we determine the most likely birth radius of

the Sun and by how much the Sun might have migrated radially within the Milky Way over its lifetime.

The displacement of stars from their birth radii is a process called radial migration. This can be produced by different processes: interaction with transient spiral structure [Sellwood & Binney, 2002; Minchev & Quillen, 2006; Roškar et al., 2008a], overlap of the dynamical resonances corresponding to the bar and spiral structure [Minchev & Famaey, 2010; Minchev et al., 2011], interference between spiral density waves that produce short lived density peaks [Comparetta & Quillen, 2012], and interaction of the Milky Way disk with in-falling satellites [Quillen et al., 2009; Bird et al., 2012].

Since radial migration is a natural process in the evolution of Galactic disks, it is very likely that the Sun has migrated from its formation place to its current position in the Galaxy. Wielen et al. [1996] argued that the Sun was born at a Galactocentric distance of 6.6 ± 0.9 kpc; roughly 2 kpc nearer to the Galactic centre. He based his conclusions on the observation that the Sun is more metal rich by 0.2 dex with respect to most stars of the same age and Galactocentric position [Holmberg et al., 2009] and the presence of a radial metallicity gradient in the Milky Way. Other studies also support the idea that the Sun has migrated from its birth place. Based on chemo-dynamical simulations of Galactic disks, Minchev et al. [2013] found that the most likely region in which the Sun was born is between 4.4 and 7.7 kpc from the Galactic centre.

However, if the metallicity of the Sun is not unusual with respect to the surrounding stars of the same age it would no longer be valid to assume that the Sun migrated from the inner parts of our Galaxy. By improving the accuracy in the determination of the effective temperature of the stars in the data of the Geneva-Copenhagen Survey, Casagrande et al. [2011] found that those stars are on average 100 K hotter and, hence, 0.1 dex more metal rich. This result shifts the peak of the metallicity distribution function to around the solar value, thus casting doubt on the observation that the Sun is metal rich with respect to its surroundings. Further studies also support the idea that the Sun is not an unusual star [Gustafsson, 1998, 2008; Gustafsson et al., 2010].

The idea that the Sun might not have migrated considerably has been explored by several authors. By solving the equations of motion of the Sun

under the influence of a disk, a dark matter halo, spiral arms, and the Galactic bar described by a multi-polar term, Klačka et al. [2012] found that the radial distance of the Sun varied between 7.6 and 8.1 kpc. They find migration only when the Sun co-rotates with the spiral arms and when these structures represent very strong perturbations. On the other hand, by using the method suggested by Wielen et al. [1996], Mishurov [2006] found that the Sun might have been born at approximately 7.4 kpc from the Galactic centre.

Has the Sun migrated considerably? And if so, what are the conditions that allow such radial migration? One way of solving these questions is by computing the motion of the Sun in the Galaxy backwards in time. Portegies Zwart [2009] used this technique to find that the Sun was born at a distance of $r = 9.4$ kpc with respect to the Galactic centre. He used an axisymmetric potential for modelling the Milky Way, which is not realistic and furthermore, he did not take into account the uncertainty in the current position and velocity of the Sun (with respect to the Galactic reference frame).

The aim of this chapter is to address the question of the Sun's birth radius by carrying out orbit integrations backward in time, using a more realistic model for the Galaxy which includes the contribution of spiral arms and a central bar. We account for the uncertainty in the parameters of the Milky Way potential as well as the uncertainty in the present day position and velocity the Sun. The resulting parameter study is used to obtain a statistical estimation of the Sun's birth radius 4.6 Gyr ago. We use the AMUSE framework [Portegies Zwart et al., 2013] to perform our computations.

This chapter is organized as follows: in section 3.2 we describe the model that we use for the Milky Way. In section 3.4 we present the methodology to survey possible past orbits of the Sun and thereby constrain its birth radius. In section 3.5 we analyse the orbit integration results and address the question of whether or not the Sun has migrated in the Galaxy and the conditions that would allow a considerable radial migration. In section 3.6 we discuss the results and in section 3.7 we present our conclusions and final remarks.

3.2. Galactic model

Since the past history of the structure of the Milky Way is unknown, we simply assume that the values of the Galactic parameters have been the same during the last 4.6 Gyr, i.e. during the lifetime of the Sun [Bonanno et al., 2002]. We model the Milky Way as a fully analytical potential that contains an axisymmetric component together with a rotating central bar and spiral arms. We use the potentials and parameters of Allen & Santillán [1991] to model the axisymmetric part of the Galaxy, which consist of a central bulge, a disk and a dark matter halo. The values of the parameters of these Galactic components are shown in table 3.1. For the central bar and spiral arms we use the models presented in Romero-Gómez et al. [2011] and Antoja et al. [2011] as detailed below.

3.2.1. Central bar

The central bar of the Milky Way is modelled as a Ferrers bar [Ferrers, 1877] which is described by a density distribution of the form:

$$\rho_{\text{bar}} = \begin{cases} \rho_0 (1 - n^2)^k & n < 1 \\ 0 & n \geq 1 \end{cases}, \quad (3.1)$$

where $n^2 = x^2/a^2 + y^2/b^2$ determines the shape of the bar potential, where a and b are the semi-major and semi-minor axes of the bar, respectively. Here, x and y are the axes of a frame that corrotates with the bar. ρ_0 represents the central density of the bar and the parameter k measures the degree of concentration of the bar. Larger values of k correspond to a more concentrated the bar. The extreme case of a constant density bar is obtained for $k = 0$ [Athanasoula et al., 2009]. Following Romero-Gómez et al. [2011] we use $k = 1$. For these models the mass of the bar is given by:

$$M_{\text{bar}} = \frac{2^{(2k+3)} \pi a b^2 \rho_0 \Gamma(k+1) \Gamma(k+2)}{\Gamma(2k+4)}, \quad (3.2)$$

where Γ is the Gamma function.

CHAPTER 3 : RADIAL MIGRATION OF THE SUN IN THE MILKY WAY: A STATISTICAL STUDY

TABLE 3.1: Parameters of the Milky Way model potential.

<i>Axisymmetric component</i>	
Mass of the bulge (M_b)	$1.41 \times 10^{10} M_\odot$
Scale length bulge (b_1)	0.3873 kpc
Disk mass (M_d)	$8.56 \times 10^{10} M_\odot$
Scale length disk 1 (a_2)	5.31 kpc
Scale length disk 2 (b_2)	0.25 kpc
Halo mass (M_h)	$1.07 \times 10^{11} M_\odot$
Scale length halo (a_3)	12 kpc
<i>Central Bar</i>	
Pattern speed (Ω_{bar})	40–70 km s ⁻¹ kpc ⁻¹
Semi-major axis (a)	3.12 kpc
Axis ratio (b/a)	0.37
Mass (M_{bar})	9.8×10^9 – $1.4 \times 10^{10} M_\odot$
Strength of the bar (ϵ_b)	0.3–0.5
Orientation	20°
<i>Spiral arms</i>	
Pattern speed (Ω_{sp})	15–30 km s ⁻¹ kpc ⁻¹
Locus beginning (R_{sp})	3.12 kpc
Number of spiral arms (m)	2, 4
Spiral amplitude (A_{sp})	650–1300 km ² s ⁻² kpc ⁻¹
Strength of the spiral arms (ϵ_s)	0.02–0.06
Pitch angle (i)	12.8°
Scale length (R_Σ)	2.5 kpc
Orientation	20°

Galactic bar parameters

Number of bars The inner part of the Galaxy has been extensively studied within the *COBE/DIRBE* [Weiland et al., 1994] and *Spitzer/GLIMPSE* [Churchwell et al., 2009] projects, which demonstrated that the centre of the Milky Way is a complex structure. While the *COBE/DIRBE* data showed that the surface brightness distribution of the bulge resembles a flattened ellipse with a minor-to-major axis ratio of ~ 0.6 , the *Spitzer/GLIMPSE* survey confirmed the existence of a second bar [Benjamin et al., 2005] which was previously observed by Hammersley et al. [2000]. Since the longitude and length ratios of these bars are in strong disagreement with both simulations and observations, Romero-Gómez et al. [2011] suggested that there is only a single bar at the centre of the Milky Way, which was confirmed by the analysis of Martínez-Valpuesta & Gerhard [2011], who show that the observations of the central region of the Milky Way can be explained by one bar. Hence we take into account the contribution of only one bar in the potential model of the Milky Way, using the parameters as obtained from the *COBE/DIRBE* survey.

Pattern speed The value of the pattern speed of the bar is uncertain. From theoretical and observational data Dehnen [2000] concluded that $\Omega_{\text{bar}} = 50 \pm 3 \text{ km s}^{-1} \text{ kpc}^{-1}$; however, Bissantz & Gerhard [2002] argued that a more suitable value for the pattern speed of the bar is $60 \pm 5 \text{ km s}^{-1} \text{ kpc}^{-1}$. Taking into account these values, we assume that the bar rotates as a rigid body with a pattern speed between 40 and 70 $\text{km s}^{-1} \text{ kpc}^{-1}$.

Semi-major axis and axis ratio Based on the best fit model by Freudenreich [1998] and on the uncertainty in the current solar Galactocentric position¹, the semi-major axis of the *COBE/DIRBE* bar is between 2.96 and 3.31 kpc. With these assumptions the axis ratio of the bar is between 0.36 and 0.38. In our simulations we maintain these two parameters constant with the values listed in table 3.1.

¹We conservatively assume the uncertainty in the distance from the Sun to the Galactic centre is 0.5 kpc

Mass and orientation of the bar Several studies suggest that the mass of the *COBE/DIRBE* bar is in the range $0.98\text{--}2\times 10^{10} M_{\odot}$ [Weiner & Sellwood, 1999; Dwek et al., 1995; Matsumoto et al., 1982; Zhao, 1996]. Given that the bar is formed from the bulge, we assume the mass of the bar is in the range $9.8 \times 10^9 - 1.4 \times 10^{10} M_{\odot}$.

The orientation of the bar is defined as the angle between its major axis and the line that joins the Galactic centre with the current position of the Sun. We fixed this angle at 20° [Pichardo et al., 2004, 2012; Romero-Gómez et al., 2011], as illustrated in Fig. 3.1.

Effect of a growing bar From N -body simulations it appears that bars in galaxies are formed during the first 1.4 Gyr of their evolution [Fux, 2000; Polyachenko, 2013]. Thus, we assume that the bar was already present in the Milky Way when the Sun was formed 4.6 Gyr ago.

3.2.2. Spiral arms

The spiral arms in our Milky Way Models are represented as periodic perturbations of the axisymmetric potential. Following Contopoulos & Grosbøl [1986] the potential of such perturbations in the plane is given by:

$$\phi_{\text{sp}} = -A_{\text{sp}} R e^{-R/R_{\Sigma}} \cos(m(\phi) - g(R)), \quad (3.3)$$

where A_{sp} is the amplitude of the spiral arms. R and ϕ are the cylindrical coordinates of a star measured in a corotating frame with the spiral arms. R_{Σ} and m are the scale length and the number of spiral arms, respectively. The function $g(R)$ defines the locus shape of the spiral arms. We use the same prescription as Antoja et al. [2011]:

$$g(R) = \left(\frac{m}{N \tan i} \right) \ln \left(1 + \left(\frac{R}{R_{\text{sp}}} \right)^N \right). \quad (3.4)$$

N is a parameter which measures how sharply the change from a bar to a spiral structure occurs in the inner regions of the Milky Way. $N \rightarrow \infty$ produces spiral arms that begin forming an angle of $\sim 90^{\circ}$ with respect to the line that joins the two starting points of the locus [Antoja et al., 2011] (as illustrated

in Fig. 3.1 below). To approximate this case we use $N = 100$. R_{sp} is the separation distance of the beginning of the spiral shape locus and $\tan i$ is the tangent of the pitch angle.

Spiral arm parameters

Pattern speed Some studies point out that the spiral arms of the Milky Way approximately rotate with a pattern speed $\Omega_{\text{sp}} = 25 \pm 1 \text{ km s}^{-1} \text{ kpc}^{-1}$ [e.g. Dias & Lépine, 2005], while others argue that the value is $\Omega_{\text{sp}} = 20 \text{ km s}^{-1} \text{ kpc}^{-1}$ [e.g. Martos et al., 2004]. Since the pattern speed of the spiral arms is uncertain, we chose a range between 15 and 30 $\text{km s}^{-1} \text{ kpc}^{-1}$, as in Antoja et al. [2011]. In addition we assume the spiral arms rotate as rigid bodies.

Locus shape, starting point, and orientation of the spiral arms In the simulations we adopt the spiral arm model obtained from a fit to the Scutum and Perseus arms. This is the so-called ‘locus 2’ in the work of Antoja et al. [2011]. We also assume that the spiral structure starts at the edges of the bar. Hence $R_{\text{sp}} = 3.12 \text{ kpc}$. With this configuration the angle between the line connecting the starting point of the spiral arms and the Galactic centre-Sun line is 20° (see Fig. 3.1).

Number of spiral arms Drimmel [2000] used K-band photometry of the Galactic plane to conclude that the Milky Way contains two spiral arms. On the other hand, Vallée [2002] reviewed a number of studies about the spiral structure of the Galaxy — mostly based on young stars, gas and dust — and he concluded that the best overall fit is provided by a four-armed spiral pattern. Given this discrepancy, we carry out simulations with $m = 2$ or $m = 4$ spiral arms.

Amplitude and strength of the spiral arms We used the amplitude of the spiral arms from the Locus 2 model in Antoja et al. [2011], which is between 650 and 1100 $\text{km}^2 \text{ s}^{-2} \text{ kpc}^{-1}$. The strength of the spiral arms [as defined in Sect. 5 of Antoja et al., 2011] corresponding to this range of amplitudes is between 0.029 and 0.05. We however explored the motion of the Sun for amplitudes of up to 1300 $\text{km}^2 \text{ s}^{-2} \text{ kpc}^{-1}$ ($\epsilon \sim 0.06$) in a two-armed spiral structure.

Other parameters We also use the value of the locus 2 model of Antoja et al. [2011] for the pitch angle (i) and scale length (R_Σ) of the spiral perturbation. These values are listed in table 3.1.

Transient spiral structure Several theoretical studies support the idea that spiral arms in galaxies are transient structures [Sellwood & Binney, 2002; Sellwood, 2011]. Nevertheless, Fujii et al. [2011] found that spiral arms in pure stellar disks can survive for more than 10 Gyr when a sufficiently large number of particles ($\sim 10^7$) is used in the simulations. In this work we use only static spiral structure.

Multiple spiral patterns Lépine et al. [2011b] have argued that the corotation radius of the spiral arms is located at solar radius, i.e. at $R = 8.4$ kpc; however based on the orbits of the Hyades and coma Berenices moving groups, Quillen & Minchev [2005] concluded that the 4:1 inner Lindblad resonance of the spiral arms is located at the solar position, placing the corotation resonance at around 12 kpc. To reconcile the uncertainty in the location of the coronation resonance of the spiral structure, Lépine et al. [2011a] suggested the existence of multiple spiral arms with different pattern speeds in the Galaxy. while the main grand-design spiral pattern has its corotation at 8.4 kpc, an outer $m = 2$ pattern would have its corotation resonance at about 12 kpc, with the 4:1 inner Lindblad resonance at the position of the Sun. These multiple spiral patterns have been observed in N-body simulations [See e.g. Quillen et al., 2011].

In this work we also consider a superposition of spiral patterns as suggested by Lépine et al. [2011a] to study the motion of the Sun in the Galaxy.

3.3. The Amuse framework

AMUSE, the Astrophysical MUltipurpose Software Environment [Portegies Zwart et al., 2013], is a framework implemented in *Python* in which different astrophysical simulation codes can be coupled to evolve complex systems involving different physical processes. For example, one can couple an N -body code with a stellar evolution code to create an open cluster simulation in which

3.3 THE AMUSE FRAMEWORK

both gravitational interactions and the evolution of the stars are included. Currently AMUSE provides interfaces to codes for gravitational dynamics, stellar evolution, hydrodynamics and radiative transfer.

AMUSE is used by writing *Python* scripts to access all the numerical codes and their capabilities. Every code incorporated in AMUSE can be used through a standard interface which is defined depending on the domain of the code. For instance, a gravitational dynamics interface defines how a system of particles moves with time and in this case, the user can add or remove particles and update their properties. We created an interface in AMUSE for the Galactic model described in Sect. 3.2. For details about how to use AMUSE we refer the reader to Portegies Zwart et al. [2013] and Pelupessy et al. [2013]. More information can be also found at <http://amusecode.org>.

The computation of the stellar motion due to an external gravitational field can be done in AMUSE through the BRIDGE [Fujii et al., 2007] interface. This code uses a second-order Leapfrog method to compute the velocity of the stars due to the gravitational field of the Galaxy. All these computations are performed in an inertial frame. Given that the potentials of the bar and spiral arms are defined to be time independent in a reference system that co-rotates either with the bar or with the spiral arms, we modified BRIDGE to compute the position and velocity of the Sun in one of such non-inertial frames. Moreover, since the time symmetry of the second-order Leapfrog is no longer valid in a rotating frame we need to use a higher order scheme. These modifications resulted in a new interface called *Rotating Bridge*. This code can also be used to perform self-consistent N -body simulations of stellar clusters that also respond to the gravitational non-static force from their parent galaxies. In these simulations the internal cluster effects like self gravity and stellar evolution can be taken into account. In chapter 2 of this thesis we derived the equations of motion for the *Rotating Bridge* for a single particle and its generalization to a system of self-interacting particles. We also show the accuracy of this code under different Galactic potentials (see e.g. Fig. 2.5).

3.4. Back-tracing the Sun's orbit

Contrary to the epicyclic trajectories that stars follow when they move under the action of an axisymmetric potential, the orbits of stars become more complicated when the gravitational fluctuations generated by the central bar and spiral arms are taken into account, specially where chaos might be important. In chaotic regions, small deviations in the initial position and/or velocity of stars produce significant variations in their final location. Hence, in order to determine the birth place of one star, it is necessary to use a precise numerical code able to resolve the substantial and sudden changes in acceleration that such star experiments. Additionally, it is necessary to compute its orbit backwards in time by using a sampling of positions and velocities around the star's current (uncertain) location in phase-space. With this last procedure we get statistical information about the region in the Galaxy where the star might have been born. We follow this methodology to find the most probable birth radius and velocity of the Sun to infer whether or not it has radially migrated during its lifetime. To ensure numerical accuracy in the orbit integration we used a 6th order Leapfrog in the *Rotating Bridge* with a time step of 0.5 Myr. This choice leads to a fractional energy error of the order of 10^{-10} .

As a first step we generate 5000 random positions and velocities which are within the measurement uncertainties from the current Galactocentric position and velocity of the Sun ($\mathbf{r}_\odot, \mathbf{v}_\odot$). This selection was made from a 4D normal distribution centred at ($\mathbf{r}_\odot, \mathbf{v}_\odot$) with standard deviations (σ) corresponding to the measured errors in these coordinates. We assume that the Sun is currently located at: $\mathbf{r}_\odot = (-R_\odot, 0)$ kpc; where the distance of the Sun to the Galactic centre is $R_\odot \pm \sigma_R = 8.5 \pm 0.5$ kpc. The uncertainty in y_\odot is set to zero as the Sun is by definition located on the x -axis of the Galactic reference frame.

Since we consider the motion of the Sun only on the Galactic plane, the velocity of the Sun is: $\mathbf{v}_\odot = (U_\odot, V_\odot)$, where:

$$\begin{aligned} U_\odot \pm \sigma_U &= 11.1 \pm 1.2 \text{ km s}^{-1} \\ V_\odot \pm \sigma_V &= (12.4 + V_{\text{LSR}}) \pm 2.1 \text{ km s}^{-1}. \end{aligned} \tag{3.5}$$

The vector $(11.1 \pm 1.2, 12.4 \pm 2.1)$ km s^{-1} is the peculiar motion of the Sun [Schönrich et al., 2010] and V_{LSR} is the velocity of the local standard of rest

3.4 BACK-TRACING THE SUN'S ORBIT

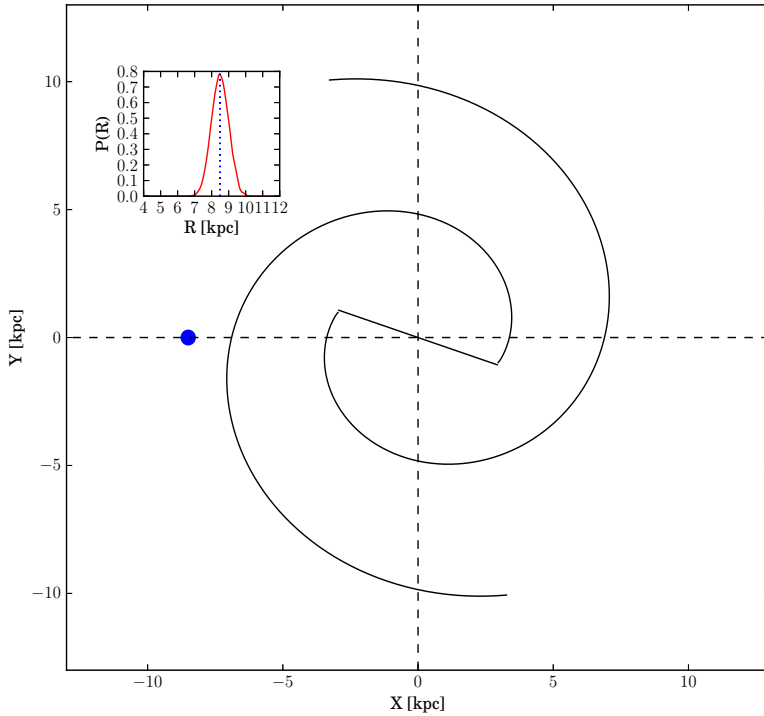


FIGURE 3.1: Configuration of the Galactic potential at the beginning of the backwards integration in time. The spiral arms are assumed to start at the ends of the major axis of the bar. The blue circle is the current position of the Sun, $r_{\odot} = (-8.5, 0)$ kpc. The angle the Sun-Galactic centre line makes with respect to the semi-major axis of the bar is 20° . The inset shows the distribution of 5000 Galactocentric distances that were selected from a 3D Gaussian centred at the current phase-space coordinates of the Sun.

which depends on the Galactic parameters that are listed in table 3.1. We use the conventional Galactocentric Cartesian coordinate system. This means that translated to a Sun-centred reference frame the x -axis points toward the Galactic centre, the y -axis in the direction of Galactic rotation, and the z -axis completes the right-handed coordinate system.

Recently Bovy et al. [2012a] found an offset between the rotational velocity of the Sun and V_{LSR} of $26 \pm 3 \text{ km s}^{-1}$, which is larger than the value measured by Schönrich et al. [2010]. We also use this value to trace back the Sun's orbit.

In Fig. 3.1 we show the configuration of the Galactic potential at the beginning of the backwards integration in time. Since it is unknown how spiral arms are oriented with respect to the bar at the centre of the Galaxy, we assume that they start at the edges of the bar. The blue circle in this Figure represents the current location of the Sun. The line from the Sun to the Galactic centre makes an angle of 20° with the semi-major axis of the bar. In the small plot located at the left top of Fig. 3.1 we show the distribution of the 5000 positions in cylindrical radius R .

Each of the 5000 positions and velocities that were generated from the 4D normal distribution are used to construct a set of present-day phase space vectors with (cylindrical) coordinates: $(R_p, \varphi_p, v_{R_p}, v_{\varphi_p})_k$; $k = 1, \dots, 5000$ (Note that φ_p is fixed at π). The Sun is then located at each of these vectors and its orbit is computed backwards in time until 4.6 Gyr have elapsed. Before starting the integration we reversed the velocity components of the Sun as well as the direction of rotation of the bar and spiral arms².

After integrating the orbit of the Sun backwards in time we obtain a sample of birth phase-space coordinates $(R_b, \varphi_b, v_{R_b}, v_{\varphi_b})_k$; $k = 1, \dots, 5000$. The distributions of present day and birth phase space coordinates then allow us to study the past motion of the Sun and infer whether or not it has migrated during its lifetime.

To take the uncertainties on the Galactic model into account we also varied the bar and spiral arm parameters according to the values listed in table 3.1. For a subset of the Galactic model parameters we verified that 5000 birth phase-space coordinates are a representative number for sampling the position

²The convention used in the *Rotating Bridge* is right-handed; hence, for the backward integration in time the pattern speed of the bar and spiral arms are positive.

and velocity of the Sun 4.6 Gyr ago. By means of the Kolmogorov-Smirnoff test, we found that the distribution of positions and velocities of the Sun after integrating its orbit backwards in time, is the same when $k = 5000$, 10 000 or 20 000. Depending on the Galactic parameters, the p -value from the test is between 0.2 and 0.98.

3.5. Results

For every choice of bar and spiral arm parameters we have the distribution of the present day phase space coordinates of the Sun $p(\mathbf{r}_p, \mathbf{v}_p)$ and of the Sun's phase space coordinates at birth $p(\mathbf{r}_b, \mathbf{v}_b)$. The amount of radial migration experienced by the Sun during its motion through the Galaxy can be obtained from the probability distribution $p(R_p - R_b)$ (referred to below as the 'migration distribution') of the difference in the radial distance between the present day and birth locations of the Sun. We use the median of the distribution to decide whether or not the Sun has migrated a considerable distance during its lifetime:

1. Median $p(R_p - R_b) > d_m$: the Sun migrated from inner regions of the Galactic disk to R_\odot (migration from inside-out).
2. Median $-d_m \leq p(R_p - R_b) \leq d_m$: the Sun has not migrated
3. Median $p(R_p - R_b) < -d_m$: the Sun migrated from outer regions of the Galactic disk to R_\odot (migration from outside-in).

The parameter d_m indicates when the value of $R_p - R_b$ is considered to indicate a significant migration of the Sun within the Galaxy. We derive the value of d_m by considering the distribution $p(R_p - R_b)$ for the case of a purely axisymmetric Galaxy, in which case for the Sun's orbital parameters the migration should be limited. The migration distribution for this case is shown in Fig. 3.2. From this distribution it can be seen that for the axisymmetric case indeed the Sun migrates only little on average (~ 0.6 kpc) and that the maximum migration distance is about 1.7 kpc (note that $p(R_p - R_b) = 0$ for $R_p - R_b \lesssim -1.7$ kpc). Based on this result we use $d_m = 1.7$ kpc in the discussions of the results below. Considering changes in the Sun's radial distance

CHAPTER 3 : RADIAL MIGRATION OF THE SUN IN THE MILKY WAY: A STATISTICAL STUDY

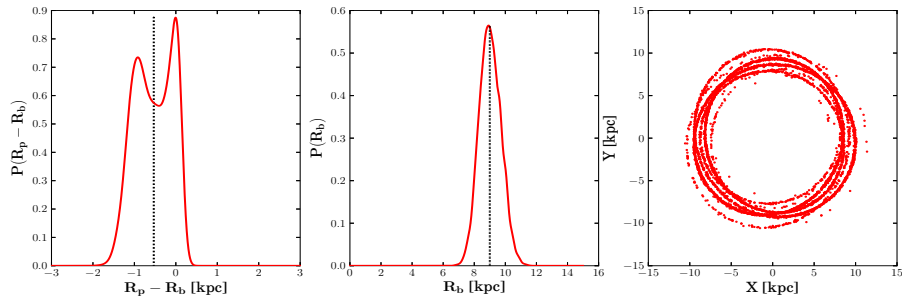


FIGURE 3.2: Results of the back-tracing of the Sun’s orbit in a purely axisymmetric Milky Way potential. *Left*: the migration distribution $p(R_p - R_b)$. *Middle*: distribution of the birth radius of the Sun $p(R_b)$. *Right*: the distribution of birth locations of the Sun on the xy -plane. The dotted black line in the top two panels represents the median of distributions. Note that this is negative for $p(R_p - R_b)$, which means that the migration of the Sun is from outer regions of the galaxy to R_\odot . The distribution of birth positions of the Sun seen on the xy plane suggest that it is not possible to determine the exact formation place of the Sun 4.6 Gyr ago.

larger than 1.7 kpc as significant migration is consistent with the estimates of the Sun’s migration made by Wielen et al. [1996] and Minchev et al. [2013].

The value of the median of $p(R_p - R_b)$ is not enough to characterize this probability distribution which is often multi-modal (see left panel of Fig. 3.2) and we thus introduce the following quantities:

$$\begin{aligned}
 P_{i-o} &= \int_{d_m}^{\infty} p(R_p - R_b) d(R_p - R_b) \\
 P_{o-i} &= \int_{-\infty}^{-d_m} p(R_p - R_b) d(R_p - R_b)
 \end{aligned}
 \tag{3.6}$$

where P_{i-o} is the probability that the Sun has experienced considerable migration from the inner regions of the Galactic disk to its present day position, while P_{o-i} is the probability that the Sun has significantly migrated in the other direction. One of the aims of our study is to find Milky Way potentials for which the above probabilities are substantial, thus indicating that the Sun has likely migrated a considerable distance over its lifetime.

We also characterize the width of the distribution $p(R_p - R_b)$ through the so-called Robust Scatter Estimate (RSE) [Lindgren et al., 2012] which is defined as $RSE = 0.390152 \times (P90 - P10)$, where $P10$ and $P90$ are the 10th and 90th

percentiles of the distribution, and the numerical constant is chosen to make the RSE equal to the standard deviation for a Gaussian distribution

The orbit integrations were carried out by using the peculiar velocity of the Sun inferred by Schönrich et al. [2010], unless otherwise stated.

3.5.1. Radial migration of the Sun as a function of bar parameters

In order to study the radial migration of the Sun under the variation of mass and pattern speed of the bar, we fixed the amplitude, pattern speed and number of spiral arms such that they have little effect on the Sun's orbit. We chose the values: $A = 650 \text{ km}^2 \text{ s}^{-2} \text{ kpc}^{-1}$, $\Omega_{\text{sp}} = 20 \text{ km s}^{-1} \text{ kpc}^{-1}$, and $m = 2$. With these values of amplitude and pattern speed we produce spiral arms with a strength at the lowest limit ($\epsilon = 0.029$) and resonances located in extreme regions of the Galactic disk. The 2:1 inner/outer Lindblad resonance of the spiral arms (ILR_{sp} , OLR_{sp}) and the co-rotation resonance (CR_{sp}), are located at 1.4 kpc, 16 kpc and 10.9 kpc respectively.

In Fig. 3.3 we show the median, RSE, $P_{\text{i-o}}$, and $P_{\text{o-i}}$ of the distribution $p(R_{\text{p}} - R_{\text{b}})$ as a function of the mass and pattern speed of the bar. The mass of the bar was varied in steps of $0.02 M_{\odot}$ and the pattern speed in steps of $0.5 \text{ km s}^{-1} \text{ kpc}^{-1}$. The maximum and minimum values of M_{bar} and Ω_{bar} were set according to the ranges listed in table 3.1. Fig. 3.3 also shows the position of the 2:1 outer Lindblad resonance of the bar (OLR_{bar}).

Note that the median of the distribution $p(R_{\text{p}} - R_{\text{b}})$ is always negative. This indicates that the migration of the Sun in this case on average is from outer regions of the Galactic disk to R_{\odot} . The median of $p(R_{\text{p}} - R_{\text{b}})$ is also always lower than 1.08 kpc, independently of the mass and pattern speed of the bar.

On the other hand from the bottom panel of Fig. 3.3 it is clear that regardless of the mass and pattern speed of the bar, it is unlikely that the Sun has migrated considerably from the inner or outer regions of the Galactic disk to R_{\odot} . The low probability of significant radial migration can also be seen in the width of the migration distribution which is always below 0.92 kpc (top right panel Fig. 3.3).

CHAPTER 3 : RADIAL MIGRATION OF THE SUN IN THE MILKY WAY: A STATISTICAL STUDY

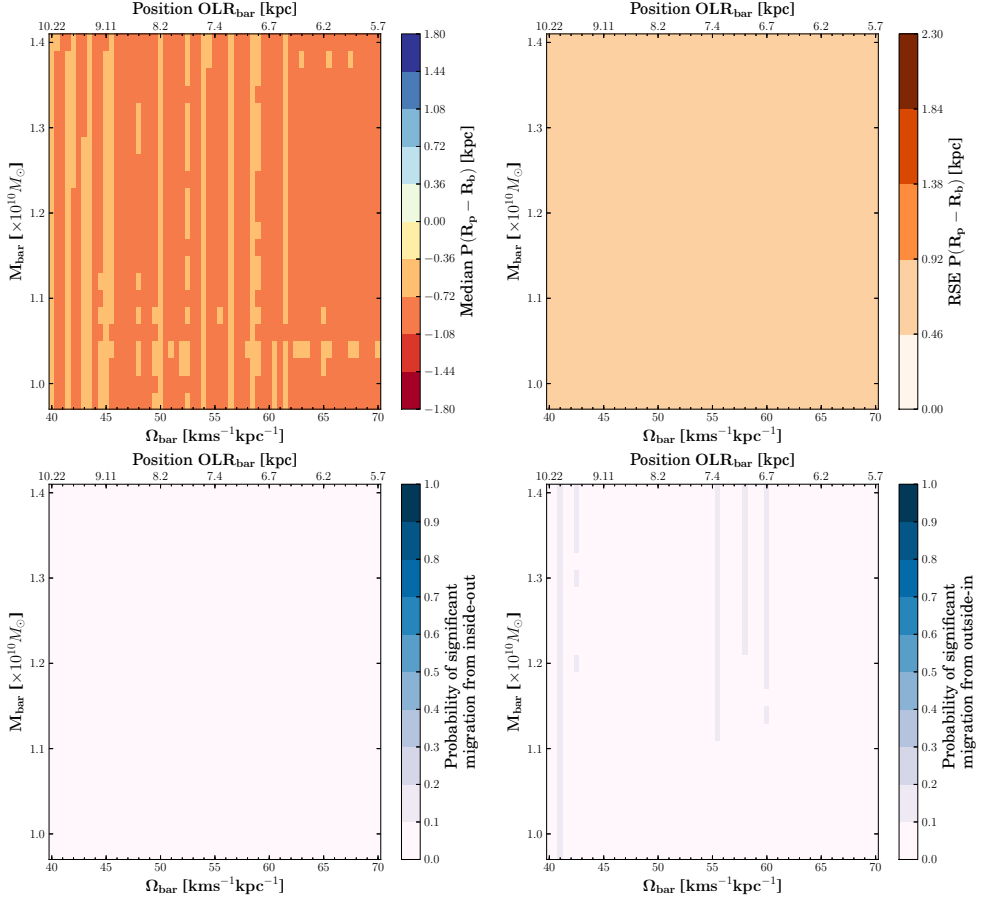


FIGURE 3.3: *Top*: Median and RSE of the migration distribution $p(R_p - R_b)$ as a function of the mass and pattern speed of the bar. Negative values in the median indicate migration from outer regions of the Galactic disk to R_{\odot} , while positive values indicate migration from inner parts to R_{\odot} . The position of the bar's outer Lindblad resonance, OLR_{bar} , with respect to the Galactic centre is also shown. For this set of simulations the position of CR_{sp} is fixed at 10.9 kpc. *Bottom*: $P_{i \rightarrow o}$ and $P_{o \rightarrow i}$ as a function of the mass and pattern speed of the bar.

3.5 RESULTS

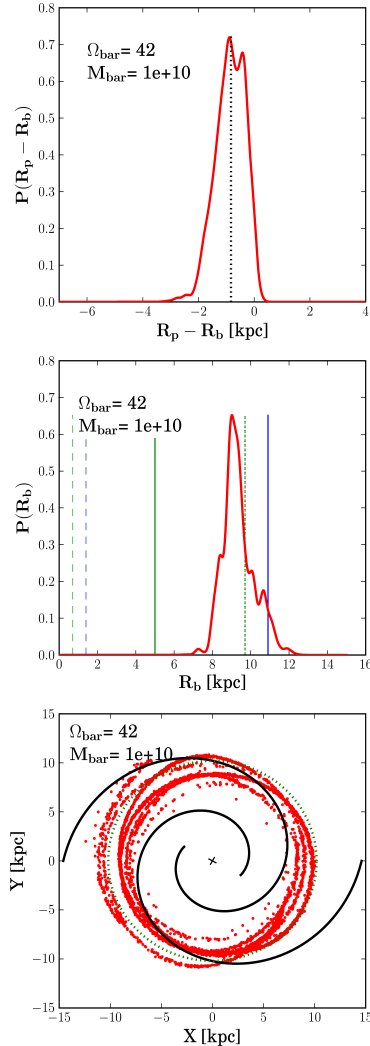


FIGURE 3.4: *Top:* Distribution function $p(R_p - R_b)$ for the Galaxy model with weak spiral arms and a central bar. The vertical dotted black line is the median of the distribution. *Middle:* Radial distribution of the birth radius of the Sun $p(R_b)$ for the same Galactic parameters. The vertical green lines represent the location of the resonances produced by the bar while the blue lines, represent the location of the resonances due to the spiral arms. The dashed, solid and dotted lines represent the 2:1 inner Lindblad (ILR), co-rotation (CR) and 2:1 outer Lindblad (OLR) resonances respectively. Hereafter, we will use this same convention. *Bottom:* Distribution of birth positions of the Sun seen on the xy plane. The OLR_{bar} is shown as the circular dotted green line. We also show the configuration of the spiral arm potential 4.6 Gyr ago.

We conclude that the presence of the central bar of the Milky Way does not produce considerable radial migration of the Sun. This result is not surprising, because although the OLR_{bar} has played an important role in shaping the stellar velocity distribution function in the solar neighbourhood [Dehnen, 2000; Minchev et al., 2010], the gravitational force produced by the bar falls steeply with radius, reaching about 1% of its total value at R_{\odot} [Dehnen, 2000]. Klačka et al. [2012] studied the motion of the Sun in an analytical model of the Galaxy that considers a multipolar expansion of the bar potential. By assuming the current location of the Sun as $\mathbf{r}_{\odot} = (-8, 0, 0)$ kpc and $\mathbf{v}_{\odot} = (0, 220, 0)$ km s⁻¹, they found that the central bar of the Galaxy does not generate considerable radial migration of the Sun if spiral arms are not considered, changing the Galactocentric distance of the Sun only 1% from its current value R_{\odot} . We find more than 1% change in radius because we take into account the potential of the spiral arms in the Galactic model.

Figure 3.4 shows the distributions $p(R_p - R_b)$ and $p(R_b)$ for a choice of bar parameters. In this specific case the median of $p(R_p - R_b)$ is -0.83 kpc, which means that the birth radius of the Sun is around 9.3 kpc. From the distribution of Sun's possible birth positions on the xy plane (bottom panel Fig. 3.4) it is clear that even for this smooth and static potential only the birth radius of the Sun can be constrained. The uncertainty in φ for the Sun's birth location is caused by the uncertainty in the present day phase space coordinates of the Sun.

In this Section we have simulated the radial migration of the Sun as a function of mass and pattern speed of the bar. We find no significant migration. In the next Section we study the motion of the Sun when the parameters of the spiral arms are varied.

3.5.2. Radial migration of the Sun as a function of spiral arm parameters

In this Section we study the effects of the spiral structure on the radial migration of the Sun and thus keep fixed the mass and pattern speed of the bar. We chose the lowest limit for the bar mass $M_{\text{bar}} = 9.8 \times 10^9 M_{\odot}$. The pattern speed of the bar was set to be $\Omega_{\text{bar}} = 40$ km s⁻¹ kpc⁻¹. With this

3.5 RESULTS

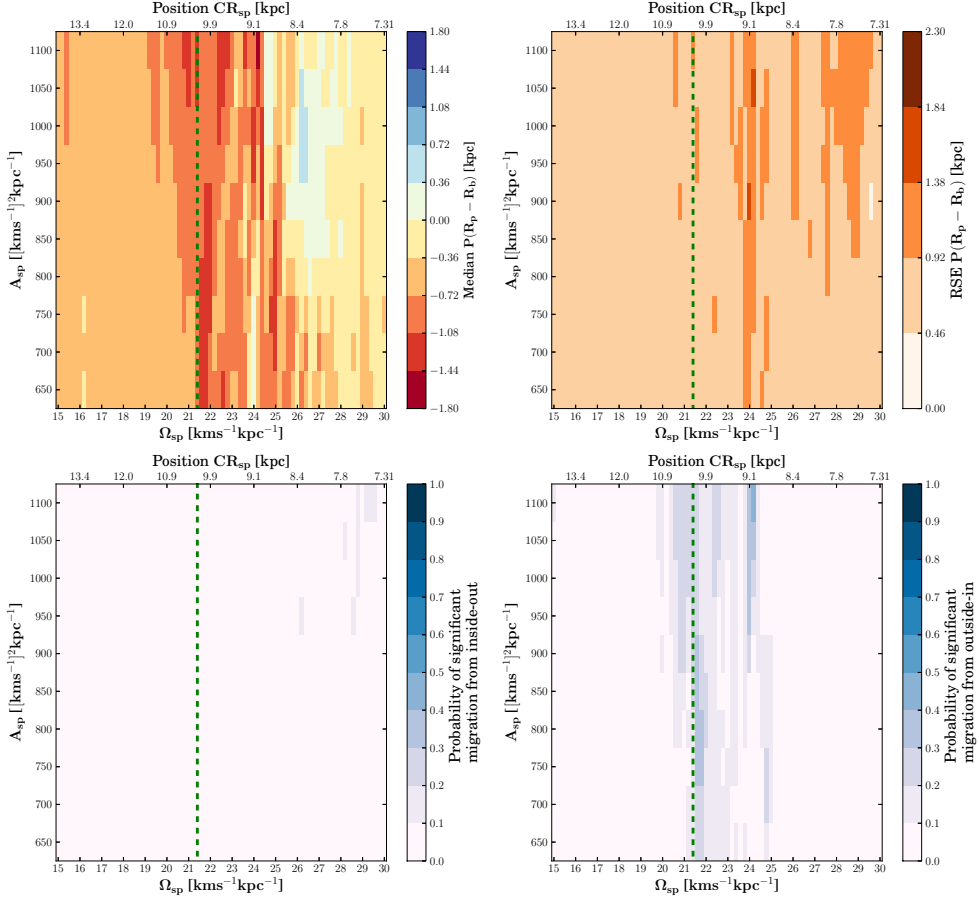


FIGURE 3.5: *Top*: Median and RSE of the distribution $p(R_p - R_b)$ as a function of the amplitude and pattern speed of a two-armed spiral structure. The location of the CR_{sp} with respect to the Galactic centre is also shown. For this set of simulations, the position of the outer Lindblad resonance of the bar, OLR_{bar} is fixed at 10.2 kpc and it is shown as the vertical dotted green line. *Bottom*: P_{i-o} and P_{o-i} also as a function of the amplitude and pattern speed of two spiral arms.

value, the resonances of the bar are located at extreme regions in the Galactic disk, in particular OLR_{bar} which is at 10.2 kpc. In Sect. 3.5.2 and 3.5.2, we explore the effects of the amplitude, CR_{sp} location and number of spiral arms on the radial migration of the Sun.

Effect of two spiral arms

In Fig. 3.5 we show the characteristics of the migration distribution as a function of the amplitude and pattern speed of two spiral arms. We varied the amplitude in steps of $50 \text{ km}^2 \text{ s}^{-2} \text{ kpc}^{-1}$ and the pattern speed in steps of $0.2 \text{ km s}^{-1} \text{ kpc}^{-1}$. Note that for most of the spiral arm parameters the median of $p(R_p - R_b)$ is negative, suggesting that the migration of the Sun has been mainly from outer regions of the Galactic disk to R_\odot . If the CR_{sp} is located between 9.0 and 10.6 kpc with respect to the Galactic centre, the median of $p(R_p - R_b)$ remains between -1.08 and -1.44 kpc for most of the values of A_{sp} . The median of $p(R_p - R_b)$ can reach values of up to -1.80 kpc if $A_{\text{sp}} = 1100 \text{ km}^2 \text{ s}^{-2} \text{ kpc}^{-1}$ and $\Omega_{\text{sp}} = 24.2 \text{ km s}^{-1} \text{ kpc}^{-1}$ (CR_{sp} at 9 kpc). For this latter case, there is a probability between 40% and 50% that the Sun has migrated considerably from outer regions of the Galactic disk to its current position (cf. Fig. 3.5, bottom right panel).

We also studied the radial migration of the Sun for amplitudes higher than $1100 \text{ km}^2 \text{ s}^{-2} \text{ kpc}^{-1}$, up to $1300 \text{ km}^2 \text{ s}^{-2} \text{ kpc}^{-1}$. We found that the migration of the Sun on average is from outer regions of the Galactic disk to R_\odot . The Sun only migrates considerably when $1200 \leq A_{\text{sp}} \leq 1300 \text{ km}^2 \text{ s}^{-2} \text{ kpc}^{-1}$ and $\Omega_{\text{sp}} = [21.4, 21.8] \text{ km s}^{-1} \text{ kpc}^{-1}$ (i.e. $\text{CR}_{\text{sp}} \sim 10.2 \text{ kpc}$). According to the former results and given that the OLR_{bar} is located at 10.2 kpc, the significant radial migration of the Sun occurs when the distance between CR_{sp} and OLR_{bar} is in the range $[0, 1] \text{ kpc}$. An illustration of the migration distribution $p(R_p - R_b)$ for these higher amplitudes is shown at the first and second rows of figure 3.6.

On the other hand, according to the bottom left panel of Fig. 3.5 we find that it is unlikely that the Sun has migrated from inner regions of the Galactic disk to R_\odot .

Other studies have also evaluated the effect of the spiral arms of the Milky Way on the motion of the Sun. Klačka et al. [2012] found that under the simultaneous effect of the central bar and spiral arms, the Sun could experience

3.5 RESULTS

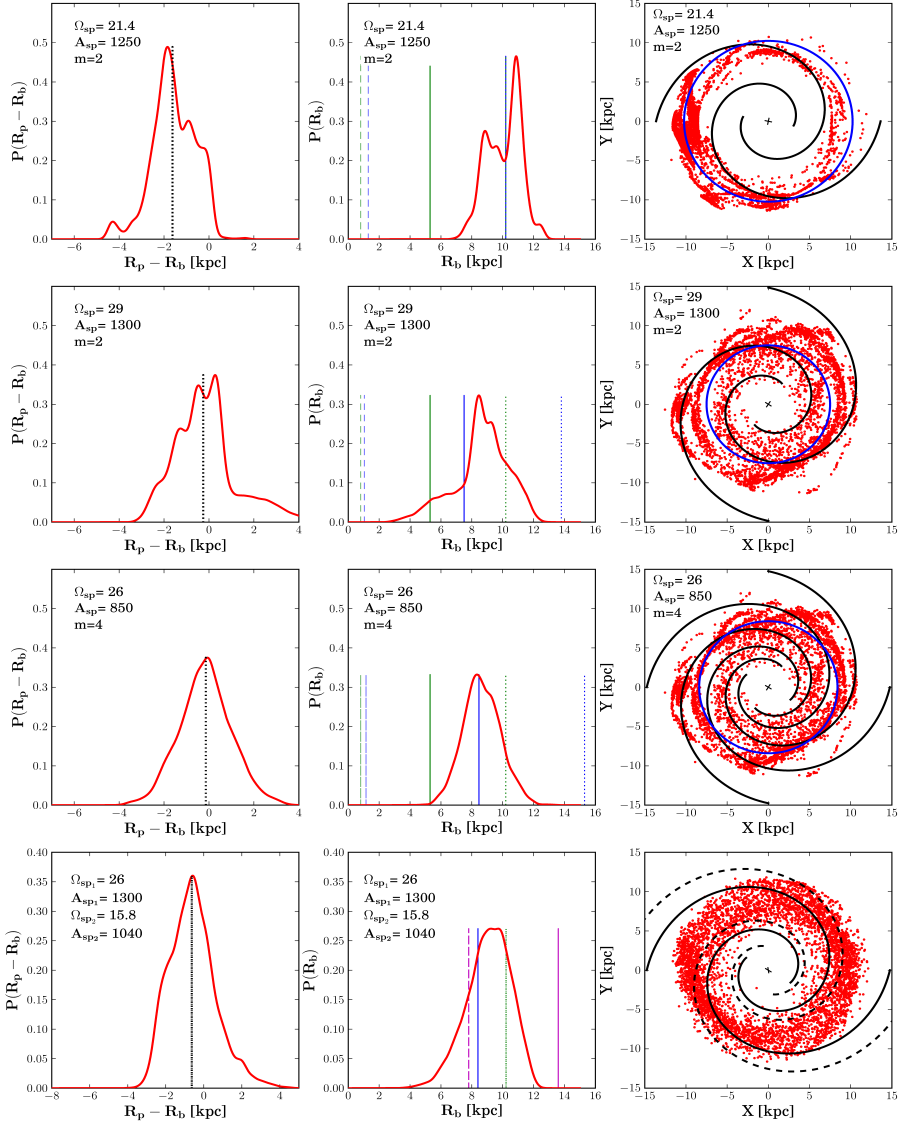


FIGURE 3.6: *Left:* Migration distribution $p(R_p - R_b)$. *Middle:* distribution of possible Sun's birth radii $P(R_b)$. *Right:* Projection on the xy plane of the possible birth radii of the Sun. In the first and second rows the Galactic potential has two spiral arms. In the third row, the Galactic potential has four spiral arms. In the bottom panel, we use a superposition of two spiral arms with different pattern speeds. The vertical dotted black lines in the left panel as well as the blue and green lines in the middle, have the same meaning as in Fig. 3.4. The dashed and solid magenta lines at the bottom panel, correspond to the ILR_{sp} and CR_{sp} of the secondary spiral structure in the composite model. The blue circles on the right panel are the position of the CR_{sp} .

considerable radial migration when it co-rotates with spiral arms that have a strength $\epsilon = 0.06$. In our simulations this strength corresponds to an amplitude $A_{\text{sp}} = 1300 \text{ km}^2 \text{ s}^{-2} \text{ kpc}^{-1}$. According to our simulations the Sun experiences considerable radial migration when $A_{\text{sp}} = 1300 \text{ km}^2 \text{ s}^{-2} \text{ kpc}^{-1}$ and $\Omega_{\text{sp}} = [21.4, 21.8] \text{ km s}^{-1} \text{ kpc}^{-1}$; therefore significant radial migration is found when $\Omega_{\text{sp}} = 1.2\Omega_{\odot}$.

By comparing Fig. 3.5 and 3.3 we can see that a 2-armed spiral pattern tends to produce more radial migration on the Sun than the central bar of the Milky way. Sellwood & Binney [2002], and more recently Minchev & Famaey [2010], found that the larger changes in angular momentum of stars always occur near the co-rotation resonance, the effect of the outer/inner Lindblad resonances being smaller. Given that in our simulations the motion of the Sun is influenced by the CR_{sp} and by the OLR_{bar} , it is expected that the spiral arms produce a stronger effect on the Sun's radial migration than the central bar of the Galaxy.

At the top panel of Fig. 3.6 we show the distributions $p(R_{\text{p}} - R_{\text{b}})$ and $p(R_{\text{b}})$ for an example of a two-arm spiral arm potential that leads to considerable radial migration of the Sun. In this case the distance between the CR_{sp} and OLR_{bar} is 0.03 kpc. For this specific set of bar and spiral arm parameters the Sun could have migrated a distance of 1.8 kpc from the outer regions of the Galactic disk to its current position. Its birth radius would then be around 11 kpc, as also indicated by the distribution $p(R_{\text{b}})$. The projection of the Sun's birth locations in the xy plane shows lots of structure, but again only the birth radius can be constrained.

In the second row of Fig. 3.6 we show the distributions $p(R_{\text{p}} - R_{\text{b}})$ and $p(R_{\text{b}})$ for a set of spiral arm parameters that produce high dispersion in the migration distribution $p(R_{\text{p}} - R_{\text{b}})$. In this case the Sun does not migrate on average (Median $p(R_{\text{p}} - R_{\text{b}}) \sim 0$). Additionally, as can be observed in the plot of the right, there is a fraction of possible birth radii at the inner regions of the Galactic disk; however, the probability of significant migration from inside-out in this case is only of 10%.

3.5 RESULTS

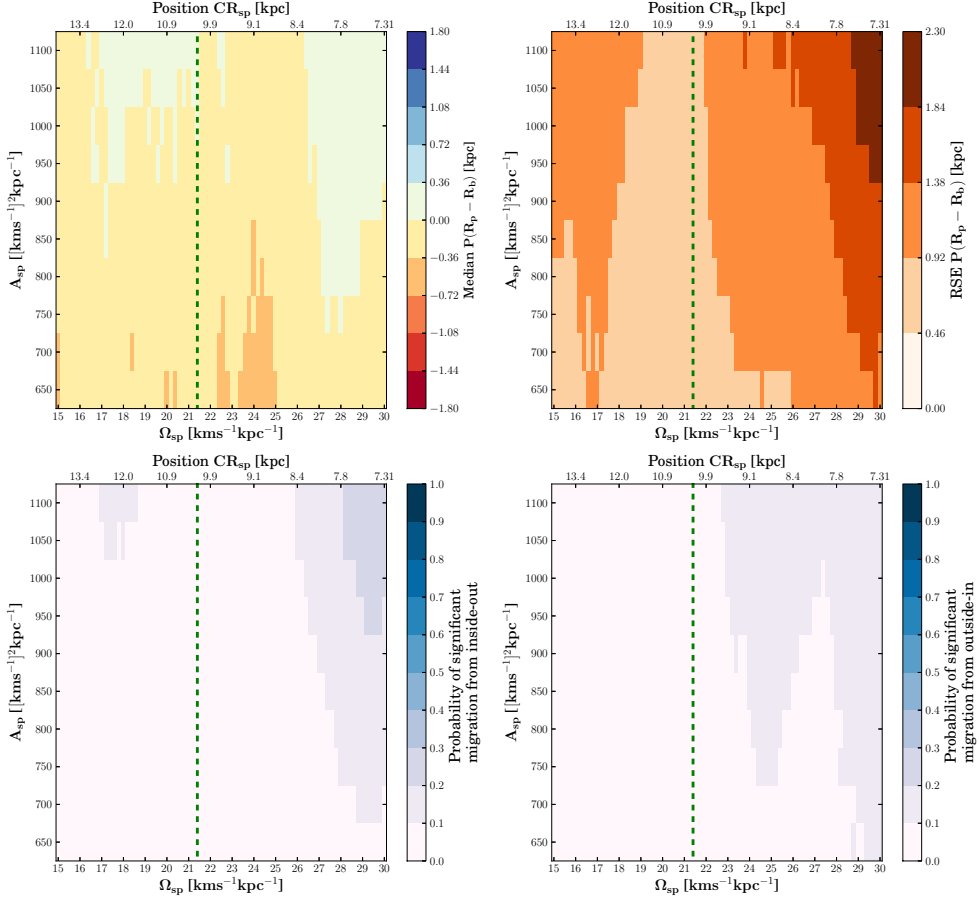


FIGURE 3.7: *Top*: Median and RSE of the distribution $p(R_p - R_b)$ as a function of the amplitude and pattern speed of a four-armed spiral structure. The location of the CR_{sp} with respect to the Galactic centre is also shown. For this set of simulations, the position of the OLR_{bar} is fixed at 10.2 kpc and it is shown as the vertical dotted green line. *Bottom*: P_{i-o} and P_{o-i} also as a function of the amplitude and pattern speed of four spiral arms.

Effect of four spiral arms

We also assess the radial migration of the Sun under the action of a Galactic potential composed of four spiral arms. The results are shown in Fig. 3.7. Note that when Ω_{sp} is between 19 and 22 $\text{km s}^{-1} \text{kpc}^{-1}$ the radial migration experienced by the Sun is less than 1 kpc. Additionally, when CR_{sp} is located between 7.3 and 8.4 kpc the median of $p(R_{\text{p}} - R_{\text{b}})$ is between -0.36 and 0.36 kpc (around zero). However the large width of the distribution leads to probabilities of up to 30% that the Sun has migrated from inner regions of the Galactic disk to its current position. The probability of significant migration in the other direction is up to 20%.

The larger width of $p(R_{\text{p}} - R_{\text{b}})$ may be due to the effect of higher order resonances (4:1 $\text{ILR}_{\text{sp}}/\text{OLR}_{\text{sp}}$) on the motion of the Sun. The fact that the width of $p(R_{\text{p}} - R_{\text{b}})$ is large for specific four-armed Galactic potentials, means that the migration of the Sun is very sensitive to its birth phase-space coordinates. This effect can be also observed in the third row of Fig. 3.6, which shows $p(R_{\text{p}} - R_{\text{b}})$ and $p(R_{\text{b}})$ when the Galactic potential has four spiral arms. In addition, the projection of the possible birth locations on the xy plane shows virtually no structure.

By comparing Figs. 3.5 and 3.7, we can see that unlike the case when the Galactic potential has two spiral arms, the median of $p(R_{\text{p}} - R_{\text{b}})$ when $m = 4$ is not much affected by small separation distances between the CR_{sp} and OLR_{bar} .

Effects of multiple spiral patterns

In addition to evaluating the motion of the Sun in a pure 2-armed or 4-armed spiral structure, we use a superposition of two spiral arms (2 + 2) with different pattern speeds, such as discussed by Lépine et al. [2011a]. We use the same values as Mishurov & Acharova [2011] to set the pitch angles of the multiple spiral patterns in the Milky Way. The parameters of the main spiral structure used in the simulations are: $A_{\text{sp}_1} = 650, 1300 \text{ km}^2 \text{ s}^{-2} \text{ kpc}^{-1}$; $i_1 = -7^\circ$ and $\Omega_{\text{sp}_1} = 26 \text{ km s}^{-1} \text{ kpc}^{-1}$. This pattern speed places the CR_{sp} of the main spiral structure at solar radius. The orientation of the main spiral pattern at the beginning of the simulations is 20° .

The parameters used to model the secondary spiral structure are: $A_{\text{sp}_2} =$

$0.8A_{\text{sp}_1}$; $i_2 = -14^\circ$ and $\Omega_{\text{sp}_2} = 15.8 \text{ km s}^{-1} \text{ kpc}^{-1}$. This pattern speed places the CR_{sp} of the secondary spiral structure at 13.6 kpc and the 4:1 ILR_{sp} at 7.8 kpc. The orientation of the secondary spiral arms with respect to the main structure at the beginning of the simulations is -200° . In addition, we fixed the mass and pattern speed of the bar to $M_{\text{bar}} = 9.8 \times 10^9 M_\odot$ and $\Omega_{\text{bar}} = 40 \text{ km s}^{-1} \text{ kpc}^{-1}$ respectively.

At the bottom panel of Fig. 3.6 we show the distributions $p(R_p - R_b)$ and $P(R_b)$ when the Galactic potential has multiple spiral patterns. In this simulation the amplitude of the main spiral structure is $A_{\text{sp}_1} = 1300 \text{ km}^2 \text{ s}^{-2} \text{ kpc}^{-1}$. We used the tangential velocity of the Sun from Bovy et al. [2012a]. As can be seen, the median of the distribution $p(R_p - R_b)$ is smaller than 1 kpc, meaning that the migration of the Sun on average is not significant. The birth radius of the Sun is therefore at 8.5 kpc, as can also be seen from the distribution $P(R_b)$. The projection of birth locations of the Sun on the xy plane suggest that there is some fraction of possible birth radii located at internal regions of the Galactic disk; however, we found that the probability of considerable migration from outer or inner regions to R_\odot is between 8% and 13%. These probabilities are even smaller when $A_{\text{sp}_1} = 650 \text{ km}^2 \text{ s}^{-2} \text{ kpc}^{-1}$. We obtain the same results when assuming V_\odot from Schönrich et al. [2010].

In Sect. 3.5.2 we have shown that the Sun might have experienced considerable migration in the Galaxy if the CR_{sp} is separated from the OLR_{bar} by a distance smaller than 1.1 kpc. In the next Section we explore in more detail the effect of the bar-spiral arm resonance overlap on the motion of the Sun.

3.5.3. Radial migration of the Sun in the presence of the bar-spiral arm resonance overlap

It has been demonstrated by Minchev & Famaey [2010] and Minchev et al. [2011] that the dynamical effects of overlapping resonances from the bar and spiral arms provide an efficient mechanism for radial migration in galaxies. Depending of the strength of the perturbations, radial mixing in Galactic disks proceeds up to an order of magnitude faster than in the case of transient spiral arms. Given that the solar neighbourhood is near to the OLR_{bar} and that the Sun is located approximately at 1 kpc from CR_{sp} [Acharova et al., 2011], it is

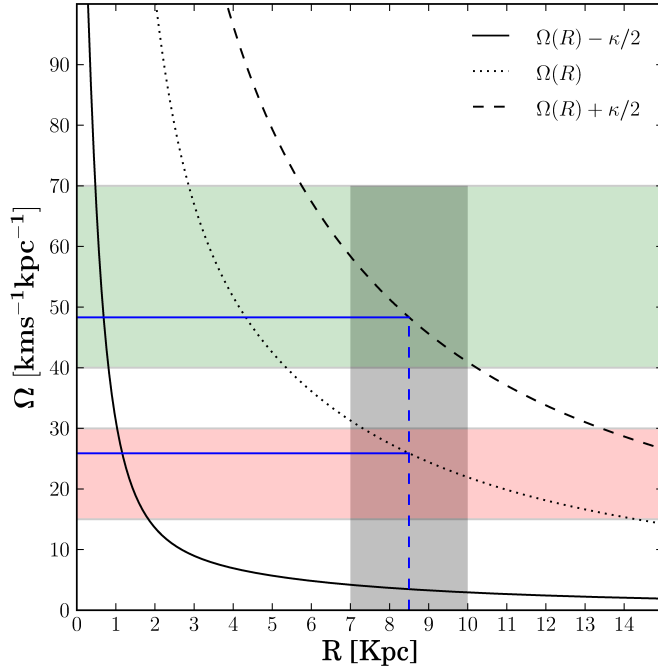


FIGURE 3.8: Resonances of second multiplicity (for $m = 2$) in galactic disks. The inner and outer Lindblad resonances (ILR, OLR) are along the solid and dashed black lines. They are given by: $\Omega(R) \pm \kappa/2$, where the minus (plus) sign corresponds to the ILR (OLR). The corotation resonance (CR) is along the dotted black line and it is given by: $CR = \Omega(R)$. The shaded green region corresponds to the pattern speed of the bar within its uncertainty. The shaded red region corresponds to the pattern speed of spiral arms within its uncertainty. Note that Ω_{bar} and Ω_{sp} only allow the overlapping between the Outer Lindblad resonance of the bar (OLR_{bar}) with the corotation of spiral arms (CR_{sp}). We refer this resonance overlap as OLR/CR overlap. The gray shaded region is the location of the OLR/CR overlap in the simulations. The blue lines show how we set Ω_{bar} and Ω_{sp} to generate the OLR/CR overlap at some desired position.

of interest to study the radial migration that the Sun might have experienced under the influence of the spiral-bar resonance overlap.

It is well known that galactic disks rotate differentially. However, the gravitational non-axisymmetric perturbations such as the central bar and spiral arms, rotate as rigid bodies. In consequence, stars at different radii will experience different forcing due to these non-axisymmetric structures [Minchev & Famaey, 2010]. There are specific locations in the Galactic disk where stars are in resonance with the perturbations. One is the corotation resonance, where stars move with the same pattern speed of the perturber, and the Lindblad resonances, where the frequency at which a star feels the the force due to the perturber coincides with its epicyclic frequency κ . Depending on the position of the star, inside or outside from the corotation radius, it can feel the Inner or Outer Lindblad resonances.

In Fig. 3.8 we show the resonances of second multiplicity (for $m = 2$) in a galactic disk. The green and red shaded regions correspond to the accepted values of the pattern speed of the bar and spiral arms of the Milky Way within the uncertainties. As can be seen, Ω_{bar} and Ω_{sp} only allow certain combinations of resonance overlaps. For the case of two spiral arms, only the overlap of the OLR_{bar} and CR_{sp} is possible³. Hereafter we refer to this resonance overlap as the OLR/CR overlap.

To explore the motion of the Sun in the presence the overlapping of resonances, we vary the pattern speed of the bar and spiral arms such that the OLR/CR overlap is located at different positions in the disk, between 7 and 10.2 kpc from the Galactic centre, as indicated by the vertical gray shaded line in Fig. 3.8. In our simulations, we varied the location of the OLR/CR overlap every 0.1 kpc. The amplitude of the spiral arms and the mass of the bar were also varied.

In Fig. 3.9 we show the median of $p(R_p - R_b)$ as a function of the position within the Galactic disk of the OLR/CR overlap. From left to right, the amplitude of spiral arms increases; from top to bottom, the mass of the bar is 9.8×10^9 and $1.3 \times 10^{10} M_{\odot}$. Note that regardless of the amplitude of the spiral arms or the mass of the bar, when the OLR/CR overlap is located at

³For $m = 2$, we do not take into account second-order resonances, i.e. 4:1 ($\text{ILR}_{\text{bar,sp}}, \text{OLR}_{\text{bar,sp}}$)

CHAPTER 3 : RADIAL MIGRATION OF THE SUN IN THE MILKY WAY: A STATISTICAL STUDY

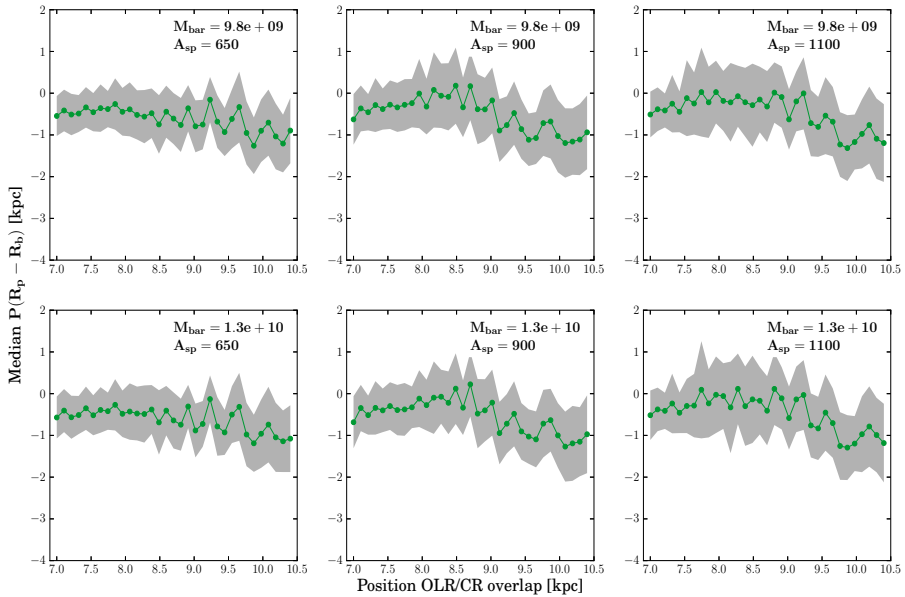


FIGURE 3.9: Median of the migration distribution $p(R_p - R_b)$ as a function of the position within the Galactic disk of the OLR/CR overlap. The shaded region corresponds to the RSE of the same distribution. From left to right, the amplitude of the spiral arms, A_{sp} takes the values 650, 900 and 1100 $\text{km}^2 \text{s}^{-2} \text{kpc}^{-1}$. From top to bottom, the mass of the bar, M_{bar} is 9.8×10^9 and $1.3 \times 10^{10} M_{\odot}$.

distances smaller than 8.5 kpc, the migration of the Sun is not considerable. In fact, for these cases, the probability that the Sun has migrated significantly in either direction is smaller than 10% (see Fig. 3.10). In contrast when the OLR/CR overlap is located at distances larger than 8.5 kpc, the median of the distribution $p(R_p - R_b)$ is shifted towards negative values, while the probability for considerable migration from the outer disk to R_{\odot} goes up reaching values up to 35%. The probability of significant migration from the inner disk to R_{\odot} remains low at values of at most a few per cent.

In Fig. 3.11 we show the migration distribution for an example of a case where the OLR/CR overlap has a strong effect, being located at 9.7 kpc from the Galactic centre. For this particular case, $M_{\text{bar}} = 9.8 \times 10^9 M_{\odot}$ and $A_{\text{sp}} = 1100 \text{ km}^2 \text{s}^{-2} \text{kpc}^{-1}$. The median of $p(R_p - R_b)$ is at -1.3 kpc and thus the radius where the Sun was born is around 10 kpc. The latter can also be seen

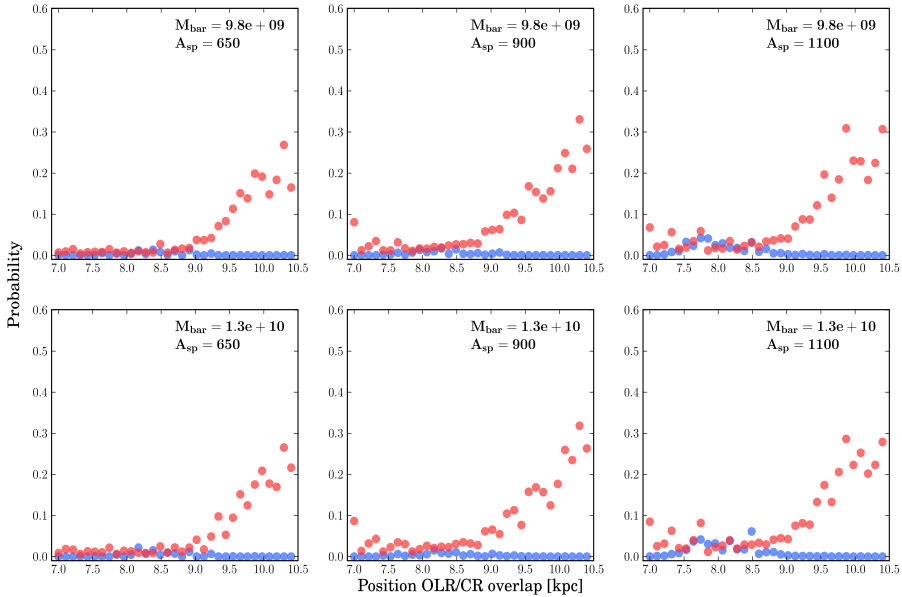


FIGURE 3.10: Probability of considerable radial migration of the Sun as a function of the location of the OLR/CR overlap. The blue points represent the probability of significant migration of the Sun from inside-out P_{i-o} , while the red points represent the significant migration from outside-in P_{o-i} . The mass of the bar and amplitude of spiral arms are the same as in Fig. 3.9.

in in the distribution $p(R_b)$. Note how the distribution of birth positions in the xy plane is clustered between the second and third quadrants. This is also seen for other cases, when the OLR/CR overlap is located between 8.5 and 9.5 kpc. However for different OLR/CR distances the clustering is toward other quadrants in the Galactic plane. Hence, taking the uncertainties in the OLR/CR location into account again only the birth radius of the Sun can be constrained.

3.5.4. Radial migration of the Sun with higher values of its tangential velocity

In this section we explore the motion of the Sun backwards in time when assuming the rotational velocity suggested by Bovy et al. [2012a]. In Fig. 3.12 we show the median of the distribution $p(R_p - R_b)$ as a function of the distance

CHAPTER 3 : RADIAL MIGRATION OF THE SUN IN THE MILKY WAY: A STATISTICAL STUDY

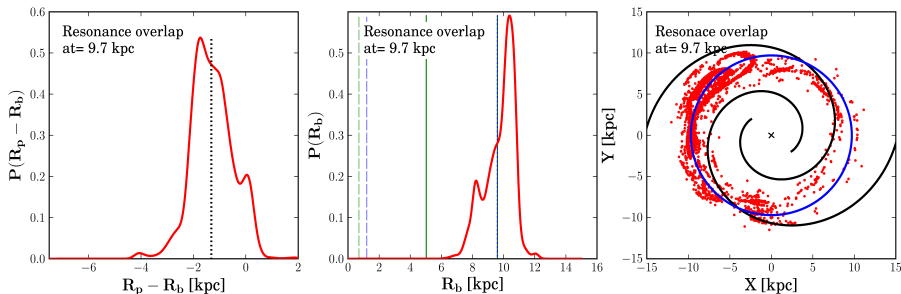


FIGURE 3.11: Example of the migration distribution for the case of the OLR/CR overlap located at 9.7 kpc from the Galactic centre. Here $A_{\text{sp}} = 1100 \text{ km}^2 \text{ s}^{-2} \text{ kpc}^{-1}$ and $M_{\text{bar}} = 9.8 \times 10^9 M_{\odot}$. *Left*: The migration distribution $p(R_p - R_b)$. The dotted black line indicates the median of the distribution. *Middle*: Distribution of the birth radius of the Sun $p(R_b)$. *Right*: Distribution of birth positions of the Sun projected on the xy plane. The location of the OLR/CR overlap is indicated by the blue circle. The configuration of the spiral arm potential 4.6 Gyr in the past is also shown.

between the OLR_{bar} and CR_{sp} . For this set of simulations we fixed the bar parameters to $M_{\text{bar}} = 9.8 \times 10^9 M_{\odot}$ and $\Omega_{\text{bar}} = 40 \text{ km s}^{-1} \text{ kpc}^{-1}$ respectively. With this pattern speed, the OLR_{bar} is located at 10.2 kpc with respect to the Galactic centre. Additionally, the amplitude of the spiral arms is fixed to $A_{\text{sp}} = 1050 \text{ km}^2 \text{ s}^{-2} \text{ kpc}^{-1}$. We varied the pattern speed of the spiral arms in steps of $1 \text{ km s}^{-1} \text{ kpc}^{-1}$ within the range listed in table 3.1. We used two and four spiral arms. For comparison we have also plotted the median of the distribution $p(R_p - R_b)$ when the tangential velocity of the Sun is taken from Schönrich et al. [2010]. As can be observed, the migration of the Sun on average is approximately 1 kpc higher when V_{\odot} is taken from Bovy et al. [2012a]. In the latter case, the median of the distribution $p(R_p - R_b)$ is negative for both $m = 2$ and $m = 4$ meaning that the Sun has migrated from outer regions of the Galactic disk to R_{\odot} . In addition, from the simulations shown at the top panel of Fig. 3.12 we found that when the OLR_{bar} and CR_{sp} are separated by $\pm 0.2 \text{ kpc}$, the Sun migrates on average a distance around 2 kpc, placing the Sun's birth place at around 10.5 kpc from the Galactic centre. For this specific case we found a probability between 55% and 60% that the Sun has migrated considerably from outer regions of the Galactic disk to its current position. On the other hand, we found unlikely that the Sun has migrated from inner regions

of the Galaxy to R_{\odot} .

Contrary to the two-armed spiral structure, the migration of the Sun on average is not significant when $m = 4$, even for small distances between the OLR_{bar} and CR_{sp} . (See bottom panel Fig. 3.12). Note that the median of $p(R_{\text{p}} - R_{\text{b}})$ is never greater than -1.7 kpc. However, Given that the width of the distribution $p(R_{\text{p}} - R_{\text{b}})$ is appreciable, specially when $\text{OLR}_{\text{bar}} - \text{CR}_{\text{sp}} \geq 2$ kpc, the probability of considerable migration from inner or outer regions to R_{\odot} can be of up to 10% or 20% respectively.

3.6. Discussion

It is well known that the metallicity of the interstellar medium (ISM) depends on time and Galactic radius. Since younger stars formed at the same Galactocentric radius have higher metallicities, the metallicity of the ISM is expected to increase with time. Additionally, it has been established that the metallicity of the ISM decreases with increasing the Galactic radius due to more efficient star formation and enrichment of the ISM in the central regions of galaxies [Dafon & Cunha, 2004; Recio-Blanco et al., 2014].

Past studies of the age-metallicity relation in the solar neighbourhood suggested that the Sun is more metal rich by typically 0.2 dex than most stars at its age and Galactocentric orbit [Edvardsson et al., 1993; Holmberg et al., 2009]. Hence, from the relationship between metallicity and Galactocentric radius, it is natural to deduce that the Sun might have migrated from the inner regions of the disk to its current position in the Galaxy [Wielen et al., 1996; Minchev et al., 2013]. However, if the observations are restricted to stars within a distance of 40 pc from the Sun it seems that its chemical composition is not unusual after all. Fuhrmann [2004] found a sample of 118 thin-disk stars with a mean age of 4.5 Gyr to have a mean metallicity of -0.04 dex. In addition Valenti & Fischer [2005], found a mean metallicity of -0.01 dex in a sample of F, G, and K stars that were observed in the context of planet search programmes. More recently Casagrande et al. [2011] found that the peak of the metallicity distribution function of stars in the Geneva-Copenhagen survey [Nordström et al., 2004], is around the solar value. As we mentioned in the introduction, if the Sun is indeed not more metal rich than the stars of its same

CHAPTER 3 : RADIAL MIGRATION OF THE SUN IN THE MILKY WAY: A STATISTICAL STUDY

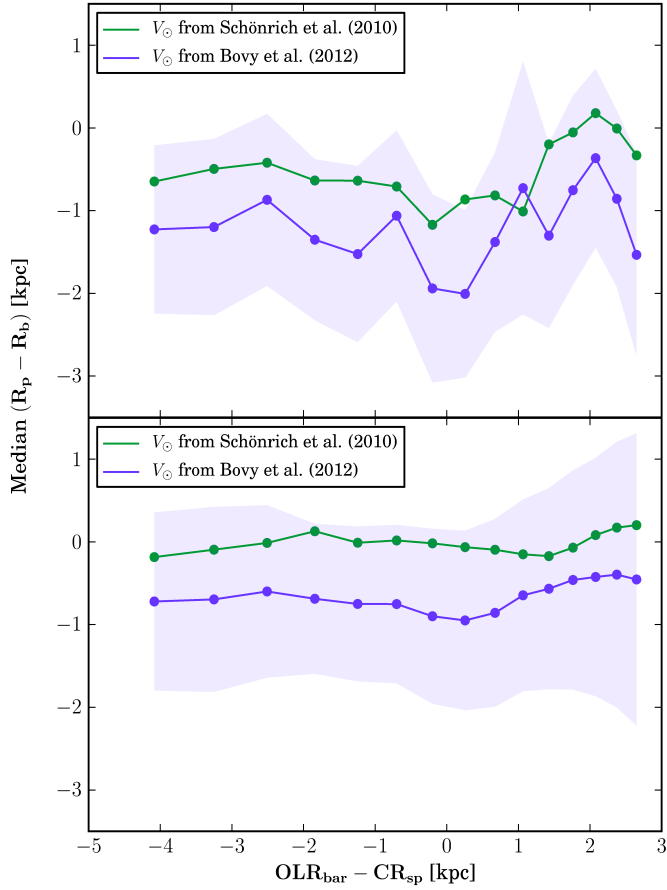


FIGURE 3.12: Median of the distribution $p(R_p - R_b)$ as a function of the distance between the OLR_{bar} and CR_{sp} . The green line is the resulting radial migration of the Sun when we assume a tangential velocity of $12.4 \pm 2.1 \text{ km s}^{-1}$ [Schönrich et al., 2010] in the orbit integration backwards in time. The blue line is the radial migration of the Sun when we assume a tangential velocity of $26 \pm 3 \text{ km s}^{-1}$ [Bovy et al., 2012a]. The blue shaded region corresponds to the RSE of $p(R_p - R_b)$ for this latter case. We used: *Top*: two spiral arms. *bottom*: four spiral arms.

age and Galactocentric radius it is probable that the Sun has not experienced considerable migration over its lifetime.

Minchev & Famaey [2010] studied the effects of the bar-spiral arm resonance overlap in the solar neighborhood. They found that a large fraction of stars that were located initially at inner and outer regions of the Galactic disk, ended up at a distance of ~ 8 kpc after 3 Gyr of evolution. This explains the observed lack of a metallicity gradient with age in the solar neighborhood [Haywood, 2008]; however, the same simulations show that after 3 Gyr of evolution, the peak of the initial radial distribution of stars that end up at 8 kpc is also around 8 kpc, meaning that most of the stars at solar radius, do not migrate. For their simulations, Minchev & Famaey [2010] modelled the central bar and spiral arms of the Galaxy as non-transient perturbations.

In this study we find that large radial migration of the Sun is only feasible when the OLR_{bar} is separated from CR_{sp} by a distance less than 1.1 kpc or when these two resonances overlap and are located further than 8.5 kpc from the Galactic centre. In these cases we find that the migration of the Sun is always from the outer regions of the Galaxy to R_{\odot} . When the CR_{sp} is located between 7.3 and 8.4 kpc and the number of spiral arms is four, the Sun migrates on average little; however, given that the width of the distribution $p(R_{\text{p}} - R_{\text{b}})$ can be up to 2.3 kpc, the radial migration of the Sun highly depends on its birth phase-space coordinates. For this latter case, the probability that the Sun has migrated considerably from inner regions of the disk to R_{\odot} can be up to 30%. Apart from the very specific cases mentioned above, we found that in general the Sun might have not experienced considerable radial migration from its birth place to its current position in the Galaxy. In the simulations we did not change the Galactic parameters (mass, scale length) of the axisymmetric components of the Milky Way. Since this is a smooth potential, we do not expect great variations on the solar motion due to the variation of these parameters.

The model that we used for the Milky Way has two restrictions: it does not take into account transient spiral structure and it assumes that the Galactic parameters have been fixed during the last 4.6 Gyr. Although there are several studies that suggest that the spiral structure in the Galaxy is transient [Sellwood, 2010, 2011], the evolutionary history of the Milky Way is quite uncertain, thus the Galactic model used is still valid. The study of the radial

migration of the Sun under the influence of transient spiral arms implies to extend the space of Galactic parameters even more. Hence, simulations taking into account transient spiral structure will be carried out in a future work.

Recently Minchev et al. [2013] made a more complex modeling of the Milky Way which involves self-consistent N-body simulations in a cosmological context together with a detailed chemical evolution model. They explored the evolution of a Galaxy for a time period of 11 Gyr, which is close to the age of the oldest disk stars in the Milky Way. They found that as the bar grows and the spiral structure start to form, the CR_{bar} and OLR_{bar} are shifted outwards of the disk producing changes in the angular momentum of stars. These changes in angular momentum can be doubled in the time interval from 4.4 to 11.2 Gyr. At the end of the simulation they found that stars of all ages end up at the solar neighborhood ($7 \leq r \leq 9$ kpc). Additionally, from the obtained metallicity distribution they conclude that the majority of stars come from inner regions of the Galactic disk ($3 \leq r \leq 7$ kpc), although a sizable fraction of stars originating from outside the solar neighborhood is also observed. By assuming an error of ± 1 dex in the metallicity, they found that the possible region where the Sun was formed is between 4.4 and 7.7 kpc, with the highest probability to be around 5.6 and 7 kpc. These results support the conclusions of Wielen et al. [1996].

According to Minchev et al. [2013] the Sun probably has migrated a distance between 1.5 and 2.9 kpc from the inner regions of the Galactic disk to R_{\odot} , which is different from what we obtained. The discrepancy in the conclusions is due to the fact that the structure of the Milky Way and its evolutionary history is quite uncertain. For instance, Minchev et al. [2013] argued that their results are strongly dependent on the migration efficiency in their simulations and also in the adopted chemical evolution model. We obtained a broad set of possible past Sun's orbits due to the large uncertainty in the bar and spiral arm parameters. Hence, a large scale determination of the phase-space of stars together with better measurements of their chemical abundances are needed to constrain the history of the Milky Way and hence, their current properties. With the *Gaia* mission [Lindgren et al., 2008] we can expect to obtain the parallaxes and proper motions of one billion of stars very accurately. The *HERMES* [Freeman & Bland-Hawthorn, 2002] and *APOGEE* [Allende Prieto et al., 2008] surveys,

will provide a complete database of chemical abundances and radial velocities for stars across all Galactic populations (bulge, disk, and halo).

With a more accurate determination of the Galactic parameters (masses, scale lengths, pattern speeds), the motion of the Sun can be better constrained.

3.7. Summary and final remarks

We studied the radial migration of the Sun within the Milky Way by computing its past orbit in an analytical potential representing the Galaxy. We took into account the uncertainties in the distance of the Sun from the centre of the Galaxy and its peculiar velocity components as well as the uncertainties in the bar and spiral arm parameters.

At the start of the simulations the phase space coordinates of the Sun are initialized to 5000 different positions and velocities which were obtained from a normal distribution centred at $(\mathbf{r}_\odot, \mathbf{v}_\odot)$, with standard deviations reflecting the uncertain present day values of \mathbf{r}_\odot and \mathbf{v}_\odot . After performing the backwards integration in time, we obtained a distribution of ‘birth’ phase-space coordinates. We computed the migration distribution function, $p(R_p - R_b)$, to study the amount of radial migration experienced by the Sun during the last 4.6 Gyr. We obtain the following results:

- For the majority of the simulations the median of the distribution $p(R_p - R_b)$ is negative. This indicates that the motion of the Sun has been on average from outer regions of the Galactic disk to R_\odot .
- The bar of the Milky Way does not produce considerable radial migration of the Sun. In contrast, the variation of amplitude and pattern speed of spiral arms produce migration on average of distances up to -1.8 kpc, if the number of spiral arms is two. Hence, the birth radius of the Sun would then be around 11 kpc. In the case of a four-armed spiral potential, the Sun does not migrate on average; however, given that the width of the migration distribution $p(R_p - R_b)$ can be up to 2.3 kpc, there is a probability of approximately 30% that the Sun has migrated considerably from inner regions of the Galactic disk to R_\odot . If the potential of

the Galaxy has multiple non-transient spiral patterns, the Sun does not migrate on average.

- Only very specific configurations of the Galactic potential lead to considerable migration of the Sun. One case is when the separation of the OLR_{bar} and CR_{sp} is less than or equal to 1 kpc. Another case is when these two resonances overlap and are located further than 8.5 kpc from the Galactic centre. For these cases there is a probability of up to **35%** or **50%** that the Sun has experienced considerable radial migration from outer regions of the Galactic disk to R_{\odot} .
- When the CR_{sp} is located between 7.3 and 8.4 kpc and the Galactic potential has four spiral arms, the probability that the Sun has migrated considerably from inner regions of the Galactic disk to its current position can be up to 30%. For other combinations of bar and spiral arm parameters, $P_{i \rightarrow o} \sim 0$. Hence, we found that in general it is unlikely that the Sun has migrated from inner regions of the Galaxy to R_{\odot} .
- Apart from the cases summarized above we find that in general the Sun might not have experienced appreciable migration from its birth place to its current position in the Galaxy.

In this study we consider the motion of the Sun in the plane. Simulations taking into account the vertical structure of the non-axisymmetric components of the Galactic potential will be carried out in future works (e.g Faure et al. [2014]; Monari et al. [2014] provide prescriptions for such potentials)

The study of the motion of the Sun during the last 4.6 Gyr has allowed us to determine its birth radius. This is the first step to understand the evolution and consequent disruption of the Sun's birth cluster in the Galaxy. In this respect, state of the art simulations are required to predict more accurately the current phase-space of the solar siblings. In these simulations, internal processes such as self gravity and stellar evolution have to be taken into account [Brown et al., 2010a]. A detailed study of the evolution and disruption of the Sun's birth cluster by using realistic simulations is shown in the next chapter.

According to the above results, the current distribution on the xy plane of the solar siblings will be different depending on the configuration of the

Galactic potential. For the bar and spiral arm parameters that produce a broad migration distribution $p(R_p - R_b)$ (cases where $\text{RSE} \geq 1.7$ kpc), we expect a high dispersion of solar siblings, spanning a large range of radii and azimuths on the disk. For the Galactic parameters that do not generate a broad distribution $p(R_p - R_b)$ (cases where $\text{RSE} \leq 1$ kpc), we expect the Sun's siblings not to have a large radial dispersion. Therefore, depending on their final distribution, it would be likely or unlikely to find solar siblings in the near vicinity of the Sun.

Mishurov & Acharova [2011] concluded that it is unlikely to find solar siblings within 100 pc from the Sun, since members of an open cluster are scattered over a large part of the Galactic disk when the gravitational field associated to the spiral arms is taken into account. Consequently, a large scale survey of phase-space is needed. Only the *Gaia* mission [Lindgren et al., 2008] will provide data at the precision needed to probe for siblings which are far away from the Sun [Brown et al., 2010a]. The realistic simulations mentioned above will have to be exploited to develop methods to look for solar siblings among the billions of stars in the *Gaia* catalogue; however, together with the kinematics provided by the simulations, a complete determination of chemical abundances of stars has to be done to find the true solar siblings [Brown et al., 2010a; Ramírez et al., 2014].

The identification of the siblings of the Sun will enable to put better constraints on the initial conditions of the Sun's birth cluster, instead of using only the current solar System properties [Brown et al., 2010a; Adams, 2010]. With well established initial conditions for the parental cluster of the Sun, the formation, evolution and current features of the solar system could finally be disentangled.

Acknowledgements

We want to thank Mercé Romero Gómez for providing us the model for the bar potential. Nathan de Vries and Inti Peluppesy for their valuable help that allowed us to make the interface of the Galactic model and to develop the *Rotating Bridge*. We also want to thank the anonymous referee, Michiko Fujii, Lucie Jilková, Kate Tolfree and Teresa Antoja for their suggestions and

CHAPTER 3 : RADIAL MIGRATION OF THE SUN IN THE MILKY WAY: A STATISTICAL STUDY

fruitful discussions that improved this manuscript. This work was supported by the Nederlandse Onderzoekschool voor Astronomie (NOVA), the Netherlands Research Council NWO (grants #639.073.803 [VICI], #614.061.608 [AMUSE] and #612.071.305 [LGM]) and by the Gaia Research for European Astronomy Training (GREAT-ITN) network Grant agreement no.: 264895

CHAPTER 4

THE EVOLUTION OF THE SUN'S BIRTH CLUSTER AND THE SEARCH FOR THE SOLAR SIBLINGS WITH *Gaia*

C.A. Martínez-Barbosa, A.G.A. Brown, T. Boekholt, S. Portegies Zwart,
E. Antiche and T. Antoja
2016, MNRAS, 457, 1062-1075

Abstract

We use self-consistent numerical simulations of the evolution and disruption of the Sun's birth cluster in the Milky Way potential to investigate the present-day phase space distribution of the sun's siblings. The simulations include the gravitational N -body forces within the cluster and the effects of stellar evolution on the cluster population. In addition the gravitational forces due to the Milky Way potential are accounted for in a self-consistent manner. Our

aim is to understand how the astrometric and radial velocity data from the *Gaia* mission can be used to pre-select solar sibling candidates. We vary the initial conditions of the Sun's birth cluster, as well as the parameters of the Galactic potential. In particular, we use different configurations and strengths of the bar and spiral arms. We show that the disruption time-scales of the cluster are insensitive to the details of the non-axisymmetric components of the Milky Way model and we make predictions, averaged over the different simulated possibilities, about the number of solar siblings that should appear in surveys such as *Gaia* or *GALAH*. We find a large variety of present-day phase space distributions of solar siblings, which depend on the cluster initial conditions and the Milky Way model parameters. We show that nevertheless robust predictions can be made about the location of the solar siblings in the space of parallaxes (ϖ), proper motions (μ) and radial velocities (V_r). By calculating the ratio of the number of simulated solar siblings to that of the number of stars in a model Galactic disk, we find that this ratio is above 0.5 in the region given by: $\varpi \geq 5$ mas, $4 \leq \mu \leq 6$ mas yr⁻¹, and $-2 \leq V_r \leq 0$ km s⁻¹. Selecting stars from this region should increase the probability of success in identifying solar siblings through follow up observations. However the proposed pre-selection criterion is sensitive to our assumptions, in particular about the Galactic potential. Using a more realistic potential (e.g., including transient spiral structure and molecular clouds) would make the pre-selection of solar sibling candidates based on astrometric and radial velocity data very inefficient. This reinforces the need for large scale surveys to determine precise astrophysical properties of stars, in particular their ages and chemical abundances, if we want to identify the solar family.

keywords: Galaxy: kinematics and dynamics; open clusters and associations: general; Sun: general

4.1. Introduction

Since most of the stars are born in star clusters [Lada & Lada, 2003], these systems are considered the building blocks of galaxies. In the Milky Way star clusters located in the Galactic halo (Globular clusters) populate the Galactic disk through mergers [Lee et al., 2013]. On the other hand star clusters formed in the Galactic disk (open clusters) supply new stars to the disk of the Galaxy through several processes, such as shocks from encounters with spiral arms and Giant Molecular Clouds [Gieles et al., 2006, 2007].

The dynamical evolution of star clusters involves several physical mechanisms. At earlier stages of their evolution, star clusters lose mass mainly due to stellar evolution and two-body relaxation processes, which in turn, enlarge the size of star clusters [Takahashi & Portegies Zwart, 2000; Baumgardt & Makino, 2003; Madrid et al., 2012]. This evolutionary stage is called the expansion phase [Gieles et al., 2011], which takes about 40% of the star cluster's lifetime. Once star clusters overcome the expansion phase, the effects of the external tidal field of the Galaxy become important, depending on their location with respect to the Galactic centre. This stage is called the evaporation phase [Gieles et al., 2011] and it is characterized by the gradual dissolution of star clusters in the Galaxy.

The dissolution rate of star clusters depends on their Galactocentric distance [Madrid et al., 2012], orbit [Baumgardt & Makino, 2003], orbital inclination [Webb et al., 2014b] and on Galaxy properties such as the mass and size of the Galactic disk [Madrid et al., 2014]. Additionally, open clusters in the Milky Way are also dissolved due to non axisymmetric perturbations such as bars [Berentzen & Athanassoula, 2012], spiral arms [Gieles et al., 2007] and giant molecular clouds [Gieles et al., 2006; Lamers & Gieles, 2006]. The strongest tidal stripping occurs at times when open clusters cross regions of high density gas, for instance, during spiral arms passages [Gieles et al., 2007; Kruijssen et al., 2011] or during collisions with giant molecular clouds [Gieles et al., 2006]. Open clusters can also radially migrate over distances of up to 1 kpc in a short time scale (~ 100 Myr) when the Galactic spiral structure is transient [Fujii & Baba, 2012]. This radial migration process can also be efficient in the absence of transient structure if the resonances due the bar and spiral structure overlap

[Minchev & Famaey, 2010]. Radial migration affects the orbits of open clusters in the Galaxy, increasing or decreasing their perigalacticon distance, which in turn influences their dissolution times [see e.g. Jílková et al., 2012].

The high eccentricities and inclinations observed in the Edgeworth-Kuiper belt objects together with the discovery of decay products of ^{60}Fe and other radioactive elements in the meteorite fossil record, suggest that the Sun was born in an open cluster 4.6 Gyr ago [Portegies Zwart, 2009, and references therein]. Identifying the stars that were formed together with the Sun (the solar siblings) would enable the determination of the Galactic birth radius of the Sun as well as further constrain the properties of its birth cluster [Bland-Hawthorn et al., 2010; Adams, 2010]. The birth radius affects the evolution of the solar system, and in particular the Oort cloud, which is sensitive to the Galactic environment the Sun passes through along its orbit [e.g. Portegies Zwart & Jílková, 2015].

The Sun's birth cluster will undergo all the disruptive processes described above and thus dissolve, leading to the spreading out of its stars over the Galactic disk. The subsequent distribution of the solar siblings was studied by Portegies Zwart [2009], who evolved the Sun's birth cluster in an axisymmetric model for the Galactic potential and concluded that tens of solar siblings might still be present within a distance of 100 pc from the Sun. Several attempts have since been made to find solar siblings [e.g. Brown et al., 2010b; Bobylev et al., 2011; Liu et al., 2015]; however, only four plausible candidates have been identified so far [Batista & Fernandes, 2012; Batista et al., 2014; Ramírez et al., 2014]. This small number of observed solar siblings might be a consequence of the lack of accurate predictions of the present-day phase space distribution of solar siblings together with insufficiently accurate stellar kinematic data.

Brown et al. [2010b] used test particle simulations to predict the current distribution of solar siblings in the Milky Way. They concluded that stars with parallaxes (ϖ) ≥ 10 mas and proper motions (μ) ≤ 6.5 mas yr $^{-1}$, should be considered solar sibling candidates. Their conclusions were criticised by Mishurov & Acharova [2011] who pointed out that in more realistic Galactic potentials the solar siblings are expected to be much more spread out over the Galactic disk. For small birth clusters (few thousand stars with a total mass of the order of $1000 M_{\odot}$) such as employed by Brown et al. [2010b] and

Portegies Zwart [2009], Mishurov & Acharova [2011] predict that practically no solar siblings will currently be located within 100 pc from the sun. However, for larger birth clusters [of order 10^4 stars, in line with predictions from e.g. Dukes & Krumholz, 2012] one can still expect to find a good number of siblings presently orbiting the Galaxy within 100 pc from the Sun.

Ongoing surveys of our galaxy, in particular the *Gaia* mission [Lindegren et al., 2008] and the *GALAH* survey [De Silva et al., 2015], will provide large samples of stars with accurately determined distances, space motions, and chemical abundance patterns, thus enabling a much improved search for the sun’s siblings. In this chapter we investigate the potential of the *Gaia* astrometric and radial velocity data to narrow down the selection of candidate solar siblings for which detailed chemical abundance studies should be undertaken in order to identify the true siblings. Our investigation is done by performing simulations of the evolution and disruption of the Sun’s birth cluster in a realistic (although static) Galactic potential, including the bar and spiral arms. The aim is to predict the present-day phase space distribution of the siblings and simulate the astrometric and radial velocity data collected by *Gaia*. We include the internal N -body processes in the cluster to account for the disruption time scale. We use a full stellar mass spectrum and a parametrized stellar evolution code to make accurate predictions of how the solar siblings are observed by *Gaia*. To this end we also account for the effects of extinction and reddening.

The rest of this chapter is organized as follows. In Sect. 4.2 we describe the simulations. In Sect. 4.3 we explore the evolution and disruption of the Sun’s birth cluster due to the bar and spiral arms of the Galaxy. In Sect. 4.4 we present the current phase-space distribution of solar siblings obtained from the simulations. In Sect. 4.5 we make use of the simulated positions and motions of the solar siblings to investigate the robustness of the selection criterion proposed by Brown et al. [2010b] to the uncertainties in the present-day phase space distribution of the solar siblings. An updated set of selection criteria based on parallax, proper motion and radial velocity information is presented. In Sect. 4.6 we use these criteria to examine stars that were previously suggested as solar siblings candidates and further discuss our results. In Sect. 4.7 we summarize.

4.2. Simulation set-up

The goals of the simulations of the Sun's birth cluster are to predict the present-day phase space distribution of the solar siblings and how these are expected to appear in the *Gaia* catalogue. In particular we wish to account for the uncertainties in the initial conditions of the birth cluster and the parameters of the Milky Way potential. The predictions of the *Gaia* observations require the use of a realistic mass spectrum for the siblings, and accounting for stellar evolution and extinction and interstellar reddening effects. We thus employ the following elements in the simulations:

Galactic model The Milky Way potential is described by an analytic model containing a disk, bulge and halo, as well as a bar and spiral arms. The parameters of the bar and spiral arms are varied in the simulations to account for uncertainties in their strengths and pattern speeds (Sect. 4.2.1).

Cluster model The Sun's birth cluster is modelled with a mass spectrum for the stars and we account for the gravitational N -body effects within the cluster as well as the effect of the Galaxy's gravitational field on the cluster stars. The use of N -body models for the birth cluster is motivated by the desire to account for the disruption time of the cluster which can be a substantial fraction of the lifetime of the Sun (Sect. 4.2.2).

Stellar evolution Predicting the observations of the Sun's birth cluster by *Gaia* requires that we account for the mass-dependent evolution of the solar siblings, in order to obtain the correct present-day apparent magnitudes and colours which are used to predict which stars end up in the *Gaia* catalogue. This prediction also requires us to account for interstellar extinction and reddening for which we employ a Galactic extinction model (Sects. 4.2.3, 4.5).

These elements are described in more detail in the subsequent subsections.

4.2.1. Galactic model

We use an analytical potential to model the Milky Way. This potential contains two parts: an axisymmetric component, which corresponds to a bulge, disk and a dark matter halo, and a non-axisymmetric component which includes a central bar and spiral arms. Bellow we explain these components in more detail.

Axisymmetric component We use the potential of Allen & Santillán [1991] to model the axisymmetric component of the Galaxy. In this approach, the bulge is modelled with a Plummer [Plummer, 1911] potential; the disk is modelled with a Miyamoto-Nagai [Miyamoto & Nagai, 1975] potential and the dark matter halo with a logarithmic potential. The parameters used to model the axisymmetric component of the Galaxy are listed in table 4.1.

The model introduced by Allen & Santillán [1991] predicts a rotational velocity of 220 km s^{-1} at the solar radius, which does not match with the recent observational estimates [see e.g McMillan, 2011; Reid et al., 2014]. However, Jílková et al. [2012] did not find substantial variations in the orbits of open clusters when using different models of the axisymmetric structure of the Galaxy. Therefore, we do not expect that the evolution of the Sun’s birth cluster and the present-day distribution of solar siblings will be affected due to the choice of the axisymmetric potential model.

The Galactic bar The central bar is modelled with a Ferrers potential [Ferrers, 1877] which describes the potential associated to an elliptical distribution of mass. In an inertial frame located at the Galactic centre, the bar rotates with a constant pattern speed of $40\text{--}70 \text{ km s}^{-1} \text{ kpc}^{-1}$ [Martínez-Barbosa et al., 2015, and references therein]. This range of angular velocities places the Outer Lindblad resonance of the bar (OLR_{bar}) at $10\text{--}5 \text{ kpc}$ from the Galactic centre. In the same inertial frame, the present-day orientation of the bar with respect to the negative x -axis is 20° [Pichardo et al., 2004, 2012; Romero-Gómez et al., 2011, and references therein]. In the left panel of Fig. 4.1 we show the present-day orientation of the Galactic bar. In Table 4.1 we show the parameters used in this study. For further details on the choice of the bar parameters, we refer

TABLE 4.1: Parameters of the Milky Way model potential.

<i>Axisymmetric component</i>	
Mass of the bulge (M_b)	$1.41 \times 10^{10} M_\odot$
Scale length bulge (b_1)	0.38 kpc
Disk mass (M_d)	$8.56 \times 10^{10} M_\odot$
Scale length disk 1 (a_2)	5.31 kpc
Scale length disk 2 (b_2)	0.25 kpc
Halo mass (M_h)	$1.07 \times 10^{11} M_\odot$
Scale length halo (a_3)	12 kpc
<i>Central Bar</i>	
Pattern speed (Ω_{bar})	40–70 km s ⁻¹ kpc ⁻¹
Semi-major axis (a)	3.12 kpc
Axis ratio (b/a)	0.37
Mass (M_{bar})	9.8×10^9 – $1.4 \times 10^{10} M_\odot$
Present-day orientation	20°
Initial orientation	1° – 167°
<i>Spiral arms</i>	
Pattern speed (Ω_{sp})	15–30 km s ⁻¹ kpc ⁻¹
Locus beginning (R_{sp})	3.12 kpc
Number of spiral arms (m)	2, 4
Spiral amplitude (A_{sp})	650–1100 km ² s ⁻² kpc ⁻¹
Pitch angle (i)	12.8°
Scale length (R_Σ)	2.5 kpc
Present-day orientation	20°
Initial orientation	103° – 173°

TABLE 4.2: Parameters of the composite Galaxy model potential.

<i>Main spiral structure</i>	
Pattern speed (Ω_{sp_1})	26 km s ⁻¹ kpc ⁻¹
Amplitude (A_{sp_1})	650–1300 km ² s ⁻² kpc ⁻¹
Pitch angle (i_1)	−7°
Present-day orientation	20°
Initial orientation	171°
<i>Secondary spiral structure</i>	
Pattern speed (Ω_{sp_2})	15.8 km s ⁻¹ kpc ⁻¹
Amplitude (A_{sp_2})	0.8 A_{sp_1}
Pitch angle (i_2)	−14°
Present-day orientation	220°
Initial orientation	158°
<i>Bar</i>	
Pattern speed (Ω_{bar})	40 km s ⁻¹ kpc ⁻¹
Semi-major axis (a)	3.12 kpc
Axis ratio (b/a)	0.37
Mass (M_{bar})	9.8 × 10 ⁹ M_{\odot}
Strength of the bar (ϵ_b)	0.3
Present-day orientation	20°
Initial orientation	1°

the reader to Martínez-Barbosa et al. [2015].

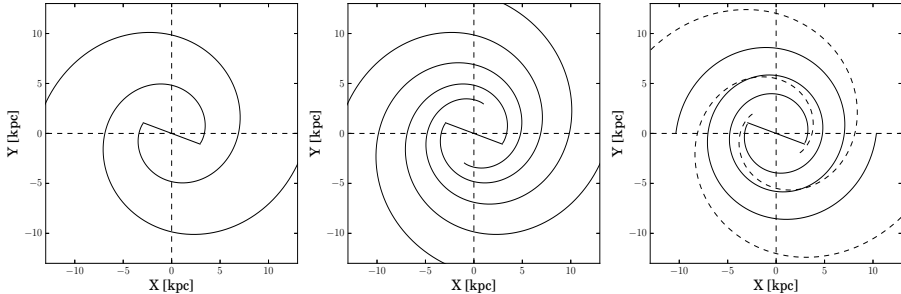


FIGURE 4.1: Configurations of the Galactic potential at the present time. *Left:* Galaxy with two spiral arms. *Middle:* Galaxy with four spiral arms. *Right:* (2 + 2) composite model.

The spiral arms We model the spiral arms as periodic perturbations of the axisymmetric potential [tight winding approximation, Lin et al., 1969]. The spiral arms rotate with a constant pattern speed of $15\text{--}30 \text{ km s}^{-1} \text{ kpc}^{-1}$ [Martínez-Barbosa et al., 2015]. This range of values places the co-rotation resonance of these structures (CR_{sp}) at $14\text{--}7 \text{ kpc}$ from the Galactic centre. We assume that the Galaxy has two or four non-transient spiral arms with the same amplitude. A schematic picture of the present-day configuration of the spiral arms is shown in the left and middle panels of Fig. 4.1. The parameters of the spiral arms used in this study are listed in Table 4.1. For further details on the choice of these parameters, we refer the reader to Martínez-Barbosa et al. [2015].

Initial orientation of the bar and spiral arms The orientation of the bar and spiral arms at the beginning of the simulations (i.e 4.6 Gyr ago) are defined through the following equations:

$$\begin{aligned}\varphi_{\text{b}} &= \varphi_{\text{b}}(0) - \Omega_{\text{bar}}t, \\ \varphi_{\text{s}} &= \varphi_{\text{s}}(0) - \Omega_{\text{spt}}t.\end{aligned}\tag{4.1}$$

Here $\varphi_{\text{b}}(0)$ is the present-day orientation of the bar. We assume that the spiral arms start at the tips of the bar, i.e. $\varphi_{\text{s}}(0) = \varphi_{\text{b}}(0)$ (see Fig. 4.1). The time,

$t = 4.6$ Gyr corresponds to the age of the Sun [Bonanno et al., 2002]. The initial orientations of the bar and spiral arms are listed in Table 4.1.

Multiple spiral patterns We also consider a more realistic Galaxy model with multiple spiral patterns, as suggested by Lépine et al. [2011a]. In this model, often called the (2+2) composite model, two spiral arms have a smaller amplitude and pattern speed than the main structure, which is also composed of two spiral arms. A schematic picture of the composite model is shown in the right panel of Fig. 4.1. We use the parameters of the composite model suggested by Mishurov & Acharova [2011] and Lépine et al. [2011a]. These values are listed in Table 4.2. Here, A_{sp_1} corresponds to a strength of 0.06; that is, the main spiral structure has 6% the strength of the axisymmetric potential. Additionally, the value of Ω_{sp_1} places the co-rotation resonance (CR) of the main spiral structure at the solar radius. The value of Ω_{sp_2} on the other hand, places the CR of the secondary spiral structure at 13.6 kpc. The orientation of the spiral arms at the beginning of the simulation is set according to Eq. 4.1, where $\varphi_{0s_1} = 20^\circ$ and $\varphi_{0s_2} = 220^\circ$ are the initial phases of the main and secondary spiral structures respectively. In the composite model we also fixed the parameters of the bar. The corresponding values are listed in Table 4.2.

4.2.2. The Sun’s birth cluster

Initial conditions

We model the Sun’s birth cluster with a spherical density distribution corresponding to a Plummer potential [Plummer, 1911]. We also assume that the primordial gas was already expelled from the cluster when it starts moving in the Galaxy. The initial mass (M_c) and radius (R_c) of the Sun’s birth cluster were set according to Portegies Zwart [2009], who suggested that the Sun was probably born in a cluster with $M_c = 500\text{--}3000 M_\odot$ and $R_c = 0.5\text{--}3$ pc. In table 4.3 we show the initial mass and radius of the Sun’s birth cluster used in the simulations. From this table we note that the number of stars belonging to the Sun’s birth cluster (N) is around $10^2\text{--}10^3$ in accordance with previous studies [see e.g. Adams & Laughlin, 2001; Adams, 2010]. In table 4.3 we also show the initial velocity dispersion of the Sun’s birth cluster (σ_v). This quan-

TABLE 4.3: Radius (R_c), mass (M_c), number of particles (N) and velocity dispersion (σ_v) adopted for the parental cluster of the Sun

R_c (pc)	M_c (M_\odot)	N	σ_v (kms $^{-1}$)
0.5	510	875	2.91
1	641	1050	2.29
	765	1050	2.27
	1007	1741	2.96
1.5	525	875	1.61
	1067	1740	2.42
2	1023	1741	2.12
	883	1350	2.05
3	804	1500	1.44

tity can be computed by means of the virial theorem. As can be observed, for the initial mass and radius adopted, σ_v is between 1.4 and 2.9 km s $^{-1}$.

We used a Kroupa initial mass-function (IMF) [Kroupa, 2001] to model the mass distribution of the Sun’s birth cluster. The minimum and maximum masses used are $0.08 M_\odot$ and $100 M_\odot$ respectively. In this regime the IMF is a two-power law function described by the relation:

$$\psi(m) = \begin{cases} A_1 m^{-1.3} & 0.08 < m \leq 0.5 M_\odot, \\ A_2 m^{-2.3} & m > 0.5 M_\odot. \end{cases} \quad (4.2)$$

Here A_1 and A_2 are normalization constants which can be determined by evaluating $\psi(m)$ at the limit masses. We also set the metallicity of the Sun’s birth cluster to $Z = 0.02$ ($[Fe/H] = 0$).

Primordial binary stars

The dynamical evolution of stellar systems is affected by a non-negligible fraction of primordial binaries (see e.g. Tanikawa & Fukushige [2009]). Therefore, we also modelled the Sun’s birth cluster with different primordial binary fractions in order to observe their effect on the current phase-space distribution of the solar siblings. We varied the primordial binary fraction from zero (only single stars) up to 0.4.

We find that binaries have an effect on the internal evolution of the Sun’s birth cluster, in the sense that they tend to halt core collapse. The influence of binaries on the dissolution of siblings throughout the Galactic disk is negligible. We observe that the current spatial distribution of the solar siblings and their astrometric properties are little affected by the primordial binary fraction of the Sun’s birth cluster. Thus hereafter we focus only on clusters with a primordial binary fraction of zero.

Initial phase-space coordinates

The initial centre of mass coordinates of the Sun’s birth cluster ($\mathbf{x}_{\text{cm}}, \mathbf{v}_{\text{cm}}$) were computed by integrating the orbit of the Sun backwards in time taking into account the uncertainty in its current Galactocentric position and velocity, using the same methods as Martínez-Barbosa et al. [2015]. In these simulations we ignore the vertical motion of the Sun.

We generate 5000 random positions and velocities from a normal distribution centred at the current Galactocentric phase-space coordinates of the Sun (r_{\odot}, v_{\odot}). Thus, the standard deviations (σ) of the normal distribution correspond to the measured uncertainties in these coordinates. We assume that the Sun is currently located at: $r_{\odot} = (-8.5, 0, 0)$ kpc, with $\sigma_r = (0.5, 0, 0)$ kpc. In this manner, the uncertainty in y_{\odot} is set to zero given that the Sun is located on the x -axis of the Galactic reference frame [see e.g. Martínez-Barbosa et al., 2015, figure 1].

The present-day velocity of the Sun is $v_{\odot} = (U_{\odot}, V_{\odot})$; where

$$\begin{aligned} U_{\odot} \pm \sigma_U &= 11.1 \pm 1.2 \text{ km s}^{-1} \\ V_{\odot} \pm \sigma_V &= (12.4 + V_{\text{LSR}}) \pm 2.1 \text{ km s}^{-1}. \end{aligned} \quad (4.3)$$

Here, the vector $(11.1 \pm 1.2, 12.4 \pm 2.1) \text{ km s}^{-1}$ is the peculiar motion of the Sun [Schönrich et al., 2010] and V_{LSR} is the velocity of the local standard of rest which depends on the choice of Galactic parameters.

We integrate the orbit of the Sun backwards in time during 4.6 Gyr, for each of the initial conditions in the ensemble. At the end of the integration, we obtain a distribution of possible phase-space coordinates of the Sun at birth ($p(\mathbf{x}_b, \mathbf{v}_b)$). This procedure was carried out for 125 different Galactic parameters and models, according to the parameter value ranges listed in Tables 4.1

and 4.2. We used 111 different combinations of bar and spiral arm parameters for the 2 and 4-armed spiral models, and 14 different parameters for the composite model.

Once the distribution $p(\mathbf{x}_b, \mathbf{v}_b)$ is obtained for a given galactic model we use the median of the values of $p(\mathbf{x}_b, \mathbf{v}_b)$ as the value for $(\mathbf{x}_{\text{cm}}, \mathbf{v}_{\text{cm}})$. For the combinations of Galactic parameters used, we found that the median value of $p(\mathbf{x}_b, \mathbf{v}_b)$ remains in the range of 8.5–9 kpc. This is consistent with Martínez-Barbosa et al. [2015], who found that the Sun hardly migrates in a Galactic potential as the one explained in Sect. 4.2.1. We therefore chose to fix $\|\mathbf{x}_{\text{cm}}\| = \|\mathbf{x}_b\|$ to a value of 9 kpc, with the velocity \mathbf{v}_{cm} corresponding to this value. We note that restricting the birth radius of the Sun for a given Galactic model (fixed bar and spiral arm parameters) limits the possible outcomes for the phase space distribution of the solar siblings. Different starting radii would lead to different orbits which are affected differently by the bar and spiral arm potentials, which in turn implies different predicted distributions of the solar siblings after 4.6 Gyr. Although we do not account for these differences in outcomes in our simulations there is still significant spread in the predicted solar sibling distribution caused by the different bar and spiral arm parameters combinations we used (as demonstrated in Sect. 4.4).

4.2.3. Numerical simulations

The various simulation elements described above were to carry out simulations of the evolution of the Sun’s birth cluster as it orbits in the Milky Way potential. We used $9 \times 125 = 1125$ different combinations of birth cluster and Galactic potential parameters, using the parameter choices listed in tables 4.1, 4.2 and 4.3, in order to study a large variety of possible present-day phase space distributions of the solar siblings.

We use the HUAYNO code [Pelupessy et al., 2012] to compute the gravity among the stars within the cluster. We set the time-step parameter to $\eta = 0.03$. We also use a softening length given by [Aarseth, 2003]:

$$\epsilon = \frac{4R_{\text{vir}}}{N}, \quad (4.4)$$

where R_{vir} is the initial virial radius of the cluster and N the number of stars.

4.3 DISRUPTION OF THE SUN’S BIRTH CLUSTER

To calculate the external force due to the Galaxy we use a 6th-order Rotating BRIDGE [Pelupessy et al. in preparation; Martínez-Barbosa et al., 2015]. We set the BRIDGE time-step to $dt = 0.5 \text{ Myr}^1$.

The stellar evolution effects were modelled with the population synthesis code SEBA [Portegies Zwart & Verbunt, 1996; Toonen et al., 2012]. The magnitudes and colours of the stars were subsequently calculated from synthetic spectral energy distributions corresponding to the present-day effective temperature and surface gravity of the solar siblings. In addition the effects of extinction are accounted for. The simulation of photometry is described further in Sect. 4.4.

The various codes used to include the simulation elements above are all coupled through the AMUSE framework [Portegies Zwart et al., 2013]. In the simulations we evolve the Sun’s birth cluster during 4.6 Gyr.

4.3. Disruption of the Sun’s birth cluster

As the Sun’s birth cluster orbits in the Milky Way potential the tidal field and the effects of the bar and spiral arms will cause the gradual dissolution of the cluster, its stars spreading out over the Galactic disk. Here we briefly summarize our findings on the cluster dissolution times in our simulations. The results are in line with what is already known about the dynamical evolution of open clusters.

To compute the disruption rate of the Sun’s birth cluster it is necessary to know its tidal radius as a function of time. In its general form, the tidal radius is defined by the following expression [Renaud et al., 2011; Rieder et al., 2013]:

$$r_t = \left(\frac{GM_c}{\lambda_{\max}} \right)^{1/3}. \quad (4.5)$$

Here G is the gravitational constant, M_c is the mass of the cluster and λ_{\max} is the largest eigenvalue of the tidal tensor T_{ij} which is defined as: $T_{ij} = -\frac{\partial^2 \phi}{\partial x_i \partial x_j}$, with ϕ being the Galactic potential.

We use the method of Baumgardt & Makino [2003] to compute the bound mass of the Sun’s birth cluster iteratively. At each time-step, we first assume

¹This set-up in the dynamical codes give a maximum energy error per time-step in the simulations of the order of 10^{-7} .

CHAPTER 4 : THE EVOLUTION OF THE SUN'S BIRTH CLUSTER AND THE SEARCH FOR THE SOLAR SIBLINGS WITH *Gaia*

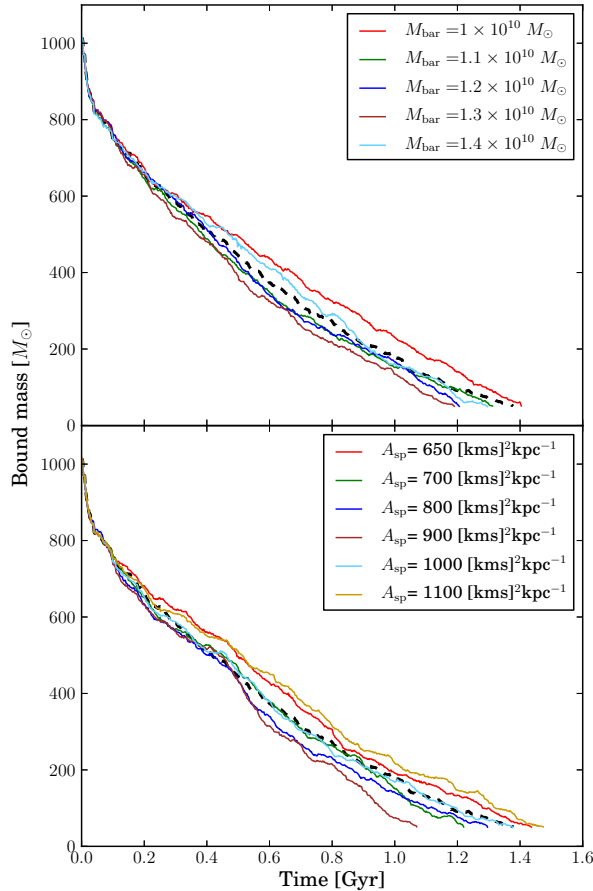


FIGURE 4.2: *Top:* Bound mass of the Sun's birth cluster as a function of time for different masses of the central bar of the Galaxy. The dashed black line corresponds to the bound mass of the Sun's birth cluster for a purely axisymmetric Galactic model. *Bottom:* Bound mass of the Sun's birth cluster as a function of time for different amplitudes of the spiral arms. The dashed black line has same meaning as above. Here the initial mass and radius of the Sun's birth cluster are 1023 M_{\odot} and 2 pc respectively.

that all stars are bound and we calculate the tidal radius of the system through Eq. 4.5, using the value of T_{ij} at the cluster centre. We use the method of Eisenstein & Hut [1998] to calculate the cluster centre. With this first estimate of r_t we compute the bound mass, which is the mass of the stars that have

4.4 CURRENT DISTRIBUTION OF SOLAR SIBLINGS IN THE MILKY WAY

a distance from the cluster centre smaller than r_t . We use this bound mass and the density centre of the bound particles to recalculate r_t and make a final estimate of the bound mass. We consider the Sun's birth cluster disrupted when 95% of its initial mass is unbound from the cluster.

We studied the effect of the mass of the bar and the spiral arms on the cluster evolution by varying the bar mass or the spiral arm strength, while keeping the other Galactic model parameters fixed. The mass of the bar was varied for a fixed pattern speed of $\Omega_{\text{bar}} = 70 \text{ km s}^{-1} \text{ kpc}^{-1}$, and with a fixed two-arm spiral with pattern speed $\Omega_{\text{sp}} = 20 \text{ km s}^{-1} \text{ kpc}^{-1}$ and amplitude $A_{\text{sp}} = 650 \text{ km}^2 \text{ s}^{-2} \text{ kpc}^{-1}$. The effect of the spiral arm amplitude was studied for a two-arm spiral with pattern speed $\Omega_{\text{sp}} = 18 \text{ km s}^{-1} \text{ kpc}^{-1}$, and a fixed bar with $M_{\text{bar}} = 9.8 \times 10^9 M_{\odot}$ and $\Omega_{\text{bar}} = 40 \text{ km s}^{-1} \text{ kpc}^{-1}$. The resulting evolution of the bound mass of the clusters is shown in Fig. 4.2, where the top panel shows the effect of varying the bar mass and the bottom panel shows the effect of varying the spiral arm strength. In both cases we also show the evolution for the case of a purely axisymmetric model of the Galaxy.

From Fig. 4.2 it is clear that the disruption time of the cluster is not very sensitive to the parameters of the Galactic model. The range of disruption times across all our simulations is 0.5–2.3 Gyr, with additional scatter introduced due to the different perigalactica and eccentricities of the cluster orbits.

4.4. Current distribution of Solar siblings in the Milky Way

If the Sun's birth cluster was completely disrupted in the Galaxy at around 1.8 Gyr, the Sun and its siblings are currently spread out over the Galactic disk, since they have been going around the Galaxy on individual orbits during the last 2.8 Gyr. In Fig. 4.3 we show four possible distributions of the solar siblings in the Galactic disk. Note that in contrast to the cluster disruption time, the present-day distribution of solar siblings depends strongly on the Galactic parameters, especially on changes in m , Ω_{sp} and Ω_{bar} . This is because the motion of the solar siblings depends on whether their orbits are affected by the CR_{sp} or by the OLR_{bar} . For instance, in panel **a** of Fig. 4.3 we observe that

CHAPTER 4 : THE EVOLUTION OF THE SUN'S BIRTH CLUSTER AND THE SEARCH FOR THE SOLAR SIBLINGS WITH *Gaia*

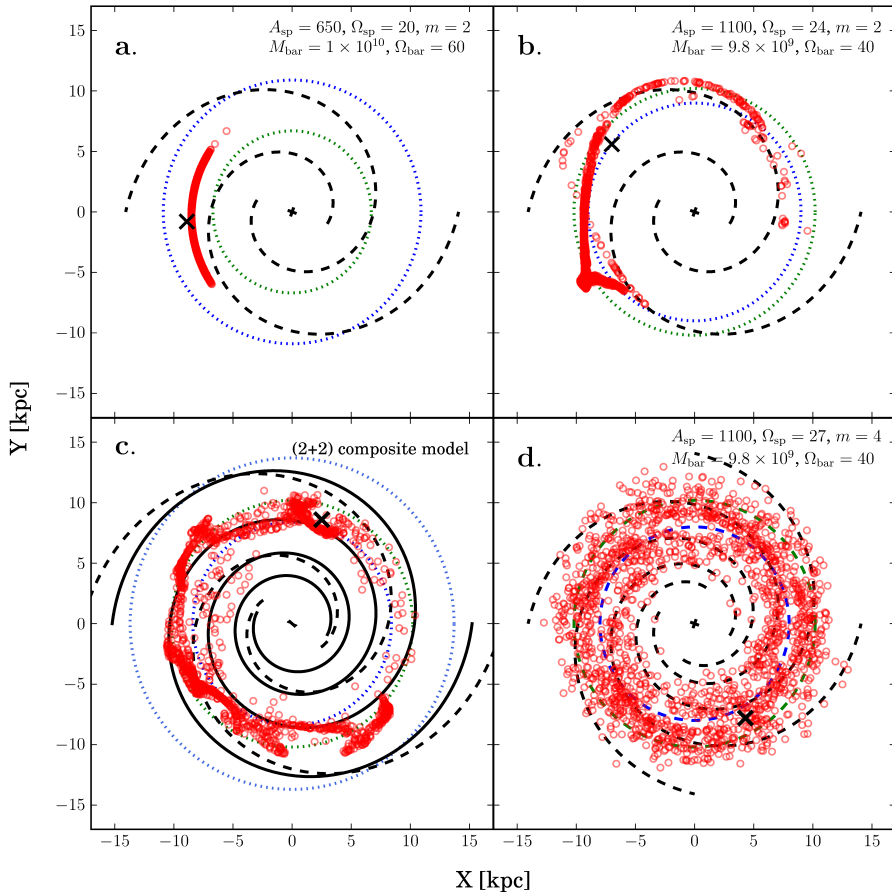


FIGURE 4.3: Present-day distribution of solar siblings in the xy plane. The point $(0,0)$ is the centre of the Milky Way. The dashed black lines represent the potential of the spiral arms at present. The dotted blue and green circles correspond to the CR_{sp} and OLR_{bar} respectively. The black crosses in each panel mark the initial location of the Sun's birth cluster, which is at 9 kpc. Here, the initial mass and radius of the Sun's birth cluster are $1023 M_{\odot}$ and 2 parsec respectively. *Top panels:* Distribution of solar siblings in a Galactic model with two spiral arms. The position of the CR_{sp} and OLR_{bar} are respectively: $(11, 6.7)$ kpc (a) and $(9, 10.2)$ kpc (b). *Bottom panels:* c. Distribution of solar siblings in a (2+2) composite model with $A_{\text{sp}1} = 1300 \text{ km}^2 \text{ s}^{-2} \text{ kpc}^{-1}$. The solid and dashed black lines represent the main and secondary spiral structures with co-rotation resonances located at 8.4 and 13.7 kpc respectively. The OLR_{bar} is at 10.2 kpc. d. Distribution of solar siblings in a Galactic model with four spiral arms. The CR_{sp} and OLR_{bar} are located at 8 and 10.2 kpc respectively.

4.4 CURRENT DISTRIBUTION OF SOLAR SIBLINGS IN THE MILKY WAY

there is not much radial migration with respect to the initial position of the Sun’s birth cluster ($\bar{R}_{\text{sib}} - R_i \sim 0.5$ kpc, where $R_i = ||\mathbf{x}_{\text{cm}}||$). In this example, the Sun and its siblings are not considerably influenced by the CR_{sp} or by the OLR_{bar} during their motion in the Galactic disk. The apocentre and pericentre of the solar siblings is at around 7 and 10 kpc; while the CR_{sp} and OLR_{bar} are located at 11 and 6.7 kpc respectively. This distribution of solar siblings is similar to the distributions predicted by Portegies Zwart [2009] and Brown et al. [2010b].

If the CR_{sp} and the OLR_{bar} are located in the same region where the Sun and its siblings move around the Galaxy, these stars will undergo constant and sudden changes in their angular momentum. As a consequence, the distribution of solar siblings will contain lots of substructures. This effect can be observed in panels **b** and **c** of Fig. 4.3.

When the Sun’s birth cluster evolves in a Galaxy containing four spiral arms, the solar siblings undergo considerable radial migration. As a consequence, the current distribution of solar siblings is highly dispersed in galactocentric radius and azimuth, as observed in panel **d** of Fig. 4.3. In this Galactic environment, some solar siblings can be located at radial distances of up to 3 kpc different from the radial distance of the Sun to the Galactic centre.

Mishurov & Acharova [2011] presented the spatial distribution of solar siblings in a Galactic potential with transient spiral structure of different life-times. They found that the solar siblings are dispersed all over the disk. Some of these stars can be even located at distances larger than 10 kpc with respect to the Galactic centre (see Figs. 9 and 10 in their paper). By comparing these results with the distributions that we obtained for a four-armed spiral structure (panel **d** Fig. 4.3), we infer that the solar siblings would be even more dispersed and located farther from the Sun if the spiral structure of the Milky Way were transient.

Bland-Hawthorn et al. [2010] used stellar diffusion modelling to predict the current distribution of solar siblings in the Galaxy. They used four different approaches, starting from constant and isotropic coefficients to models where they accounted for the impact of churning on the solar siblings. In their approach the solar siblings are always spread all over the Galactic disk (all azimuths), in a configuration like the one shown in Fig. 4.3d. None of their solar sib-

CHAPTER 4 : THE EVOLUTION OF THE SUN'S BIRTH CLUSTER AND THE SEARCH FOR THE SOLAR SIBLINGS WITH *Gaia*

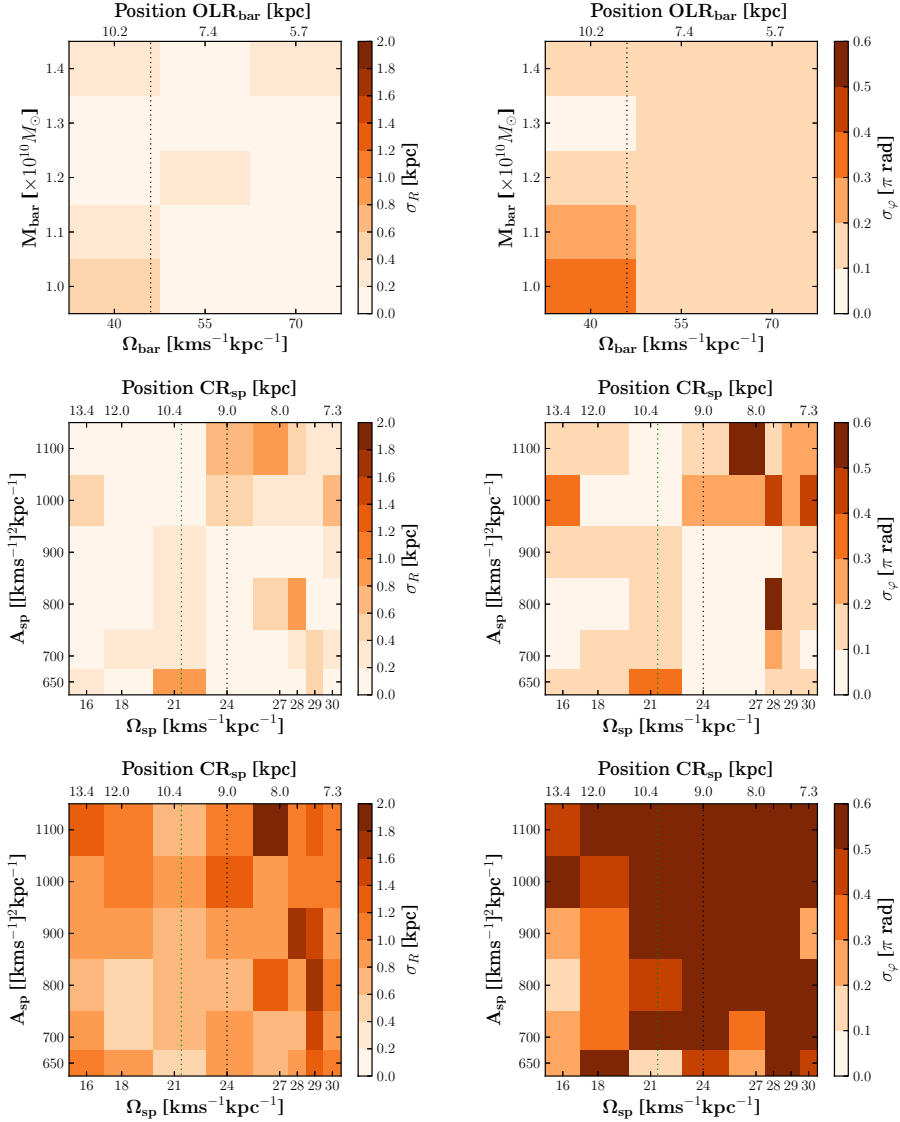


FIGURE 4.4: Radial and angular dispersion of the current distribution of solar siblings as a function of different Galactic parameters. *Top*: The bar parameters vary. Here $A_{\text{sp}} = 650 \text{ km}^2 \text{ s}^{-2} \text{ kpc}^{-1}$, $\Omega_{\text{sp}} = 20 \text{ km s}^{-1} \text{ kpc}^{-1}$ and $m = 2$. *Middle*: The spiral arms parameters change. Here $m = 2$. *Bottom*: The same as in the middle panel but for a Galaxy with $m = 4$. In the Middle and bottom panels, $M_{\text{bar}} = 9.8 \times 10^9 M_\odot$ and $\Omega_{\text{bar}} = 40 \text{ km s}^{-1} \text{ kpc}^{-1}$. For this set of simulations $M_c = 1023 M_\odot$ and $R_c = 2 \text{ pc}$. The dotted black line in the panels corresponds to $\|\mathbf{x}_{\text{cm}}\|$. The dotted green line in the middle and bottom panels represents the OLR_{bar}. In the top panel the value of CR_{sp} is fixed at 10.9 kpc.

4.4 CURRENT DISTRIBUTION OF SOLAR SIBLINGS IN THE MILKY WAY

lings distributions show substructures or stellar concentrations in radius and azimuth, as is shown in Figs. 4.3a–c. Bland-Hawthorn et al. [2010] found that a substantial fraction of solar siblings may be located at galactic longitudes of $l = 90^\circ\text{--}120^\circ$ or $l = 30^\circ\text{--}60^\circ$, depending on the diffusion model employed.

We characterize our predicted present-day distributions of solar siblings by means of their radial and azimuthal dispersion (σ_R and σ_ϕ). These quantities are computed using the Robust Scatter Estimate (RSE) [Lindegren et al., 2012]. The radial dispersion of the distributions shown in panels a–d in Fig. 4.3 are $\sigma_R = 0.1, 0.4, 0.9,$ and 1.8 kpc, respectively. The angular dispersion of these distributions is: $\sigma_\phi = 0.1\pi, 0.2\pi, 0.4\pi,$ and 0.6π rad. Since 0.6π corresponds to the standard deviation of a uniform distribution in azimuth, a highly dispersed distribution (as in panel d of Fig. 4.3) satisfies $\sigma_R > 0.9$ kpc and $\sigma_\phi > 0.4\pi$ rad.

In Fig. 4.4 we show the radial and angular dispersion of the current distribution of solar siblings as a function of different Galactic parameters. In the top panel we varied the parameters of the bar. In the middle and bottom panels, we varied the amplitude and pattern speed of the spiral arms. Note that there is a remarkable increase in σ_R and σ_ϕ when the Galaxy has four spiral arms. In that Galactic potential, 83% of the simulations result in the solar siblings currently being dispersed all over the Galactic disk ($\sigma_R > 0.9$ kpc and $\sigma_\phi > 0.4\pi$ rad). On the contrary, in a Galaxy with two spiral arms (e.g. Fig. 4.4, top and middle panels), the spatial distribution of solar siblings is more ‘clustered’ in radius and azimuth. We found that in 84% of these simulations, $\sigma_R < 0.4$ kpc and $\sigma_\phi < 0.2\pi$ rad.

We computed σ_R and σ_ϕ for different initial conditions of the Sun’s birth cluster, according to the values presented in table 4.3. We found that σ_R and σ_ϕ do not depend on M_c and R_c . The maximum difference in radial and angular dispersion is $\Delta\sigma_{R,\max} = 0.2$ kpc and $\Delta\sigma_{\phi,\max} = 0.2\pi$ rad.

The current distribution of solar siblings constrains the number of stars that can be observed near the Sun. For instance, if the solar siblings are ‘clustered’ in galactocentric radius and azimuth (as shown at the top and middle panels of Fig. 4.4), the probability of finding a large fraction of solar siblings in the vicinity of the Sun increases. Conversely, in more dispersed solar siblings distributions (e.g. bottom panel Fig. 4.4), we expect to find a smaller fraction of solar siblings in the solar vicinity.

We next consider the prospects of identifying solar sibling candidates from the future *Gaia* catalogue data.

4.5. The search for the solar siblings with *Gaia*

The *Gaia* mission will provide an astrometric and photometric survey of more than one billion stars brighter than magnitude $G = 20$ [Lindegren et al., 2008], where G denotes the apparent magnitude in the white light band of used for the astrometric measurements, covering the wavelength range $\sim 350\text{--}1050$ nm [see Jordi et al., 2010]. Parallaxes (ϖ) and proper motions (μ) will be measured with accuracies ranging from 10 to 30 micro-arcseconds (μas) for stars brighter than 15 mag, and from 130 to 600 μas for sources at $G = 20$. For ~ 100 million stars brighter than $G = 16$ *Gaia* will also measure radial velocities (V_r), with accuracies ranging from 1 to 15 km s^{-1} . *Gaia* will not only revolutionize the current view of the Galaxy but will generate a data set which should in principle allow for a search for solar siblings even far away from the Sun.

In this section we use our simulations to predict the number of solar siblings that will be seen by *Gaia*, and to study their distribution in the space of parallax, proper motion, and radial velocity with the aim of establishing efficient ways of selecting solar sibling candidates from the *Gaia* catalogue.

4.5.1. The solar siblings in the *Gaia* catalogue

We first compare the predicted *Gaia* survey of the solar siblings with predictions by Bland-Hawthorn et al. [2010], who considered the prospects for a survey like *GALAH* [De Silva et al., 2015] to varying limiting magnitudes. Following Bland-Hawthorn et al. [2010] we broadly distinguish the possible present-day phase configurations for the solar siblings by referring to the cases shown in the panels of Fig. 4.3 as model **a** and model **b** (compact spatial distribution of solar siblings), model **c** (spatial distribution of solar siblings obtained with the 2 + 2 composite model) and model **d** (highly dispersed spatial distribution of solar siblings).

In predicting the observed kinematic properties of the solar siblings we want to account for the fact that we do not know which of the stars in our simulated

4.5 THE SEARCH FOR THE SOLAR SIBLINGS WITH *Gaia*

clusters is the Sun. The location of the Sun with respect to its siblings will affect the number of siblings that can be observed, especially for clusters that during their dissolution have not spread all over the Galactic disk in azimuth. We therefore proceed as follows. All stars in the simulated cluster located at Galactocentric distances of $R = 8\text{--}9$ kpc and with stellar masses around $1 M_{\odot}$ are considered possible ‘suns’. The *Gaia* observables (ϖ, μ, V_r) of the siblings are then calculated with respect to each of these candidate suns. This results in a set of distributions of siblings over the observables which can be considered collectively in order to account for the uncertain position of the Sun within its dissolved birth cluster.

We used the PYGAIA² code to compute the astrometric properties of the solar siblings. Since we are interested in solar siblings that can be observed by *Gaia*, we only include stars for which $G \leq 20$.

The apparent G magnitude is given by the following equation [Jordi et al., 2010]:

$$G = -2.5 \log \left(\frac{\int_{\lambda_{\min}}^{\lambda_{\max}} F(\lambda) 10^{-0.4A_{\lambda}} S_x(\lambda) d\lambda}{\int_{\lambda_{\min}}^{\lambda_{\max}} F^{\text{Vega}}(\lambda) S_x(\lambda) d\lambda} \right) + G^{\text{Vega}}. \quad (4.6)$$

Here $F(\lambda)$ and $F^{\text{Vega}}(\lambda)$ are the fluxes of a solar sibling and Vega, respectively, as measured above the atmosphere of the Earth (in photons $\text{s}^{-1} \text{nm}^{-1}$). We obtain $F(\lambda)$ through the BaSeL library of synthetic spectra [Lejeune et al., 1998], by searching for the stellar spectral energy distribution which best matches the mass (M_s), radius (R_s) and effective temperature (T_{eff}) of a given solar sibling, where the latter quantities are obtained from the stellar evolution part of the simulations. $F^{\text{Vega}}(\lambda)$ was obtained in the same way by using the following parameters [Jordi et al., 2010]: $T_{\text{eff}} = 9550$ K, $\log g = 3.95$ dex, $[\text{Fe}/\text{H}] = -0.5$ dex and $\epsilon_t = 2 \text{ km s}^{-1}$.

A_{λ} in Eq. 4.6 is the extinction, which is described by:

$$A_{\lambda} = A_V \left(a_{\lambda} + \frac{b_{\lambda}}{R_V} \right), \quad (4.7)$$

where A_V is the extinction in the visual (at $\lambda = 550$ nm). The value of A_V within our simulated Galaxy is computed by means of the Drimmel extinction

²<https://pypi.python.org/pypi/PyGaia/>

CHAPTER 4 : THE EVOLUTION OF THE SUN'S BIRTH CLUSTER AND THE SEARCH FOR THE SOLAR SIBLINGS WITH *Gaia*

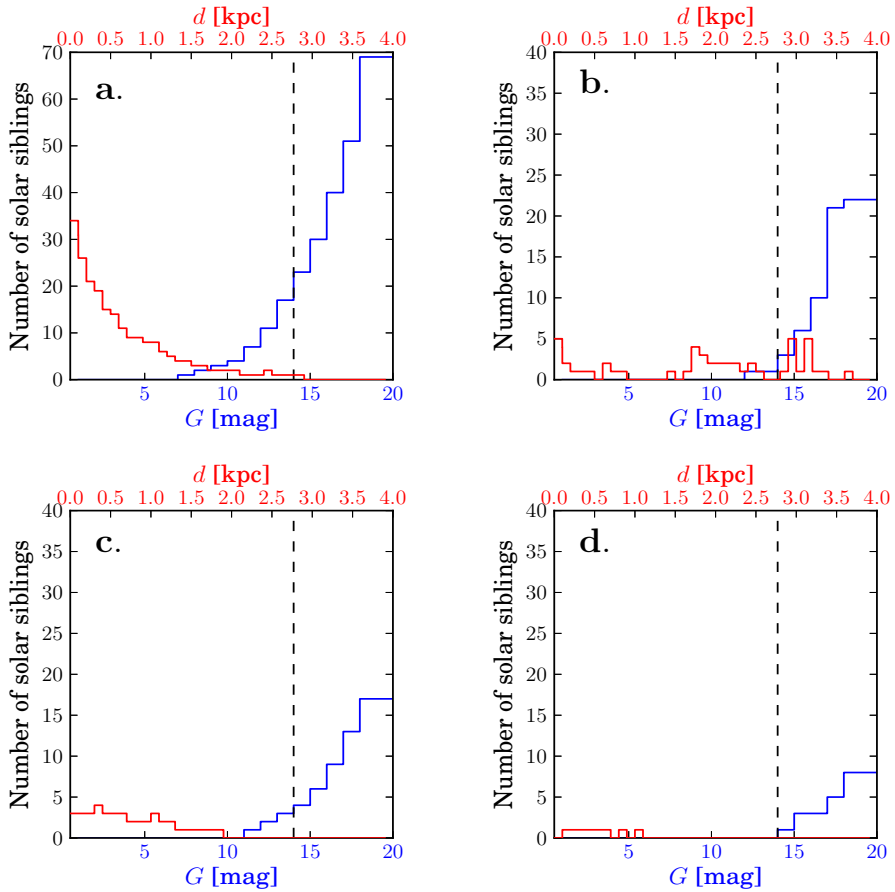


FIGURE 4.5: Median number of solar siblings that *Gaia* is predicted to observe, as a function of their heliocentric distances d (red histograms) and G magnitudes (blue histograms). The letters in the left corner correspond to the distributions shown in Fig. 4.3. The vertical dotted black lines in each panel represent the limiting magnitude of the *GALAH* survey, $G \sim 14$ mag.

4.5 THE SEARCH FOR THE SOLAR SIBLINGS WITH *Gaia*

TABLE 4.4: Median and RSE of the number of solar siblings observed at different heliocentric distances and to different limits in G . The last column lists the total number of solar siblings out to the magnitude limit listed. The first column refers to the distributions shown in Fig. 4.3. The statistics for a given model were obtained from the distribution of the number of observable solar siblings predicted for each of the candidate Suns.

Model	G [mag]	$d \leq 100$ pc	$d \leq 500$ pc	$d \leq 1$ kpc	total
a	≤ 14	14 ± 5	26 ± 7	30 ± 7	31 ± 7
	≤ 16	22 ± 8	50 ± 16	62 ± 18	72 ± 19
	≤ 18	31 ± 13	95 ± 33	121 ± 39	146 ± 38
	≤ 20	33 ± 14	145 ± 49	199 ± 62	268 ± 57
b	≤ 14	1 ± 0.3	1 ± 0.6	1 ± 0.6	1 ± 0.6
	≤ 16	1 ± 0.9	3 ± 1	3 ± 1	4 ± 1
	≤ 18	3 ± 2	8 ± 4	10 ± 6	19 ± 2
	≤ 20	5 ± 3	14 ± 8	19 ± 11	61 ± 0.3
c	≤ 14	1 ± 1	4 ± 2	5 ± 3	6 ± 3
	≤ 16	1 ± 1	8 ± 4	11 ± 5	15 ± 6
	≤ 18	2 ± 2	13 ± 7	19 ± 11	33 ± 16
	≤ 20	2 ± 2	18 ± 10	37 ± 18	61 ± 31
d	≤ 14	0	0	1 ± 0.7	1 ± 1
	≤ 16	0	1 ± 1	2 ± 1	4 ± 1
	≤ 18	0	2 ± 1	4 ± 1	9 ± 2
	≤ 20	0	4 ± 1	10 ± 2	22 ± 4

model [Drimmel et al., 2003]. R_V is the ratio between the extinction and colour excess in the visual band; we use $R_V = 3.1$. a_λ and b_λ are coefficients calculated through the Cardelli extinction law [Cardelli et al., 1989].

The function $S_x(\lambda)$ in Eq. 4.6 corresponds to the *Gaia* pass-bands, which depend on the telescope transmission and the CCD quantum efficiency. To compute the stellar magnitude in G , we use the corresponding pass-band described in Jordi et al. [2010].

Finally, G^{Vega} is the magnitude zero point which is fixed through the measurement of the flux of Vega, such that $G^{\text{Vega}} = 0.03$ mag.

In Fig. 4.5 and Table 4.4 we show the number of solar siblings that might be observed by *Gaia* as a function of their heliocentric distances d and their magnitudes G , where we have averaged over each of the candidate Suns per model. Note that for models **a**, **c** and **d** the largest fraction of solar siblings is located within ~ 500 pc from the Sun. Yet, the number of solar siblings located at this distance is rather small for some cases. In models **c** and **d** for instance, just 18 and 4 solar siblings are at $d \leq 500$ pc on average (see table 4.4). In model **a**, on the other hand, 145 ± 49 solar siblings might be identified. In model **b** the solar siblings are almost uniformly distributed throughout the entire range of d , with more stars at $1.5 \lesssim d \lesssim 3.3$ kpc. A closer look at Fig. 4.5 (and also at table 4.4) reveals that only in the most ‘clustered’ spatial distribution of solar siblings (model **a**) there is a chance to observe tens of solar siblings within 100 pc from the Sun, in accordance with Portegies Zwart [2009] and Valtonen et al. [2015]. In model **d**, on the contrary, it is not possible to observe substantial numbers of solar siblings near the Sun.

Similar predictions of the observable number of solar siblings were made by Bland-Hawthorn et al. [2010] in the context of preparations for chemical tagging surveys, (their table 1). They assumed a larger birth cluster of the Sun (with 2×10^4 stars) with a slightly more massive lower limit on the IMF ($0.15 M_\odot$ vs. $0.08 M_\odot$ in our case).

4.5.2. Selecting solar sibling candidates from the *Gaia* catalogue

Brown et al. [2010b] used their simulated distribution of solar siblings to

4.5 THE SEARCH FOR THE SOLAR SIBLINGS WITH *Gaia*

propose a criterion for the selection of solar sibling candidates on the basis of their observed parallax and proper motion. They basically proposed to select nearby stars with small motions with respect to the Sun. This was motivated by the observation that in that region of the parallax vs. proper motion plane the ratio between the number of siblings and the number of disk stars (in the Hipparcos catalogue) was largest. Given that this contrast between the number solar siblings and disk stars depends on the details of the Galactic potential (as illustrated in Fig. 4.3) we revisit the selection criterion proposed by Brown et al. [2010b] in order to assess how robust it is against the uncertainties in the present-day distribution of solar siblings. We proceed in a similar way as Brown et al. [2010b] and examine the simulated present-day distribution of solar siblings in the space of the astrometric observables (parallax, proper motion, radial velocity), and compare that to the distribution of disk stars. We then search for regions in (ϖ, μ, V_r) where the contrast between solar siblings and disk stars is high.

We illustrate this procedure in Fig. 4.6. Here, the distribution of solar siblings in the proper motion-parallax plane is represented by the red contours. The black contours correspond to a simulation of field disk stars as measured by *Gaia*. We use the *Gaia* Universe Model Snapshot (GUMS) [Robin et al., 2012] to generate a simulated sample of 2.6×10^7 field disk stars. GUMS represents a synthetic catalogue of stars that simulates what *Gaia* will observe. To select only disk stars, we used only the GUMS stars located in a cylindrical region of radius 8 kpc and height 300 pc (i.e. $|z| \leq 150$ pc) centred on to the Sun. The GUMS model includes multiple-star systems. We determine which ones will be resolved by *Gaia* by using a prescription employed within the Data Processing and Analysis Consortium [DPAC, Mignard et al., 2008]³. In this approach the angular separation on the sky that *Gaia* can resolve depends on the apparent magnitudes of the stars in the system, with the minimum separation being ~ 38 mas. For the unresolved cases, a single detection is considered by computing the total integrated magnitude and averaging positions and velocities.

As can be seen in Fig. 4.6, most of the solar siblings are located well within the overall disk population (at distances over 100 pc) making the selection of sibling candidates on the basis of astrometric and radial velocity data alone

³<http://www.cosmos.esa.int/web/gaia/dpac>

CHAPTER 4 : THE EVOLUTION OF THE SUN'S BIRTH CLUSTER AND THE SEARCH FOR THE SOLAR SIBLINGS WITH *Gaia*

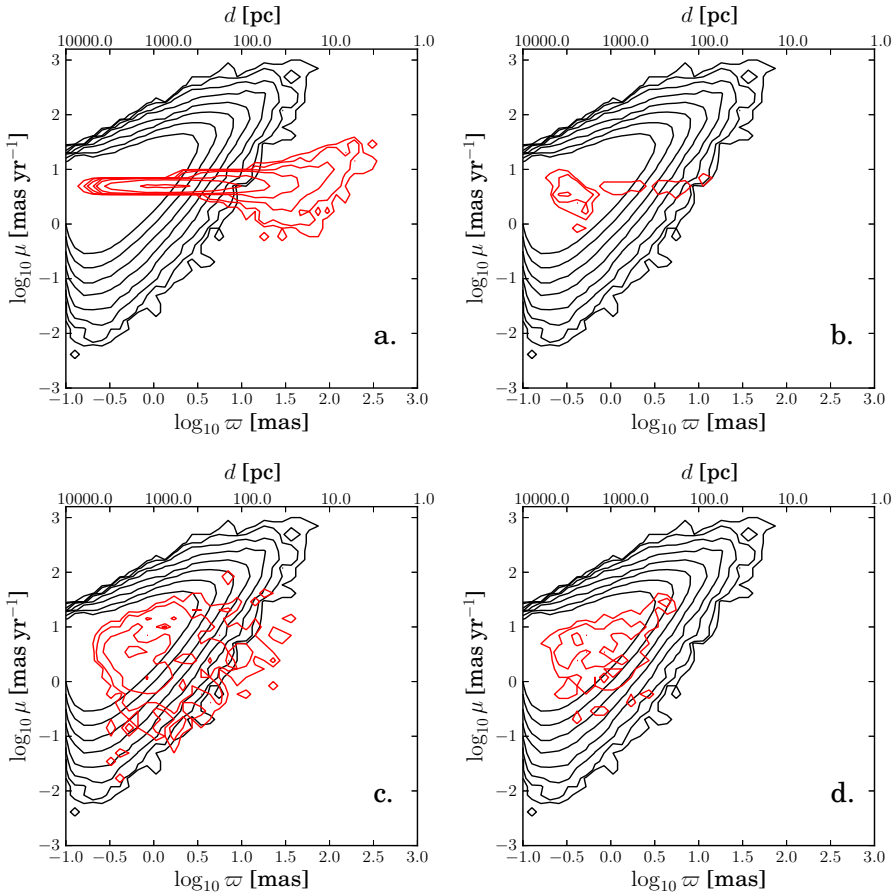


FIGURE 4.6: Distribution of solar siblings (red contours) and simulated *Gaia* data for disk stars (black contours) in the proper motion-parallax plane. Each panel corresponds to the distributions shown in Fig. 4.3. The red and black contours indicate the number of stars in bins of $0.1 \times 0.15 \text{ mas}^2 \text{ yr}^{-1}$. The contour levels are at 1, 3, 10, 30, 100, 300, 1000 and 3000 stars/bin. In the labels of the top, we also show the heliocentric distance corresponding to each parallax. The proper motion axis represents to total proper motion of the star.

4.5 THE SEARCH FOR THE SOLAR SIBLINGS WITH *Gaia*

very difficult. The only area where a high contrast between the number of siblings and disk stars can be expected is at large parallax and small proper motion values. However, and as expected, this contrast depends strongly on the Galactic potential used in predicting the solar sibling distribution. In order to evaluate the robustness of a selection of sibling candidates in (ϖ, μ, V_r) we must take the uncertainties in their distribution into account and we proceed as follows.

We divide the space ϖ , μ and V_r into discrete (3D) bins and determine for a given simulated solar sibling distribution the number of solar siblings N_{sib} in each bin. We also determine the number of disk stars N_{disk} in each bin and then calculate the number $f_{\text{sib}} = N_{\text{sib}}/N_{\text{disk}}$, which we refer to as the sibling fraction. The idea is that a high value of f_{sib} (say $f_{\text{sib}} > 0.5$) suggests that selecting stars from the corresponding (ϖ, μ, V_r) bin in the *Gaia* catalogue should increase the success rate of subsequent searches for solar siblings that examine the astrophysical properties of those stars (age, metallicity, chemical abundance pattern). Alternatively the number f_{sib} can be interpreted as meaning that a star selected from the corresponding bin in (ϖ, μ, V_r) has a probability f_{sib} of being a solar sibling (provided of course that the simulated population of siblings and disk stars is representative of reality).

To account for the uncertainties in the phase space distribution of siblings we repeat the above procedure for each of our 1125 simulated solar sibling populations and for each of the ‘suns’ within a given population of siblings. This leads to a distribution of values of f_{sib} , $p(f_{\text{sib}})$, for each bin in (ϖ, μ, V_r) . This distribution thus reflects different Galactic potential parameters, different initial conditions for the Sun’s birth cluster, and different possible locations of the Sun within the dispersed sibling population. In Fig. 4.7 we show the mean value (top panel), the RSE (middle panel) and the survival function ($sf(0.5)$) (bottom panel) of $p(f_{\text{sib}})$. The survival function corresponds to the fraction of simulations for which $f_{\text{sib}} > 0.5$, which provides a more robust indication of bins in (ϖ, μ, V_r) where a high fraction of solar siblings is likely to be found. Note that the figure shows the statistics for $p(f_{\text{sib}})$ marginalized over the coordinate not included in the plot.

The statistics of f_{sib} shown in Fig. 4.7 show that the proposal by Brown et al. [2010b], to search for solar siblings among nearby stars with small motions with

CHAPTER 4 : THE EVOLUTION OF THE SUN'S BIRTH CLUSTER AND THE SEARCH FOR THE SOLAR SIBLINGS WITH *Gaia*

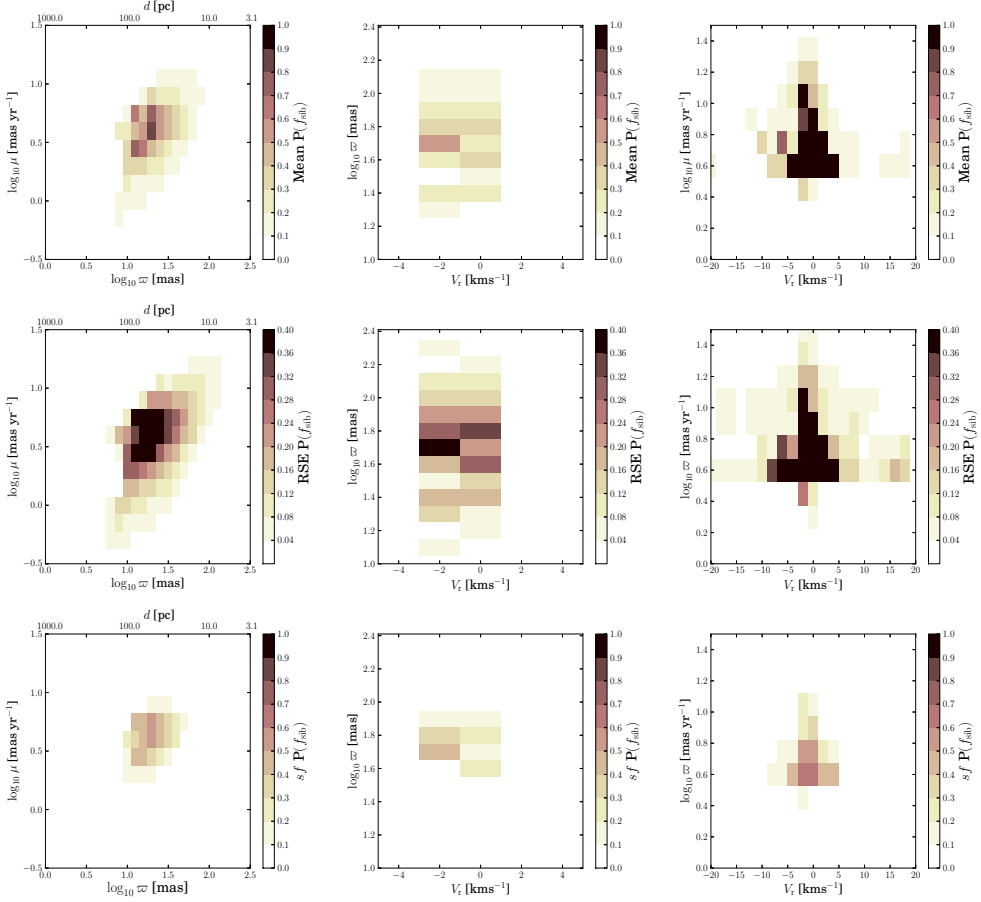


FIGURE 4.7: Mean (top), RSE (middle) and survival function (bottom) of $P(f_{\text{sib}})$ (see text). We show the projections of such a distribution in the proper motion versus parallax plane (left), in the parallax versus radial velocity plane (middle) and in the proper motion versus radial velocity plane (right). The bin area in each column is $(0.1 \times 0.15) \text{ mas}^2 \text{ yr}^{-1}$, $(2 \times 0.15) \text{ km s}^{-1} \text{ mas}$ and $(2 \times 0.1) \text{ km s}^{-1} \text{ mas yr}^{-1}$ respectively.

respect to the Sun, is robust to the uncertainties in the distribution of the solar siblings due to the uncertain Galactic potential and birth cluster conditions. By examining the (ϖ, μ, V_r) in three dimensions and looking for regions where the mean of $p(f_{\text{sib}})$ is above 0.5, we refine the solar sibling candidate selection criterion by Brown et al. [2010b] to:

$$\begin{aligned} \varpi &\geq 5 \text{ mas}; \\ 4 &\leq \mu \leq 6 \text{ mas yr}^{-1}; \\ -2 &\leq V_r \leq 0 \text{ km s}^{-1}. \end{aligned} \tag{4.8}$$

The survival function in this region goes from 0.42 to 0.54. This indicates that despite the uncertainties in the spatial distributions of solar siblings it is still possible to identify regions in the space of ϖ, μ and V_r where more than a half of the stars might be a solar sibling.

4.6. Discussion

4.6.1. Re-evaluation of existing solar sibling candidates

We now use the updated selection criterion from Eq. 4.8 to examine the stars that have been proposed in the literature as solar sibling candidates. The results are shown in table 4.5. In the first column we list the names of the solar siblings candidates. From the second to the ninth columns we show the value and uncertainty of their heliocentric distances, parallaxes, proper motions and radial velocities respectively. These values were obtained from the SIMBAD catalogue [Wenger et al., 2000]. The tenth column lists mean value of f_{sib} for each star, given its coordinates in the space of ϖ, μ and V_r . The corresponding RSE and the survival fraction for that region of phase space are shown in the eleventh and twelfth columns respectively.

Note that the stars HD 147443 and HD 196676 have phase space coordinates corresponding to sibling fractions of 0.76 ± 0.20 and 0.56 ± 0.38 , respectively. Their ages and metallicities are also consistent with those of the Sun [Ramírez et al., 2014]. However, given that these stars do not have solar chemical composition [Ramírez et al., 2014], we can not identify them as solar siblings. This is consistent with the fact that the value of f_{sib} for these stars still allows for

TABLE 4.5: Current Solar siblings candidates. They are sorted by the value of f_{sib} .

Star name (HD no.)	d (pc)	σ_d (pc)	ϖ (mas)	σ_ϖ (mas)	μ (mas yr ⁻¹)	σ_μ (mas yr ⁻¹)	V_r (km s ⁻¹)	σ_{V_r} (km s ⁻¹)	f_{sib}	RSE	sf	Ref.*
147443	92.0	8.38	10.87	0.99	5.26	0.69	-2.1	7.1	0.76	0.20	0.47	1
196676	74.4	2.77	13.44	0.5	5.06	0.54	-0.79	0.1	0.56	0.38	0.42	1
192324	67.11	4.82	14.9	1.07	6.36	2.01	-4.4	0.4	0.02	0.01	0.01	1
46301	107.64	6.6	9.29	0.57	5.85	0.71	-6.7	0.7	0.01	0.005	0.01	3
162826	33.6	0.41	29.76	0.36	20.14	0.38	1.88	0.0063	0.003	0.001	$\sim 10^{-4}$	2
26690	36.34	0.77	27.52	0.58	3.62	0.58	2.4	1.9	0.003	0.001	$\sim 10^{-4}$	3
207164	76.1	3.82	13.14	0.66	3.06	0.7	-7.0	0.3	0.001	0.0005	$\sim 10^{-4}$	3
35317	55.71	2.39	17.95	0.77	6.08	0.51	15.0	0.1	$\sim 10^{-4}$	$\sim 10^{-4}$	$\sim 10^{-4}$	3
175740	81.97	1.75	12.2	0.26	2.95	0.26	-9.18	0.25	$\sim 10^{-4}$	$\sim 10^{-4}$	$\sim 10^{-4}$	1,3
199881	72.2	3.65	13.85	0.7	2.64	0.8	-15.7	0.3	$\sim 10^{-4}$	$\sim 10^{-4}$	$\sim 10^{-4}$	3
101197	82.99	6.82	12.05	0.99	5.66	0.62	7.5	0.3	$\sim 10^{-4}$	$\sim 10^{-4}$	$\sim 10^{-4}$	3
105678	74.02	1.7	13.51	0.31	5.82	0.26	-17.4	0.5	$\sim 10^{-4}$	$\sim 10^{-4}$	$\sim 10^{-4}$	3
219828	72.31	3.87	13.83	0.74	5.86	0.77	-24.14	0.17	$\sim 10^{-4}$	$\sim 10^{-4}$	$\sim 10^{-4}$	3
28676	38.7	0.88	25.84	0.59	4.47	0.73	6.71	0.09	$\sim 10^{-4}$	$\sim 10^{-4}$	$\sim 10^{-4}$	1,3
52242	68.17	2.74	14.67	0.59	5.07	0.64	31.3	0.9	$\sim 10^{-4}$	$\sim 10^{-4}$	$\sim 10^{-4}$	3
95915	66.62	2.13	15.01	0.48	5.09	0.53	16.9	0.3	$\sim 10^{-4}$	$\sim 10^{-4}$	$\sim 10^{-4}$	3
105000	71.07	2.98	14.07	0.59	4.73	0.75	-14.8	1.5	$\sim 10^{-4}$	$\sim 10^{-4}$	$\sim 10^{-4}$	3
148317	79.62	3.49	12.56	0.55	3.45	0.69	-37.6	0.4	$\sim 10^{-4}$	$\sim 10^{-4}$	$\sim 10^{-4}$	3
44821	29.33	0.53	34.1	0.62	5.0	0.44	18.3	0.76	$\sim 10^{-4}$	$\sim 10^{-4}$	$\sim 10^{-4}$	1,3
68814	80.45	7.57	12.43	1.17	3.65	1.03	34.5	0.3	$\sim 10^{-4}$	$\sim 10^{-4}$	$\sim 10^{-4}$	4
7735	85.69	8.81	11.67	1.2	3.5	1.18	21.7	1.4	$\sim 10^{-4}$	$\sim 10^{-4}$	$\sim 10^{-4}$	3
100382	93.98	3.0	10.64	0.34	4.89	0.35	-10.9	0.4	$\sim 10^{-4}$	$\sim 10^{-4}$	$\sim 10^{-4}$	1
199951	70.22	1.28	14.24	0.26	1.78	0.21	17.6	0.8	$\sim 10^{-4}$	$\sim 10^{-4}$	$\sim 10^{-4}$	3
168769	50.18	3.7	19.93	1.47	2.14	1.33	26.4	0.2	$\sim 10^{-4}$	$\sim 10^{-4}$	$\sim 10^{-4}$	1
46100	55.46	2.61	18.03	0.85	9.35	0.94	21.3	0.3	$\sim 10^{-4}$	$\sim 10^{-4}$	$\sim 10^{-4}$	3
83423	72.1	4.94	13.87	0.95	7.96	1.2	-7.3	3.4	$\sim 10^{-4}$	$\sim 10^{-4}$	$\sim 10^{-4}$	2,3
91320	90.5	6.88	11.05	0.84	5.18	0.63	17.5	0.4	$\sim 10^{-4}$	$\sim 10^{-4}$	$\sim 10^{-4}$	1
102928	91.41	4.18	10.94	0.5	0.63	0.34	14.12	0.06	$\sim 10^{-4}$	$\sim 10^{-4}$	$\sim 10^{-4}$	1
168442	19.56	0.62	51.12	1.63	2.3	1.56	-13.8	0.3	$\sim 10^{-4}$	$\sim 10^{-4}$	$\sim 10^{-4}$	1
154747	97.85	8.9	10.22	0.93	8.58	0.78	-14.9	0.3	$\sim 10^{-4}$	$\sim 10^{-4}$	$\sim 10^{-4}$	3
183140	71.84	6.61	13.92	1.28	13.97	0.91	-28.8	0.4	$\sim 10^{-4}$	$\sim 10^{-4}$	$\sim 10^{-4}$	3

*1= Brown et al. [2010b]; 2= Bovyev et al. [2011]; 3= Batista & Fernandes [2012]; 4= Liu et al. [2015]

a significant fraction of stars that are not solar siblings located in the same region of phase space.

Conversely, Ramírez et al. [2014] found that the stars HD 28676, HD 91320, HD 154747 and HD 162826 have the same age, metallicity and chemical composition as the Sun, within the observational errors. However, according to the numbers in Table 4.5 these stars have a low probability of being solar siblings. This also holds for the star HD 68814, which is chemically homogeneous with the Sun [Liu et al., 2015] but is located in a phase space region where $f_{\text{sib}} \sim 10^{-4}$. This discrepancy may be due to the limitations in our simulations, which may lead to underestimates of f_{sib} (see Sect. 4.6.2) or may be attributed to the observation that there is chemical abundance overlap between different clusters [Blanco-Cuaresma et al., 2015], which implies the presence of stars that look like solar siblings even if their phase space properties are very different.

From the small number of stars examined as potential solar siblings it is not possible to draw further conclusions. For more progress on this issue the results of *Gaia* and the complementary abundance surveys, such as *GALAH*, will have to be awaited.

4.6.2. Applicability of the sibling selection criteria

We have shown in this study that despite uncertainties in the Galactic potential parameters and solar birth cluster initial conditions, it is possible to identify a region in the space of parallaxes, proper motion, and radial velocities which is robustly predicted to contain a high fraction of solar siblings with respect to disk stars. However, the selection criterion shown in Eq. 4.8 is only valid for the cluster initial conditions and Galaxy models considered here. Changes in the mass and size of the Sun’s birth cluster or in the modelling of the Milky Way, might alter the region in phase-space where it is more likely to identify solar siblings. For instance, massive clusters (with 10^4 stars) evolving in the Galactic potential described in Sect. 4.2.1 might have lifetimes of around 20 Gyr [Gieles et al., 2007]. Thus, after 4.6 Gyr of evolution, most of the solar siblings would still be bound to the cluster, showing a clumped distribution in the phase-space for most of the Galactic parameters. Conversely, small open clusters (as those described in Sect. 4.2.2) only survive a few Myr in a Galaxy

model containing transient spiral structure and giant molecular clouds [see e.g. Gieles et al., 2006; Lamers & Gieles, 2006; Gieles et al., 2007; Kruijssen et al., 2011]. In such a more realistic potential the solar siblings would be more dispersed in both radius and azimuth, completely mixed with other disk stars, which would (much) lower the mean value of f_{sib} in any given region of (ϖ, μ, V_r) . Another limitation is that we do not consider the vertical motion of the Sun and the vertical force of the bar and spiral arms in the cluster simulations. Although the solar siblings are stars that move within the Galactic disk, the mean value of f_{sib} might change when considering a three-dimensional potential for the Galaxy. For the types of solar birth clusters studied in this work the results thus strongly support the need for chemical abundance surveys to attempt to identify the sun's siblings (and other disrupted clusters).

One could consider making more sophisticated phase space searches for the solar siblings by making use of conserved quantities (energy, angular momentum). However, if open clusters contribute a significant fraction of the stars to the Galactic disk (and all stars existing on somewhat similar orbits) it is not obvious that disrupted open clusters would stand out in integrals of motion spaces. Our simple selection criterion also has the advantage of being defined entirely in the space of observables where the properties of the errors are well understood.

4.7. Summary

We used numerical simulation to study the evolution and disruption of the Sun's birth cluster in the Milky Way. In the simulations we include the gravitational force among the stars in the cluster and the stellar evolution effects on the cluster population. We also include the external tidal field of the Galaxy, which was modelled as an analytical potential containing a bar and spiral arms. We used two Galactic models: one in which the Galaxy has two or four spiral arms and a $(2 + 2)$ composite model in which two spiral arms have smaller strength and pattern speed than the other two arms. The aim of this study is to predict the present-day phase space distribution of the solar siblings (as observed in astrometry and radial velocities) and to understand how *Gaia* data might be used to pre-select solar siblings candidates for follow-up chemical

abundance studies.

We found that the dissolution time-scale of the Sun’s birth cluster is insensitive to the details of the Galactic model, in particular to the parameters of the bar and spiral arms. For the set of simulations carried out in this study, the Sun’s birth cluster is completely disrupted in a time-scale of $0.5 - 2.3$ Gyr, where the differences are due to different eccentricities and perigalactica of the cluster orbits.

After the dissolution of the Sun’s birth cluster, the solar siblings move independently within the potential of the Galaxy. Depending on the Galactic parameters, the solar siblings may currently be more or less dispersed in Galactic radius and azimuth. If the orbits of the solar siblings are not influenced by the CR_{sp} or by the OLR_{bar} , the present-day distribution of the solar siblings is such that most of these stars are in the close vicinity of the Sun. Conversely, if the orbits of the solar siblings are influenced by these two resonances, the current spatial distribution of the siblings is more dispersed in radius and azimuth, with substructures in some regions of the Galactic disk (this is also observed in the $(2 + 2)$ composite model). In Galaxy models with four spiral arms, the solar siblings are spread all over the Galactic disk.

We predicted the *Gaia* observations (astrometry and radial velocities) of solar siblings brighter than $G = 20$ mag. We use the GUMS simulation [Robin et al., 2012] to generate a large sample of stars which mimic the disk stars that *Gaia* will observe. With this information, we computed the sibling fraction $f_{sib} = N_{sib}/N_{disk}$, which can be interpreted as the probability of finding solar siblings in a certain region of the space of ϖ , μ and V_r . Regions in this phase-space where $f_{sib} > 0.5$ indicate that a large fraction of stars located there might be solar siblings. Thus exploring those regions would increase the success rate in finding solar siblings candidates in the future. We found that $f_{sib} > 0.5$ when $\varpi \geq 5$ mas, $4 \leq \mu \leq 6$ masyr $^{-1}$, and $-2 \leq V_r \leq 0$ km s $^{-1}$. This result is very similar to that by Brown et al. [2010b] but is now obtained for a large fraction of simulations covering a broad range of Galactic parameters and initial conditions for the Sun’s birth cluster.

However, this selection criterion is only valid under the assumptions made in this study. Introducing more realism into the simulations (transient spiral arms, molecular clouds) would lower f_{sib} and make the pre-selection of solar

siblings on the basis of distance and kinematic data very inefficient (unless the sun's birth cluster was originally much more massive). This reinforces the conclusion already reached by Bland-Hawthorn et al. [2010] that large scale surveys are needed which are aimed at precisely determining the astrophysical properties of stars, in particular their ages and chemical abundances, if we want to identify the solar family.

Acknowledgements

We thank the anonymous referee for his/her suggestions that greatly improved the manuscript. This work was supported by the Nederlandse Onderzoekschool voor Astronomie (NOVA), the Netherlands Research Council NWO (grants #639.073.803 [VICI], #614.061.608 [AMUSE] and #612.071.305 [LGM]) and by the Gaia Research for European Astronomy Training (GREAT-ITN) network Grant agreement no.: 264895.

CHAPTER 5

THE EFFECT OF GALACTIC STELLAR ENCOUNTERS ON THE OUTER EDGE OF THE SOLAR SYSTEM'S PARKING ZONE

C.A. Martínez-Barbosa, L. Jílková, S. Portegies Zwart and A.G.A. Brown
Article in preparation.

Abstract

The frequency of Galactic stellar encounters the Solar System experienced depends on the local density and velocity dispersion at each position along the orbit of the Sun. The stronger encounters establish the outer limit of the so-called parking zone, which is the region in the plane of the orbital eccentricities and semi-major axes where the planetesimals of the solar system have been perturbed only by interactions with stars belonging to the Sun's birth cluster. We aim to improve the estimate of the number of encounters experienced

by the Sun in the past, as it serves to determine more accurately the outer edge of the parking zone. As a first step, we integrate the orbit of the Sun backwards in time in an analytical potential of the Milky Way. We use different present-day phase-space coordinates of the Sun, according to the measured uncertainties. The resulting orbits are then inserted in an N-body simulation of the Galaxy, where the stellar velocity dispersion is estimated at each position. We compute the Galactic stellar encounters by employing three different solar orbits. We found that the strongest stellar encounters have been with stars with $M = 0.1 M_{\odot}$ and at distances of 741 – 1320 AU. These encounters set the outer edge of the Solar System's parking zone at semi-major axes of 300 – 1300 AU, depending on the orbit of the Sun. These estimates are around one order of magnitude smaller than the determination made by Portegies Zwart & Jilková [2015].

keywords: planets and satellites: dynamical evolution and stability; Sun: general

5.1. Introduction

The Sun orbits in the gravitational potential of the Galaxy. The perturbations by passing stars [Oort, 1950] and by the Galactic gravitational field [Heisler & Tremaine, 1986] play an important role in the evolution of the most remote part of the Solar System, the so called Oort cloud. Oort [1950] suggested that more than 10^{11} icy bodies orbit the Sun with aphelia of $5\text{--}15 \times 10^4$ AU, and isotropically distributed inclinations of their orbital planes. The existence of the Oort cloud was proposed to explain the constant rate of observed new long period comets. The two mechanisms — the gravitational perturbation by the Galactic tide and the encounters with passing field stars — constantly perturb the Oort cloud sending some of its objects back into the planetary region. The Galactic tide has a stronger overall effect when averaged over long time scales [for example Heisler & Tremaine, 1986]. The effect of the encounters is stochastic and helps to keep the Oort cloud isotropic [e.g. Kaib et al., 2011,

and references therein]. The two mechanisms act together and combine in a non-linear way [Rickman et al., 2008].

It is well known that the disc of the Milky Way contains non-axisymmetric rotating patterns — the Galactic bar and spiral arms — which strongly influence the orbits of stars in the Galactic disc. For example, the stars can undergo so-called radial migration [for example Sellwood & Binney, 2002; Roškar et al., 2008a; Minchev & Famaey, 2010] which causes their orbital radii to change by up to several kiloparsec. It is possible that the Sun has experienced radial migration and spent a substantial time close to [Wielen et al., 1996; Minchev et al., 2013] or farther away from the Galactic centre compared to its present distance of about 8 kpc. However, some observational [e.g. Casagrande et al., 2011] and theoretical [e.g. Martínez-Barbosa et al., 2015] studies suggest that the Sun may not have migrated considerably.

The orbit of the Sun in the Galaxy determines the intensity of the gravitational tides the Solar System was exposed to, as well as the number of stars around the Sun that could pass close enough to perturb the Oort cloud. Kaib et al. [2011] investigated the effect of encounters with the field stars and the Galactic tides on the Oort cloud, considering the effect of the radial migration. They simulated the Oort cloud around the Sun, adopting possible solar orbits from the simulation of a Milky Way-like galaxy of Roškar et al. [2008a], including those that experienced no migration and those that experienced strong radial migration (some of their solar analogues get as close as 2 kpc from the Galactic centre and as far as 13 kpc, respectively). They found that the present day structure of the Oort Cloud depends rather strongly on the Sun’s orbital history, in particular on its minimum past Galactocentric distance. The distance of the inner edge of the Oort cloud shows a similar dependence on the orbital history of the Sun and is in addition influenced by the effect of a few strong encounters between the Sun and other stars.

With the increasing amount of precise astrometric and radial velocity data for the stars in the solar neighborhood, several studies have focused on the identification of stars that passed close to the Solar System in the recent past, or will pass close by in the future [Mamajek et al., 2015; Bailer-Jones, 2015; Dybczyński & Berski, 2015]. For example, Mamajek et al. [2015] identified the star that is currently known to have made the closest approach to the Sun —

the so called Scholz's star that passed the Solar System at $0.25_{-0.07}^{+0.11}$ pc. Feng & Bailer-Jones [2015] studied the effect of recent and future stellar encounters, that is, those that are identified based on the observed positions and velocities of the stars in the solar neighborhood. They carried out simulations of the Oort cloud, considering perturbations by the identified encounters and a constant Galactic field at the current solar Galactocentric radius, and kept track of the flux of long-period comets injected into the inner Solar System as a consequence of the encounters. Unlike Kaib et al. [2011], Feng & Bailer-Jones [2015] focused only on the effect of the actually observed perturbers. They conclude that past encounters in their sample explain about 5% of the currently observed long period comets and they suggest that the Solar System experienced more strong, as yet unidentified, encounters.

Portegies Zwart & Jílková [2015] discuss the effect of the stellar encounter history on the structure of the system of planetesimals surrounding the Sun. They considered encounters with stars in the Sun's birth cluster (early on in the history of the Sun) and encounters with field stars that occur as the Sun orbits the Galaxy. The encounters with the field stars set the outer edge of the so called Parking zone of the Solar System [Portegies Zwart & Jílková, 2015]. The parking zone is defined as a region in the plane of semi-major axis and eccentricity of objects orbiting the Sun that have been perturbed by the parental star cluster but not by the planets or the Galactic perturbations. The orbits located in the parking zone maintain a record of the interaction of the Solar System with stars belonging to the Sun's birth cluster. Therefore, these orbits carry information that can constrain the natal environment of the Sun. Recently, Jílková et al. [2015] argued that a population of observed planetesimals with semi-major axes > 150 au and perihelia > 30 au, would live in the parking zone of the Solar System. They also found that such a population might have been captured from a debris disc of another star during a close flyby that happened in the Sun's birth cluster.

The outer edge of the parking zone is defined by the strongest encounter the Solar System experienced after it left its birth cluster. The strength of the encounter is measured by the perturbation of semi-major axes and eccentricity of the bodies in their orbit around the Sun. Portegies Zwart & Jílková [2015] used the impulse approximation [Rickman, 1976] to estimate the effect and

defined the outer edge of the Solar System’s parking zone as corresponding to the perturbation caused by the Scholz’s star [Mamajek et al., 2015]. However, stronger encounters might have happened in the past, as the Sun orbited in the Galactic disc. These encounters would alter the outer edge of the Solar System’s parking zone moving it closer to the Sun. The perturbation strength of the stellar encounters depends on the characteristics of the close encounters with field stars — the mass of the other star, its closest approach and relative velocity. Similar to Scholz’s star, the parameters of some of the recent close encounters can be derived from the observed data [for example Feng & Bailer-Jones, 2015; Dybczyński & Berski, 2015].

Estimates of the number and strength of past encounters are difficult to make because of the large uncertainties in the Galactic environment where the Sun has been moving since it left its birth cluster. These uncertainties are due to the unknown evolution of the Galactic potential (leading to uncertainties in the Sun’s past orbit), which is in turn related to the unknown (population dependent) density and velocity dispersion of the Milky Way stars along the Sun’s orbit. García-Sánchez et al. [2001] studied the recent encounter history of the Sun by integrating its orbit in an analytical Milky Way potential together with 595 stars from the Hipparcos catalogue in order to identify recent and near future encounters. In addition they estimated the encounter frequency for the Sun in its present environment by considering the velocity dispersions and number densities of different types of stars. Rickman et al. [2008] simulated the stellar encounters by assuming random encounter times (for a fixed number of encounters) over 5 billion years and using velocity dispersions for 13 different types of stars (different masses), with relative encounter frequencies for these types taken from García-Sánchez et al. [2001]. An alternative approach based on a numerical model of the Milky Way was taken by Kaib et al. [2011]. The orbits of solar analogues in this model were extracted from a simulation of a Milky Way-like galaxy and then the encounters were simulated by tracking the stellar number density and velocity dispersion along the orbit and then generating random encounters by starting stars at random orientations 1 pc from the Sun. The encounter velocities were generated using the recipe by Rickman et al. [2008].

In this chapter we set out to improve the estimate of the number of encounters the Sun may have experienced in the past, as this serves to better predict the location of the outer edge of the Solar System's parking zone. We compute the number of encounters by employing the largest Milky Way simulation to date, which contains 51 billion particles, divided over a central bulge, a disk and a dark matter halo [Bédorf et al., 2014]. This Galaxy model is used to estimate the velocity dispersion of the stars encountered by the Sun along its orbit. To achieve this we integrate the Sun's orbit back in time using an analytical potential for the Milky Way. The orbit of the Sun is then inserted in a snapshot of the particle simulation and the velocity dispersion of the disk stars is estimated at each position. We employ three different orbits for the Sun (no radial migration, migration inward, migration outward) and use the resulting estimates of the encounter frequencies as a function of stellar mass to discuss the implications for the location of the outer edge of the Solar System's parking zone.

This chapter is organized as follows: In Sect. 5.2 we explain the Galaxy model and we show three possible orbital histories of the Sun. In Sect. 5.3 we use the particle simulation of the Milky Way to estimate the number of encounters along each of these solar orbits, as a function of the mass and closest approach of the encountering star. In Sect. 5.4 we discuss the consequences of this computation on the estimation of the outer edge of the Solar System's parking zone. In Sect. 5.5 we discuss the limitations of our computation and the improvements that might be done in future studies. Finally in Sect. 5.6 we conclude.

5.2. Galaxy model and the solar orbit

We use an analytical potential to model the Milky Way to calculate potential past solar orbits. This Galactic potential is composed of two parts: an axisymmetric component (bulge, disk and dark matter halo) and a non-axisymmetric component (bar and spiral arms). Hereafter r and R represent the spherical and cylindrical radial coordinates respectively, φ is the azimuthal angle measured from the axis of the bar or spiral arms and in the direction opposite to the Galactic rotation, and z is the vertical component, perpendicular

5.2 GALAXY MODEL AND THE SOLAR ORBIT

TABLE 5.1: Modeling parameters of the Milky Way.

<i>Axisymmetric component</i>		
Mass of the bulge (M_b)	$1.41 \times 10^{10} M_\odot$	
Scale length bulge (b_1)	0.3873 kpc	
Disk mass (M_d)	$8.56 \times 10^{10} M_\odot$	
Scale length 1 disk (a_2)	5.31 kpc	1)
Scale length 2 disk (b_2)	0.25 kpc	
Halo mass (M_h)	$1.07 \times 10^{11} M_\odot$	
Scale length halo (a_3)	12 kpc	
<i>Central Bar</i>		
Pattern speed (Ω_{bar})	$55 \text{ km s}^{-1} \text{ kpc}^{-1}$	2)
Mass (M_{bar})	$9.8 \times 10^9 M_\odot$	4)
Semi-major axis (a)	3.1 kpc	5)
Axis ratio (b/a)	0.37	5)
Vertical axis (c)	1 kpc	6)
Orientation	20°	3)
<i>Spiral arms</i>		
Pattern speed (Ω_{sp})	$25 \text{ km s}^{-1} \text{ kpc}^{-1}$	2)
Number of spiral arms (m)	2	7)
Amplitude (A_{sp})	$3.9 \times 10^7 M_\odot \text{ kpc}^{-3}$	4)
Pitch angle (i)	15.5°	4)
Scale length (R_Σ)	2.6 kpc	7)
Scale height (H)	0.3 kpc	7)
Orientation	20°	5)

References: 1) Allen & Santillán [1991]; 2) Gerhard [2011];
3) Romero-Gómez et al. [2011]; 4) Jílková et al. [2012];
5) Martínez-Barbosa et al. [2015]; 6) Monari et al. [2014];
7) Drimmel [2000]; 8) Jurić et al. [2008]

to the plane of the Galactic disk. In the computation of the solar orbit, r , R , φ and z are measured in a frame co-rotating with the bar. The force due to the spiral arms is therefore calculated by translating these coordinates to a frame co-rotating with the spiral arms.

In Sects. 5.2.1- 5.2.3 we give a detailed description of the axisymmetric and non-axisymmetric components of the Galactic potential.

5.2.1. Axisymmetric component

As mentioned before, the axisymmetric component of the Galaxy consists of a bulge, disk and a dark matter halo. We model the bulge of the Milky Way as a Plummer potential [Plummer, 1911]:

$$\Phi_{\text{bulge}} = -\frac{GM_{\text{b}}}{\sqrt{r^2 + b_1^2}}, \quad (5.1)$$

where G corresponds to the gravitational constant, M_{b} is the mass of the bulge, and b_1 is its corresponding scale length.

The disk of the Milky Way was modelled by using a Miyamoto-Nagai potential [Miyamoto & Nagai, 1975], which is described by the expression:

$$\Phi_{\text{disk}} = -\frac{GM_{\text{d}}}{\sqrt{R^2 + \left(a_2 + \sqrt{z^2 + b_2^2}\right)^2}}. \quad (5.2)$$

Here M_{d} corresponds to the mass of the disk. The parameters a_2 and b_2 are constants that modulate its shape. In particular, when $a_2 = 0$, Eq. 5.2 represents a spherical distribution of mass. In the case where $b_2 = 0$, Eq. 5.2 corresponds to the potential of a completely flattened disk.

Finally, we model the dark matter halo by means of a logarithmic potential of the form:

$$\Phi_{\text{halo}} = -\frac{GM(r)}{r} - \frac{GM_{\text{h}}}{1.02a_3} \left[-\frac{1.02}{1 + \mathfrak{R}^{1.02}} + \ln \left(1 + \mathfrak{R}^{1.02} \right) \right]_r^{100}, \quad (5.3)$$

where

$$M(r) = \frac{M_h \mathfrak{R}^{2.02}}{1 + \mathfrak{R}^{1.02}} \quad \text{and}$$

$$\mathfrak{R} = \frac{r}{a_3}.$$

In the expression of above, M_h represents the mass of the halo and a_3 its scale length.

The parameters in Eqs. 5.1, 5.2 and 5.3 were taken from Allen & Santillán [1991] and they are listed in Table 5.1. Although the model introduced by Allen & Santillán [1991] does not precisely represent the current estimates of the mass distribution in the Galaxy, this model has been widely used in studies of orbits of open clusters [Allen et al., 2006; Bellini et al., 2010] and in studies of moving groups in the solar neighbourhood [Antoja et al., 2009, 2011]. Moreover, Jílková et al. [2012] did not find substantial differences in the orbit of an open cluster when the axisymmetric component is described by a different more up-to-date model. Therefore, we do not expect that the modelling of the axisymmetric component of the Galaxy influences the results obtained in this study.

5.2.2. Galactic bar

We model the bar of the Galaxy with a three-dimensional Ferrers potential [Ferrers, 1877], which is represented by the following density

$$\rho_{\text{bar}} = \begin{cases} \rho_0 (1 - n^2)^k & n < 1 \\ 0 & n \geq 1 \end{cases}. \quad (5.4)$$

Here $n^2 = x^2/a^2 + y^2/b^2 + z^2/c^2$ determines the shape of the bar potential, where x , y and z correspond to coordinates measured in a frame corotating with the bar. The parameters a , b and c are the semi-major, semi-minor and vertical axes of the bar, respectively. ρ_0 represents the central density of the bar and k its concentration. Following Romero-Gómez et al. [2011], we chose $k = 1$.

The parameters that describe the bar such as its pattern speed, mass, orientation and axes are currently under debate [for a complete discussion see e.g. Martínez-Barbosa et al., 2015]. Hence, we used values that are within the ranges reported in the literature. These values are listed in Table 5.1.

5.2.3. Spiral arms

The spiral arms are usually represented as periodic perturbations of the axisymmetric potential. We use the prescription given by Cox & Gómez [2002], which models such perturbations in the three-dimensional space. The potential of the spiral arms is given by the following expression:

$$\Phi_{\text{sp}} = -4\pi GHA_{\text{sp}} \exp\left(-\frac{r}{R_{\Sigma}}\right) \sum_n \left(\frac{C_n}{K_n D_n}\right) \times \cos(n\gamma) \left[\text{sech}\left(\frac{K_n z}{\beta_n}\right)\right]^{\beta_n}, \quad (5.5)$$

where H is the scale height, A_{sp} is the amplitude of the spiral arms and R_{Σ} is the scale length. We use $n = 1$ term only, with $C_1 = 8/3\pi$ and the parameters K_1, D_1 and β_1 given by:

$$\begin{aligned} K_1 &= \frac{m}{r \sin i}, \\ \beta_1 &= K_1 H (1 + 0.4 K_1 H), \\ D_1 &= \frac{1 + K_1 H + 0.3 (K_1 H)^2}{1 + 0.3 K_1 H}, \end{aligned}$$

where m and i correspond to the number of arms and pitch angle of the spiral structure respectively.

Finally, the term γ in Eq. 5.5 represents the shape of the spiral structure, which is described by the expression:

$$\gamma = m \left[\varphi - \frac{\ln(r/r_0)}{\tan i} \right].$$

Here r_0 is a parameter which determines the scale length of the spiral arms. Following Jílková et al. [2012], $r_0 = 5.6$ kpc.

As for the bar, the parameters that describe the spiral structure of the Galaxy are rather uncertain [See e.g. Jílková et al., 2012; Martínez-Barbosa et al., 2015]. Therefore, we chose the values that are consistent with the current picture of the spiral arms. These values are listed in table 5.1.

5.2 GALAXY MODEL AND THE SOLAR ORBIT

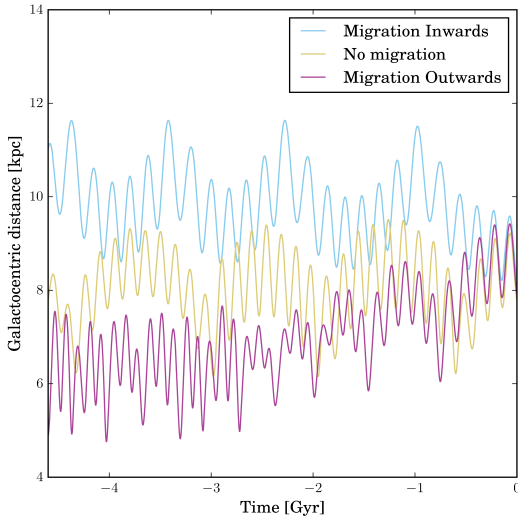


FIGURE 5.1: Possible trajectories of the Sun under the Galactic parameters listed in Table. 5.1. $t = 0$ Gyr represents the current time. The Galactocentric distance is measured in an inertial reference frame.

5.2.4. Solar orbits

We compute the orbit of the Sun backwards in time using the analytical Galaxy model described previously. In this calculation we account for the uncertainty in the present-day Galactocentric phase-space coordinates of the Sun. We employ the same methodology as used by Martínez-Barbosa et al. [2015] for this purpose¹. Thus, we select a sample of 5000 random positions and velocities from a normal distribution centred at the current phase-space coordinates of the Sun. The normal distribution is then centred at (r_{\odot}, v_{\odot}) with standard deviations (σ) corresponding to the uncertainties in these coordinates. The present day location of the Sun is:

$$r_{\odot} = (-8.5, 0, 0.02) \text{ kpc} \quad \text{and}$$

$$\sigma_r = (0.5, 0, 0.005) \text{ kpc}.$$

¹Unlike Martínez-Barbosa et al. [2015] we use a three-dimensional model for the Galaxy in this study.

The present day velocity of the Sun is given by:

$$v_{\odot} = (11.1, 12.4 + V_{\text{LSR}}, 7.25) \text{ km s}^{-1} \quad \text{and}$$

$$\sigma_v = (1.2, 2.1, 0.6) \text{ km s}^{-1}.$$

where v_{\odot} and σ_v were taken from Schönrich et al. [2010] and V_{LSR} corresponds to the velocity in the Local Standard of Rest. According to the Milky Way model parameters listed in Table 5.1, $V_{\text{LSR}} = 226 \text{ km s}^{-1}$.

We integrate the orbit of the Sun backwards in time using each of the 5000 positions and velocities as initial phase-space coordinates. The solar orbits were computed during 4.6 Gyr by using a 6th-order integrator called Rotating BRIDGE [Martínez-Barbosa et al., 2015, Pelupessy et al. in prep.]. This integrator is implemented in the AMUSE framework [Portegies Zwart et al., 2013; Pelupessy et al., 2013].

At the end of the simulation, we obtain a collection of solar orbits, from which we chose three. These orbits are shown in Fig. 5.1 and they represent different orbital histories of the Sun through the Galaxy. The blue orbit for instance shows that the Sun might have been born at $\sim 11 \text{ kpc}$ from the Galactic centre, suggesting migration from outer regions of the Galactic disk to R_{\odot} . Martínez-Barbosa et al. [2015] argued that such a migration could only have happened if the Sun was influenced by the overlapping of the co-rotation resonance of the spiral arms with the Outer Lindblad resonance of the bar. Conversely, the violet orbit shows an example where the Sun migrated from inner parts of the disk to R_{\odot} , in accordance with Wielen et al. [1996] and Minchev et al. [2013]. The yellow orbit represents the case where the Sun does not migrate on average.

The stellar encounter rate experienced by the Sun during the last 4.6 Gyr depends on the solar orbit, due to differences in the stellar density and in the local stellar velocity dispersion. Therefore we compute the number of stellar encounters in each of the orbits shown in Fig. 5.1. The methodology is described in Sect. 5.3.

5.3. Galactic stellar encounters

The frequency of stellar passages between the Sun and other stars in the Galaxy is given by the following expression [i.e. Portegies Zwart & Jílková, 2015]:

$$\Gamma = n(t, x, y, z)\sigma(M, V, r_{\text{enc}})\nu(x, y, z), \quad (5.6)$$

where x, y, z are the Galactocentric coordinates of the Sun at a given time t , measured in an inertial reference frame. M is the mass of the encountering star, V is its heliocentric velocity and r_{enc} is the closest approach distance of such a star to the Sun. The function $n(t, x, y, z)$ corresponds to the number of stars with mass M per unit volume, $\sigma(M, V, r_{\text{enc}})$ is the gravitationally focused cross section and $\nu(x, y, z)$ is the local velocity dispersion. In the next paragraphs we describe the procedure to calculate these functions in detail.

The number of stars with mass M per volume is given by the expression: $n(t, x, y, z) = f\rho(t, x, y, z)$, where f is the fraction of stars with mass M and $\rho(t, x, y, z)$ is the local stellar density. f is calculated by the integration of an initial mass function (IMF) in a mass interval around M . We used a Kroupa IMF [Kroupa, 2001], with limiting masses between 0.08 and $100 M_{\odot}$ to calculate f . In this mass range, the Kroupa IMF is described by the following expression:

$$\phi(m) = \begin{cases} \xi_1 m^{-1.3} & 0.08 < m \leq 0.5M_{\odot}, \\ \xi_2 m^{-2.3} & m > 0.5M_{\odot}. \end{cases} \quad (5.7)$$

Here ξ_1 and ξ_2 are normalization constants. For the mass range mentioned above, $\xi_1 = 1/4$ and $\xi_2 = 1/8$. The local stellar density on the other hand, is computed through the Poisson's equation using the Galaxy potential described in Sect. 5.2. In the calculation of the local stellar density, we do not include the dark matter halo potential.

The gravitationally focused cross-section in Eq. 5.6 can be computed from energy and angular momentum conservation laws. This quantity is thus given by the following expression [Binney & Tremaine, 1987]:

$$\sigma(M, V, r_{\text{enc}}) = \pi r_{\text{enc}}^2 \left(1 + \frac{2GM}{V^2 r_{\text{enc}}} \right). \quad (5.8)$$

Here M and r_{enc} are independent free parameters, while V depends on the mass of the star. This heliocentric velocity is calculated by combining the peculiar velocity of the encountering star with the apex velocity of the Sun². We refer the reader to Rickman et al. [2008] for further details on the calculation of V . In this study we use the final values of V listed in Rickman et al. [2008], Table 1.

Finally, we compute the velocity dispersion (ν) in all the regions of the Galaxy. We obtain ν by using the largest N-body simulation of the Milky Way, which employs a total number of 51 billion particles [Bédorf et al., 2014]. We did not use the Galactic model described in Sect. 5.2 given the complexity in the estimate of ν from an analytical Galaxy model. Although the computation of ν by means of a different Galaxy model is not consistent, we notice that the simulations of Bédorf et al. [2014] have successfully reproduced the stellar velocity distribution within 500 pc from the Sun (see e.g. Fig. 3 in their paper). For simplicity, we also do not take the temporal evolution of ν into account, that is, we calculate ν from a single snapshot. An approach in which the computation of $\rho(t, x, y, z)$ and $\nu(t, x, y, z)$ is made consistently is left for a future work.

We compute ν by using the snapshot of Bédorf's simulation corresponding to 5.6 Gyr of evolution. We chose this snapshot because it corresponds well to the current picture of the Milky Way. In this snapshot, we discretize the space in bins of $(\Delta_R, \Delta_\varphi, \Delta_z) = (0.3 \text{ kpc}, 0.26 \text{ rad}, 5 \text{ pc})$ respectively. This choice ensures a robust estimate of ν because of the number of particles located at each bin. The region in the Galaxy where we determine ν is: $0 \leq R \leq 15 \text{ kpc}$; $0 \leq \varphi \leq 2\pi \text{ rad}$ and $-200 \leq z \leq 200 \text{ pc}$.

The velocity dispersion is given by the following expression:

$$\nu^2 = \frac{\sum_{i=1}^N \left[(v_{R_i} - \bar{v}_R)^2 + (v_{\varphi_i} - \bar{v}_\varphi)^2 + (v_{z_i} - \bar{v}_z)^2 \right]}{N - 1}, \quad (5.9)$$

where v_{R_i} , v_{φ_i} and v_{z_i} are the radial, tangential and vertical velocities of the i -th star in a bin of N stars. \bar{v}_R , \bar{v}_φ and \bar{v}_z are the mean values of the former velocities respectively.

²These two vectors are measured in the local standard of rest of the encountering star.

5.3 GALACTIC STELLAR ENCOUNTERS

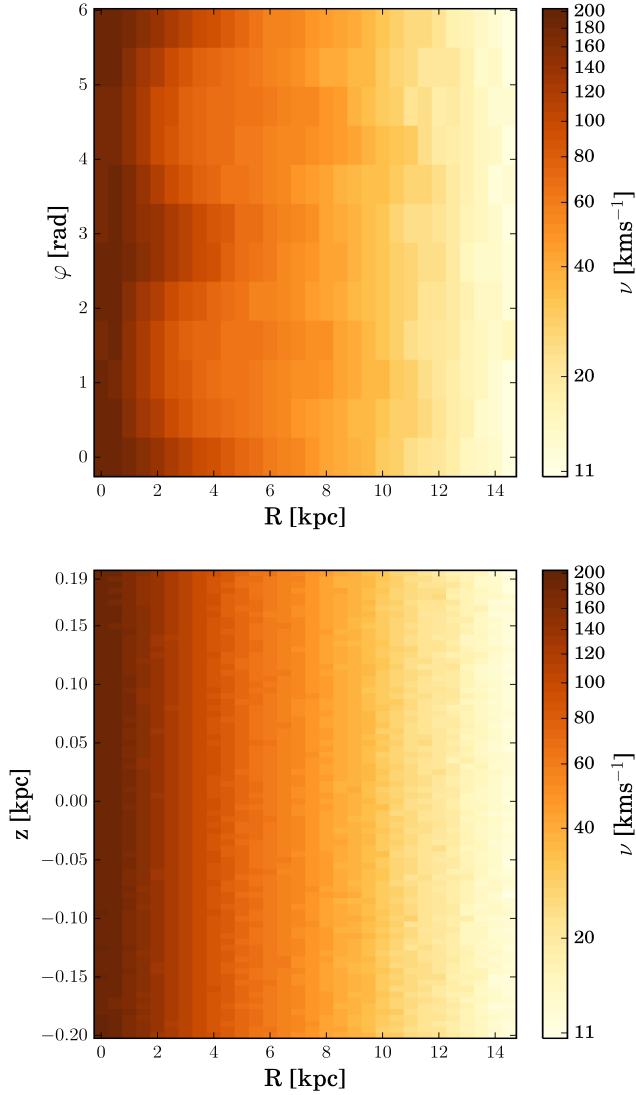


FIGURE 5.2: *Top*: Stellar velocity dispersion of the Milky Way as a function of Galactocentric radius and azimuth where $0 \leq z \leq 5$ pc. *Bottom*: Stellar velocity dispersion as a function of Galactocentric radius and vertical distance where $0 \leq \varphi \leq \pi/6$ rad.

In Fig. 5.2 we show ν as a function of the radius and azimuth (top panel) and as a function of the radius and vertical distance (bottom panel). As is expected, the velocity dispersion decreases with radius, due to a reduction of the stellar density in the outer regions of the Galaxy. At the solar position, we observe that $\nu \simeq 40 \text{ km s}^{-1}$, which is in agreement with measurements of the local velocity dispersion [Nordström et al., 2004; Holmberg et al., 2009].

The velocity dispersion varies periodically with azimuth, being higher in the inner disk (e.g. top panel Fig. 5.2). This variation is a signature of the presence of the bar which extends up to $\sim 4 \text{ kpc}$ from the Galactic centre. The variation of ν with azimuth is smaller in outer regions of the disk and it is due to the presence of spiral arms. From Fig. 5.2 we also observe that the variation of the velocity dispersion with the vertical distance z is low compared to the change with radius or azimuth.

As we mention before, Eq. 5.6 gives the number of encounters between the Sun and another star in the Galaxy over a unit of time. The total number of encounters along the orbit of the Sun is thus given by:

$$n_{\text{enc}} = \int_{t=0}^{4.6 \text{ Gyr}} \Gamma(t, x, y, z, M, V, r_{\text{enc}}) dt. \quad (5.10)$$

In Fig. 5.3 we show contour lines of n_{enc} in terms of the mass and the closest distance of approach of the encountering star, for the three solar orbits shown in Fig. 5.1. The small bumps in the contours, specially when $n_{\text{enc}} = 10^4$, are due to the binning in r_{enc} , which is logarithmic and therefore, they are not related to some physical phenomenon. We analyze the number of encounters with stars that have a mass of $M = [0.1 - 5] M_{\odot}$, and the closest approach distance of $r_{\text{enc}} = [10 - 10^6] \text{ AU}$ (or $4 \times 10^{-5} - 5 \text{ pc}$). As we can observe, the orbit moving closer to the Galactic centre (migration outwards) experiences more stellar encounters of a given mass and closest approach distance than the orbit that moves farther (migration inwards). This is expected, since the stellar density and the velocity dispersion are higher in regions closer to the Galactic centre.

From the large set of stellar encounters obtained, we can look for those that produce the strongest perturbation in the outer regions of the Solar System. These stellar encounters will set the outer edge of the parking zone. Portegies

5.3 GALACTIC STELLAR ENCOUNTERS

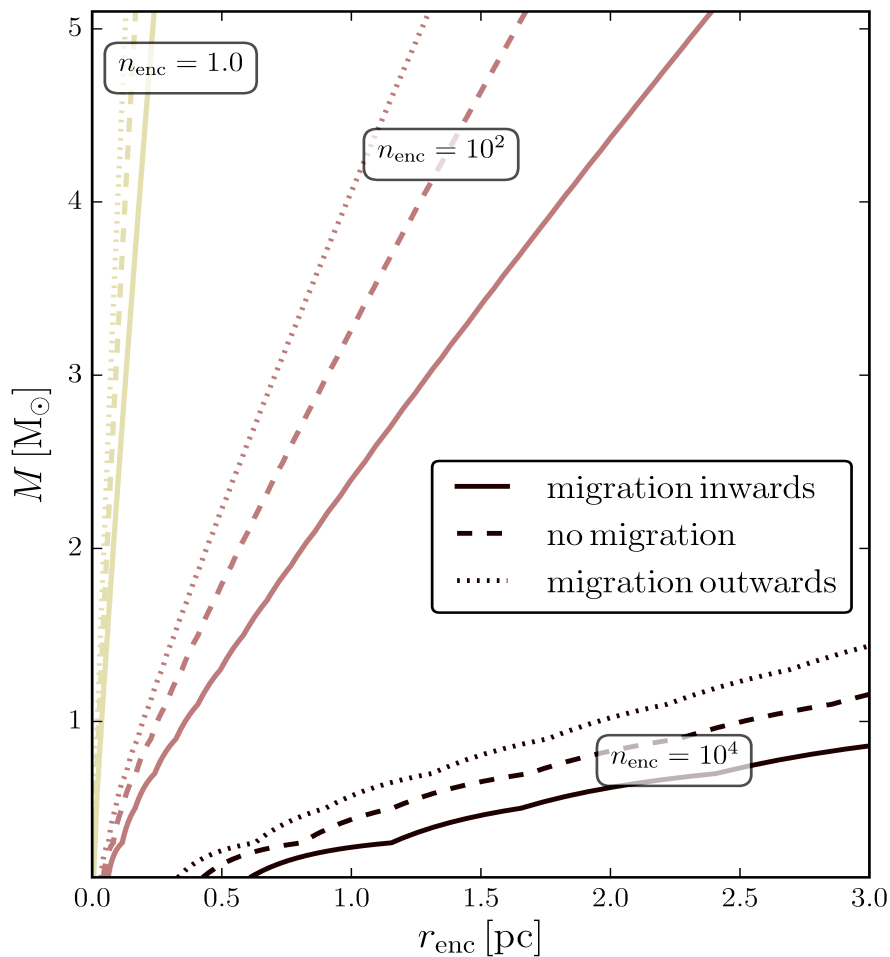


FIGURE 5.3: Contour lines of the Number of stellar encounters experienced by the Sun along its orbit (n_{enc}) in terms of the mass and the closest distance of the encountering star. The different line styles correspond to the solar orbits shown in Fig. 5.1.

TABLE 5.2: Stellar encounters that produce the strongest perturbation on objects orbiting the Sun. These encounters satisfy the condition $n_{\text{enc}} \geq 1$.

Orbit	$M [M_{\odot}]$	$r_{\text{enc}} [\text{AU}]$	$V [\text{kms}^{-1}]$
Migration inwards	0.1	1320	5.1
No migration	0.1	932	5.1
Migration outwards	0.1	741	5.1

Zwart & Jílková [2015], used the encounter with Scholz’s star to determine the location of the outer edge of the Solar System’s parking zone. They found that the effect of this particular encounter has hardly perturbed the Oort cloud down to a distance of 10^5 AU. If the Sun experienced stronger stellar encounters (i.e. with closer and/or more massive stars), the perturbations in the Oort cloud might become important at smaller semi-major axes, shifting inwards the outer edge of the parking zone. In the next section we determine the strongest stellar encounters experienced by the Sun and we make a new estimate of the location of the outer edge of the Solar System’s parking zone.

5.4. The outer limit of the parking zone

The outer edge of the parking zone is estimated for each of the studied orbits by considering the stellar encounters that have occurred at least once. That is, the stellar encounters that satisfy $n_{\text{enc}} \geq 1$. From such encounters we determine—through the impulse approximation [Rickman, 1976]—the encounters that produce the strongest perturbation of the Solar system objects; that is, the perturbation for which the impulse gained is comparable to the velocity at aphelion, as calculated by Portegies Zwart & Jílková [2015].

In Table 5.2 we present the mass, distance of closest approach and relative velocity of the stellar encounters that produce the strongest perturbation of the Solar system for each studied orbit. Note that these encounters come from stars with $M = 0.1 M_{\odot}$, passing at distances comparable to the border between the inner and classical Oort cloud [~ 1500 AU, Trujillo & Sheppard, 2014]. These encounters are stronger than the one with Scholz’s star, a binary system of $0.15 M_{\odot}$ that has recently encountered the Sun at a distance of

5.4 THE OUTER LIMIT OF THE PARKING ZONE

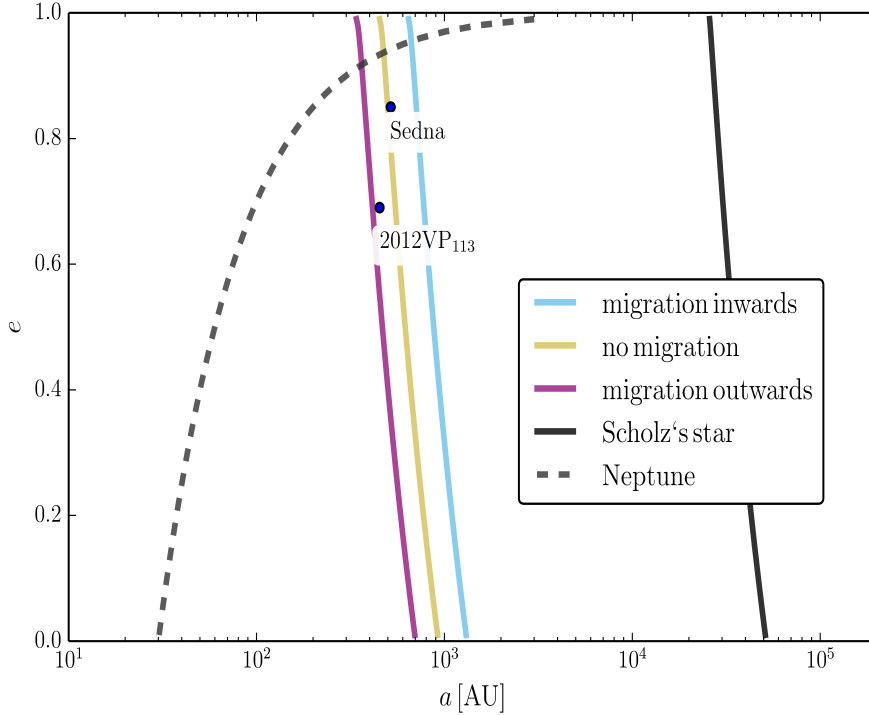


FIGURE 5.4: The penetration to which random Galactic stellar encounters affect the inner Solar System. e and a stand for eccentricity and semi-major axis respectively. The blue, yellow and purple lines show the outer edge of the Solar system’s parking zone according to the solar orbits shown in Fig. 5.1. The black line is the estimate using Scholz’s star [Portegies Zwart & Jílková, 2015]. The dashed black curve corresponds to the Neptune’s perturbing distance, and indicates the inner edge of the parking zone. The two bullets give the orbital parameters for Sedna [Brown et al., 2004] and 2012VP₁₁₃ [Trujillo & Sheppard, 2014].

$$r_{\text{enc}} = 0.25_{-0.07}^{+0.11} \text{ pc [or 50000 AU, Mamajek et al., 2015].}$$

In Fig. 5.4 we show the outer edge of the Solar System's parking zone for the stellar encounters listed in Table 5.2. The solid black line corresponds to the previous estimate made by Portegies Zwart & Jílková [2015] using the Scholz's star. The outer edge of the parking zone given by the encounters derived here is located in the region corresponding to the inner Oort cloud, where objects like Sedna [Brown et al., 2004] and 2012VP₁₁₃ [Trujillo & Sheppard, 2014] reside. The orbit migrating outwards from the denser inner regions of the Galaxy (violet line in Figs. 5.1 and 5.4), results in the smallest parking zone. The orbit migrating inwards from the less dense outer regions (blue line in Figs. 5.1 and 5.4) results in a parking zone that would not perturb the objects on Sedna-like orbits. This picture is consistent with Kaib et al. [2011], who concluded that the inner edge of the classical Oort cloud strongly depends on the orbit of the Sun, being smaller for the orbits that moved closer to the Galactic center.

5.5. discussion

We computed the Galactic stellar encounters in a more complete fashion than in Portegies Zwart & Jílková [2015]. However, we notice that our approach has some limitations. First, we use different Galaxy models to compute the local stellar density and the velocity dispersion along the orbit of the Sun. This is inconsistent, because the local density and the stellar velocity dispersion might be different in the two Galaxy models used, even when these models might reproduce the observed properties of the Milky Way locally. Second, since we used only one snapshot from the N-body Galaxy model, the velocity dispersion along the orbit of the Sun does not evolve with time.

We can improve the estimate of the stellar encounters by computing in a consistent manner the local stellar density and the velocity dispersion along the orbit of the Sun. This can be achieved by using either the analytical or the N-body Galaxy model. In the analytical Galaxy model, the velocity dispersion can be derived by solving the Jeans equations. In this way the temporal evolution of the velocity dispersion is also taken into account. However, several assumptions have to be made in order to obtain an uncomplicated solution for $\nu(t, x, y, z)$. For instance, it is necessary to assume an initial velocity dispersion profile and

the velocity ellipsoid aligned with the R and z axes. [Monari et al., 2013, Sect. 2.3]. In the analytical model of the Galaxy, the local stellar density is computed through the Poisson’s equation, as explained in Sect. 5.3.

In the N-body Galaxy model on the other hand, it is necessary to integrate the orbit of the Sun and to compute $\rho(t, x, y, z)$ and $\nu(t, x, y, z)$ using this model to make a consistent determination of n_{enc} . To account for the temporal evolution of ρ and ν , such calculations must include all the snapshots obtained from the N-body simulation. This procedure however, is not easy to execute given the complexity at handling the huge amount of data provided by each snapshot in the simulation.

The improvements mentioned above require further work and are outside the scope of this chapter. The computation of the encounter probability by using either of the two methods is left for a future work.

5.6. Summary and conclusions

We estimate the number of Galactic stellar encounters the Sun may have experienced in the past, along its orbit through the Galaxy. We aim to improve the previous estimates of the outer edge of the Solar System’s parking zone made by Portegies Zwart & Jílková [2015]. The parking zone is the region in the plane of the eccentricity and semi-major axis where objects orbiting the Sun have been perturbed by stars belonging to the Sun’s birth cluster but not by the planets or by Galactic perturbations. As a consequence, the orbits of objects located in the parking zone maintain a record of the interaction of the Solar System with the so called solar siblings [Portegies Zwart, 2009]. These orbits carry information that can constrain the natal environment of the Sun.

We use an analytical potential containing a bar and spiral arms to model the Galaxy. In this potential we integrate the orbit of the Sun back in time during 4.6 Gyr. Since we include the uncertainties in the present-day phase-space coordinates of the Sun, we obtain a collection of possible orbital histories. Here we study three different orbits, depending on the migration experienced by the Sun namely: migration inwards, no migration and migration outwards. The Galactic stellar encounters are estimated for each of these orbits.

We compute the number of Galactic stellar encounters by employing the

largest Milky Way simulation to date [Bédorf et al., 2014]. We insert the orbits of the Sun in a snapshot of this particle simulation and we estimate the velocity dispersion of the stars at each position. The resulting estimates of the encounter frequencies as a function of stellar mass and closest approach distance are used in the impulse approximation [Rickman, 1976] to determine the encounters that produce the strongest perturbation on the objects in the Oort cloud. Such stellar encounters determine the outer edge of the parking zone of the Solar System.

We found that the location of the outer edge of the parking zone depends on the solar orbit and that the Sun experienced stronger stellar encounters than those with the Scholz's star. As a consequence, the location of the outer edge of the parking zone is closer to the Sun than the previous estimates made by Portegies Zwart & Jílková [2015] and is comparable to the border between the inner and outer Oort cloud. Regardless of the migration of the solar orbit, we find that objects in the Solar System with semi-major axis smaller than 300 AU have not been perturbed by encounters with field stars. However, depending on the migration of the solar orbit, it is possible that the inner Oort cloud (including Sedna) has been perturbed.

To make a better estimate of the Galactic stellar encounters, it is necessary to evaluate the stellar density and the velocity dispersion at each position along the solar orbit using a Galaxy model that accounts for the evolution of the Milky Way. This would lead to a more refined determination of the outer edge of the parking zone.

Acknowledgements

This work was supported by the Nederlandse Onderzoekschool voor Astronomie (NOVA), the Netherlands Research Council NWO (grants #639.073.803 [VICI], #614.061.608 [AMUSE] and #612.071.305 [LGM]).

BIBLIOGRAPHY

- S. J. Aarseth, 2003. *Gravitational N-Body Simulations*.
- I. A. Acharova, Y. N. Mishurov, & M. R. Rasulova, 2011. *MNRAS*, 415:L11–L15.
- F. C. Adams, 2010. *ARA&A*, 48:47–85.
- F. C. Adams & G. Laughlin, 2001. *Icarus*, 150:151–162.
- A. Ahmad & L. Cohen, 1973. *ApJ*, 179:885–896.
- C. Allen, E. Moreno, & B. Pichardo, 2006. *ApJ*, 652:1150–1169.
- C. Allen & A. Santillán, 1991. *Rev.Mex.Astron.Astrofis.*, 22:255–263.
- L. Allen, S. T. Megeath, R. Gutermuth, et al., 2007. *Protostars and Planets V*, pages 361–376.
- C. Allende Prieto, S. R. Majewski, R. Schiavon, et al., 2008. *Astronomische Nachrichten*, 329:1018.
- T. Antoja, F. Figueras, M. Romero-Gómez, et al., 2011. *MNRAS*, 418:1423–1440.
- T. Antoja, O. Valenzuela, B. Pichardo, et al., 2009. *ApJ*, 700:L78–L82.
- E. Athanassoula, M. Romero-Gómez, & J. J. Masdemont, 2009. *MNRAS*, 394:67–81.
- C. A. L. Bailer-Jones, 2015. *A&A*, 575:A35.
- J. Bakos, I. Trujillo, & M. Pohlen, 2008. *ApJ*, 683:L103–L106.
- S. F. A. Batista, V. Z. Adibekyan, S. G. Sousa, et al., 2014. *A&A*, 564:A43.

BIBLIOGRAPHY

- S. F. A. Batista & J. Fernandes, 2012. *New Astron.*, 17:514–519.
- H. Baumgardt & J. Makino, 2003. *MNRAS*, 340:227–246.
- J. Bédorf, E. Gaburov, M. S. Fujii, et al., 2014. In *Proceedings of the International Conference for High Performance Computing, Networking, Storage and Analysis*, p. 54-65, pages 54–65.
- R. Belleman, J. Bédorf, & S. F. Portegies Zwart, 2014. “Kirin: N-body simulation library for GPUs.” Astrophysics Source Code Library.
- A. Bellini, L. R. Bedin, B. Pichardo, et al., 2010. *A&A*, 513:A51.
- R. A. Benjamin, E. Churchwell, B. L. Babler, et al., 2005. *ApJ*, 630:L149–L152.
- T. Bensby, S. Feltzing, & M. S. Oey, 2014. *A&A*, 562:A71.
- T. Bensby, A. R. Zenn, M. S. Oey, et al., 2007. *ApJ*, 663:L13–L16.
- I. Berentzen & E. Athanassoula, 2012. *MNRAS*, 419:3244–3257.
- M. Bergemann, G. R. Ruchti, A. Serenelli, et al., 2014. *A&A*, 565:A89.
- J. Binney & S. Tremaine, 1987. *Galactic dynamics*.
- J. C. Bird, S. Kazantzidis, & D. H. Weinberg, 2012. *MNRAS*, 420:913–925.
- N. Bissantz & O. Gerhard, 2002. *MNRAS*, 330:591–608.
- S. Blanco-Cuaresma, C. Soubiran, U. Heiter, et al., 2015. *A&A*, 577:A47.
- J. Bland-Hawthorn, M. R. Krumholz, & K. Freeman, 2010. *ApJ*, 713:166–179.
- V. V. Bobylev & A. T. Bajkova, 2014. *MNRAS*, 437:1549–1553.
- V. V. Bobylev, A. T. Bajkova, A. Mylläri, et al., 2011. *Astronomy Letters*, 37:550–562.
- T. Boekholt & S. Portegies Zwart, 2015. *Computational Astrophysics and Cosmology*, 2:2.
- S. Boissier & N. Prantzos, 2000. *MNRAS*, 312:398–416.
- A. Bonanno, H. Schlattl, & L. Paternò, 2002. *A&A*, 390:1115–1118.
- J. Bovy, C. Allende Prieto, T. C. Beers, et al., 2012a. *ApJ*, 759:131.
- J. Bovy, H.-W. Rix, & D. W. Hogg, 2012b. *ApJ*, 751:131.
- R. Brasser & M. E. Schwamb, 2015. *MNRAS*, 446:3788–3796.
- A. G. A. Brown, S. F. Portegies Zwart, & J. Bean, 2010a. *MNRAS*, 407:458–464.
- A. G. A. Brown, S. F. Portegies Zwart, & J. Bean, 2010b. *MNRAS*, 407:458–464.
- M. E. Brown, C. Trujillo, & D. Rabinowitz, 2004. *ApJ*, 617:645–649.
- J. A. Cardelli, G. C. Clayton, & J. S. Mathis, 1989. *ApJ*, 345:245–256.

- D. Carollo, T. C. Beers, M. Chiba, et al., 2010. *ApJ*, 712:692–727.
- D. Carollo, T. C. Beers, Y. S. Lee, et al., 2007. *Nature*, 450:1020–1025.
- G. Carraro, 2014. In *IAU Symposium*, editors S. Feltzing, G. Zhao, N. A. Walton, et al., volume 298 of *IAU Symposium*, pages 7–16.
- L. Casagrande, R. Schönrich, M. Asplund, et al., 2011. *A&A*, 530:A138.
- C. Chiappini, F. Matteucci, & D. Romano, 2001. *ApJ*, 554:1044–1058.
- M. Chiba & T. C. Beers, 2000. *AJ*, 119:2843–2865.
- E. Churchwell, B. L. Babler, M. R. Meade, et al., 2009. *PASP*, 121:213–230.
- J. Comparetta & A. C. Quillen, 2012. *ArXiv e-prints*.
- G. Contopoulos & P. Grosbol, 1986. *A&A*, 155:11–23.
- D. P. Cox & G. C. Gómez, 2002. *ApJS*, 142:261–267.
- S. Daflon & K. Cunha, 2004. *ApJ*, 617:1115–1126.
- G. M. De Silva, K. C. Freeman, J. Bland-Hawthorn, et al., 2007. *AJ*, 133:694–704.
- G. M. De Silva, K. C. Freeman, J. Bland-Hawthorn, et al., 2015. *MNRAS*, 449:2604–2617.
- G. M. De Silva, C. Sneden, D. B. Paulson, et al., 2006. *AJ*, 131:455–460.
- W. Dehnen, 2000. *AJ*, 119:800–812.
- W. Dehnen, 2014. *Computational Astrophysics and Cosmology*, 1:1.
- W. Dehnen & J. J. Binney, 1998. *MNRAS*, 298:387–394.
- W. S. Dias & J. R. D. Lépine, 2005. *ApJ*, 629:825–831.
- L. Dones, P. R. Weissman, H. F. Levison, et al., 2004. In *Star Formation in the Interstellar Medium: In Honor of David Hollenbach*, editors D. Johnstone, F. C. Adams, D. N. C. Lin, et al., volume 323 of *Astronomical Society of the Pacific Conference Series*, page 371.
- R. Drimmel, 2000. *A&A*, 358:L13–L16.
- R. Drimmel, A. Cabrera-Lavers, & M. López-Corredoira, 2003. *A&A*, 409:205–215.
- D. Dukes & M. R. Krumholz, 2012. *ApJ*, 754:56.
- E. Dwek, R. G. Arendt, M. G. Hauser, et al., 1995. *ApJ*, 445:716–730.
- P. A. Dybczyński & F. Berski, 2015. *MNRAS*, 449:2459–2471.
- B. Edvardsson, J. Andersen, B. Gustafsson, et al., 1993. *A&A*, 275:101.
- D. J. Eisenstein & P. Hut, 1998. *ApJ*, 498:137–142.
- C. Faure, A. Siebert, & B. Famaey, 2014. *MNRAS*, 440:2564–2575.

BIBLIOGRAPHY

- F. Feng & C. A. L. Bailer-Jones, 2013. *ApJ*, 768:152.
- F. Feng & C. A. L. Bailer-Jones, 2014. *MNRAS*, 442:3653–3673.
- F. Feng & C. A. L. Bailer-Jones, 2015. *ArXiv e-prints*.
- F. Fermani & R. Schönrich, 2013. *MNRAS*, 432:2402–2419.
- N. M. Ferrers, 1877. *Pure Appl. Math.*, 14:1.
- K. Freeman & J. Bland-Hawthorn, 2002. *ARA&A*, 40:487–537.
- H. T. Freudenreich, 1998. *ApJ*, 492:495–510.
- E. D. Friel, 1995. *ARA&A*, 33:381–414.
- K. Fuhrmann, 2004. *Astronomische Nachrichten*, 325:3–80.
- K. Fuhrmann, 2008. *MNRAS*, 384:173–224.
- M. Fujii, M. Iwasawa, Y. Funato, et al., 2007. *PASJ*, 59:1095–.
- M. S. Fujii & J. Baba, 2012. *MNRAS*, 427:L16–L20.
- M. S. Fujii, J. Baba, T. R. Saitoh, et al., 2011. *ApJ*, 730:109.
- R. Fux, 2000. In *Dynamics of Galaxies: from the Early Universe to the Present*, editors F. Combes, G. A. Mamon, & V. Charmandaris, volume 197 of *Astronomical Society of the Pacific Conference Series*, page 27.
- J. García-Sánchez, P. R. Weissman, R. A. Preston, et al., 2001. *A&A*, 379:634–659.
- O. Gerhard, 2011. *Memorie della Societa Astronomica Italiana Supplementi*, 18:185.
- M. Gieles, E. Athanassoula, & S. F. Portegies Zwart, 2007. *MNRAS*, 376:809–819.
- M. Gieles, D. C. Heggie, & H. Zhao, 2011. *MNRAS*, 413:2509–2524.
- M. Gieles, S. F. Portegies Zwart, H. Baumgardt, et al., 2006. *MNRAS*, 371:793–804.
- G. Gilmore, S. Randich, M. Asplund, et al., 2012. *The Messenger*, 147:25–31.
- G. Gilmore & N. Reid, 1983. *MNRAS*, 202:1025–1047.
- S. P. Goodwin & A. P. Whitworth, 2004. *A&A*, 413:929–937.
- B. Gustafsson, 1998. *Space Sci. Rev.*, 85:419–428.
- B. Gustafsson, 2008. *Physica Scripta Volume T*, 130(1):014036.
- B. Gustafsson, J. Meléndez, M. Asplund, et al., 2010. *Ap&SS*, 328:185–191.
- P. L. Hammersley, F. Garzón, T. J. Mahoney, et al., 2000. *MNRAS*, 317:L45–L49.
- M. Haywood, 2008. *MNRAS*, 388:1175–1184.

- M. Haywood, P. Di Matteo, M. D. Lehnert, et al., 2013. *A&A*, 560:A109.
- D. C. Heggie & R. D. Mathieu, 1986. In *The Use of Supercomputers in Stellar Dynamics*, editors P. Hut & S. L. W. McMillan, volume 267 of *Lecture Notes in Physics*, Berlin Springer Verlag, page 233.
- E. Heirer, C. Lubich, & G. Wanner, 2006. *Geometric numerical integration*, volume 31.
- J. Heisler & S. Tremaine, 1986. *Icarus*, 65:13–26.
- C. Hellström & S. Mikkola, 2010. *Celestial Mechanics and Dynamical Astronomy*, 106:143–156.
- A. Helmi, S. D. M. White, P. T. de Zeeuw, et al., 1999. *Nature*, 402:53–55.
- A. Higuchi & E. Kokubo, 2015. *AJ*, 150:26.
- A. Higuchi, E. Kokubo, H. Kinoshita, et al., 2007. *AJ*, 134:1693–1706.
- J. Holmberg, B. Nordström, & J. Andersen, 2009. *A&A*, 501:941–947.
- P. Hut, W. Alvarez, W. P. Elder, et al., 1987. *Nature*, 329:118–126.
- P. Hut, J. Makino, & S. McMillan, 1995. *ApJ*, 443:L93–L96.
- R. A. Ibata, G. Gilmore, & M. J. Irwin, 1994. *Nature*, 370:194–196.
- Ž. Ivezić, B. Sesar, M. Jurić, et al., 2008. *ApJ*, 684:287–325.
- M. Iwasawa, S. Portegies Zwart, & J. Makino, 2015. *Computational Astrophysics and Cosmology*, 2:6.
- L. Jílková, G. Carraro, B. Jungwiert, et al., 2012. *A&A*, 541:A64.
- L. Jílková, S. Portegies Zwart, T. Pijloo, et al., 2015. *MNRAS*, 453:3157–3162.
- C. I. Johnson, R. M. Rich, C. Kobayashi, et al., 2013. *ApJ*, 765:157.
- C. Jordi, M. Gebran, J. M. Carrasco, et al., 2010. *A&A*, 523:A48.
- M. Jurić, Ž. Ivezić, A. Brooks, et al., 2008. *ApJ*, 673:864–914.
- N. A. Kaib, R. Roškar, & T. Quinn, 2011. *Icarus*, 215:491–507.
- J. S. Kalirai, 2012. *Nature*, 486:90–92.
- I. R. King, 1966. *AJ*, 71:64.
- J. Kláčka, R. Nagy, & M. Jurči, 2012. *MNRAS*, 427:358–371.
- G. Kordopatis, G. Gilmore, R. F. G. Wyse, et al., 2013. *MNRAS*, 436:3231–3246.
- P. Kroupa, 2001. *MNRAS*, 322:231–246.
- J. M. D. Kruijssen, F. I. Pelupessy, H. J. G. L. M. Lamers, et al., 2011. *MNRAS*, 414:1339–1364.
- C. J. Lada & E. A. Lada, 2003. *ARA&A*, 41:57–115.

BIBLIOGRAPHY

- H. J. G. L. M. Lamers & M. Gieles, 2006. *A&A*, 455:L17–L20.
- Y.-W. Lee, S.-I. Han, S.-J. Joo, et al., 2013. *ApJ*, 778:L13.
- T. Lejeune, F. Cuisinier, & R. Buser, 1998. *A&AS*, 130:65–75.
- J. R. D. Lépine, I. A. Acharova, & Y. N. Mishurov, 2003. *ApJ*, 589:210–216.
- J. R. D. Lépine, P. Cruz, S. Scarano, Jr., et al., 2011a. *MNRAS*, 417:698–708.
- J. R. D. Lépine, A. Roman-Lopes, Z. Abraham, et al., 2011b. *MNRAS*, 414:1607–1616.
- C. C. Lin, C. Yuan, & F. H. Shu, 1969. *ApJ*, 155:721.
- L. Lindegren, C. Babusiaux, C. Bailer-Jones, et al., 2008. In *IAU Symposium*, editors W. J. Jin, I. Platais, & M. A. C. Perryman, volume 248 of *IAU Symposium*, pages 217–223.
- L. Lindegren, U. Lammers, D. Hobbs, et al., 2012. *A&A*, 538:A78.
- C. Liu, G. Ruchti, S. Feltzing, et al., 2015. *A&A*, 575:A51.
- J. P. Madrid, J. R. Hurley, & M. Martig, 2014. *ApJ*, 784:95.
- J. P. Madrid, J. R. Hurley, & A. C. Sippel, 2012. *ApJ*, 756:167.
- L. Magrini, S. Randich, P. Donati, et al., 2015. *A&A*, 580:A85.
- L. Magrini, P. Sestito, S. Randich, et al., 2009. *A&A*, 494:95–108.
- J. Makino, P. Hut, M. Kaplan, et al., 2006. *New Astron.*, 12:124–133.
- E. E. Mamajek, S. A. Barenfeld, V. D. Ivanov, et al., 2015. *ApJ*, 800:L17.
- C. A. Martínez-Barbosa, A. G. A. Brown, & S. Portegies Zwart, 2015. *MNRAS*, 446:823–841.
- I. Martinez-Valpuesta & O. Gerhard, 2011. *ApJ*, 734:L20.
- M. Martos, X. Hernandez, M. Yáñez, et al., 2004. *MNRAS*, 350:L47–L51.
- T. Matsumoto, S. Hayakawa, H. Koizumi, et al., 1982. In *The Galactic Center*, editors G. R. Riegler & R. D. Blandford, volume 83 of *American Institute of Physics Conference Series*, pages 48–52.
- F. Matteucci & P. Francois, 1989. *MNRAS*, 239:885–904.
- P. J. McMillan, 2011. *MNRAS*, 414:2446–2457.
- P. J. McMillan & J. J. Binney, 2010. *MNRAS*, 402:934–940.
- S. L. W. McMillan & S. J. Aarseth, 1993. *ApJ*, 414:200–212.
- A. L. Melott, R. K. Bambach, K. D. Petersen, et al., 2012. *Journal of Geology*, 120:217–226.
- F. Mignard, C. Bailer-Jones, U. Bastian, et al., 2008. In *IAU Symposium*, editors W. J. Jin, I. Platais, & M. A. C. Perryman, volume 248 of *IAU*

- Symposium*, pages 224–230.
- M. Miholics, J. J. Webb, & A. Sills, 2015. *ArXiv e-prints*.
- I. Minchev, C. Boily, A. Siebert, et al., 2010. *MNRAS*, 407:2122–2130.
- I. Minchev, C. Chiappini, & M. Martig, 2013. *A&A*, 558:A9.
- I. Minchev & B. Famaey, 2010. *ApJ*, 722:112–121.
- I. Minchev, B. Famaey, F. Combes, et al., 2011. *A&A*, 527:A147.
- I. Minchev & A. C. Quillen, 2006. *MNRAS*, 368:623–636.
- Y. N. Mishurov, 2006. *Astronomical and Astrophysical Transactions*, 25:129–133.
- Y. N. Mishurov & I. A. Acharova, 2011. *MNRAS*, 412:1771–1777.
- M. Miyamoto & R. Nagai, 1975. *PASJ*, 27:533–543.
- G. Monari, T. Antoja, & A. Helmi, 2013. *ArXiv e-prints*.
- G. Monari, A. Helmi, T. Antoja, et al., 2014. *ArXiv e-prints*.
- B. Nordström, M. Mayor, J. Andersen, et al., 2004. *A&A*, 418:989–1019.
- R. P. Olling & M. R. Merrifield, 1998. *MNRAS*, 297:943–952.
- J. H. Oort, 1950. *BAN*, 11:91–110.
- F. I. Pelupessy, J. Jänes, & S. Portegies Zwart, 2012. *New Astron.*, 17:711–719.
- F. I. Pelupessy, A. van Elteren, N. de Vries, et al., 2013. *A&A*, 557:A84.
- M. A. C. Perryman, A. G. A. Brown, Y. Lebreton, et al., 1998. *A&A*, 331:81–120.
- D. Pfenniger & D. Friedli, 1993. *A&A*, 270:561–572.
- B. Pichardo, M. Martos, & E. Moreno, 2004. *ApJ*, 609:144–165.
- B. Pichardo, E. Moreno, C. Allen, et al., 2012. *AJ*, 143:73.
- H. C. Plummer, 1911. *MNRAS*, 71:460–470.
- E. V. Polyachenko, 2013. *Astronomy Letters*, 39:72–82.
- M. Portail, C. Wegg, O. Gerhard, et al., 2015. *MNRAS*, 448:713–731.
- S. Portegies Zwart & J. Bédorf, 2014. *ArXiv e-prints*.
- S. Portegies Zwart, S. L. W. McMillan, E. van Elteren, et al., 2013. *Computer Physics Communications*, 183:456–468.
- S. F. Portegies Zwart, 2009. *ApJ*, 696:L13–L16.
- S. F. Portegies Zwart & L. Jílková, 2015. *MNRAS*, 451:144–148.
- S. F. Portegies Zwart, S. L. W. McMillan, & M. Gieles, 2010. *ARA&A*, 48:431–493.
- S. F. Portegies Zwart & F. Verbunt, 1996. *A&A*, 309:179–196.

BIBLIOGRAPHY

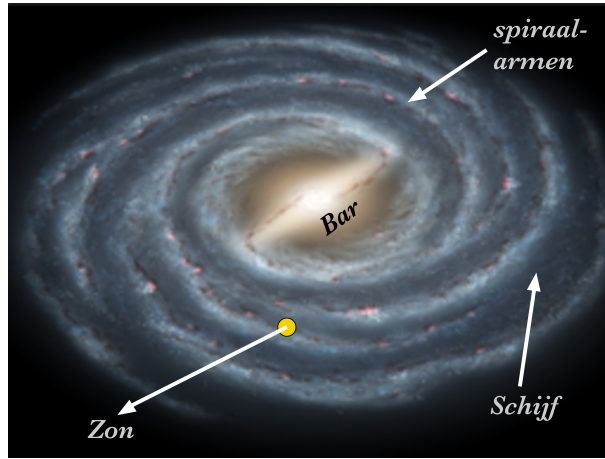
- A. C. Quillen, J. Dougherty, M. B. Bagley, et al., 2011. *MNRAS*, 417:762–784.
- A. C. Quillen & I. Minchev, 2005. *AJ*, 130:576–585.
- A. C. Quillen, I. Minchev, J. Bland-Hawthorn, et al., 2009. *MNRAS*, 397:1599–1606.
- I. Ramírez, A. T. Bajkova, V. V. Bobylev, et al., 2014. *ApJ*, 787:154.
- A. Recio-Blanco, P. de Laverny, G. Kordopatis, et al., 2014. *ArXiv e-prints*.
- M. J. Reid, K. M. Menten, A. Brunthaler, et al., 2014. *ApJ*, 783:130.
- F. Renaud, M. Gieles, & C. M. Boily, 2011. *MNRAS*, 418:759–769.
- H. Rickman, 1976. *Bulletin of the Astronomical Institutes of Czechoslovakia*, 27:92–105.
- H. Rickman, M. Fouchard, C. Froeschlé, et al., 2008. *Celestial Mechanics and Dynamical Astronomy*, 102:111–132.
- S. Rieder, T. Ishiyama, P. Langelaan, et al., 2013. *MNRAS*, 436:3695–3706.
- A. C. Robin, X. Luri, C. Reylé, et al., 2012. *A&A*, 543:A100.
- M. Romero-Gómez, E. Athanassoula, T. Antoja, et al., 2011. *MNRAS*, 418:1176–1193.
- R. Roškar & V. P. Debattista, 2014. *ArXiv e-prints*.
- R. Roškar, V. P. Debattista, T. R. Quinn, et al., 2008a. *ApJ*, 684:L79–L82.
- R. Roškar, V. P. Debattista, T. R. Quinn, et al., 2012. *MNRAS*, 426:2089–2106.
- R. Roškar, V. P. Debattista, G. S. Stinson, et al., 2008b. *ApJ*, 675:L65–L68.
- S. Ruphy, A. C. Robin, N. Epchtein, et al., 1996. *A&A*, 313:L21–L24.
- T. R. Saitoh & J. Makino, 2010. *PASJ*, 62:301–.
- R.-D. Scholz, N. V. Kharchenko, A. E. Piskunov, et al., 2015. *A&A*, 581:A39.
- R. Schönrich, J. Binney, & W. Dehnen, 2010. *MNRAS*, 403:1829–1833.
- M. E. Schwamb, 2014. *Nature*, 507:435–436.
- J. A. Sellwood, 2010. *MNRAS*, 409:145–155.
- J. A. Sellwood, 2011. *MNRAS*, 410:1637–1646.
- J. A. Sellwood & J. J. Binney, 2002. *MNRAS*, 336:785–796.
- E. M. Shoemaker & R. F. Wolfe, 1986. In *The Galaxy and the Solar System*, editors R. Smoluchowski, J. M. Bahcall, & M. S. Matthews, pages 338–386.
- M. Sofroniou & G. Spaletta, 2005. *Optimization Methods and Software*, 20:597–613.
- Y. Sofue, M. Honma, & T. Omodaka, 2009. *PASJ*, 61:227–.
- K. Takahashi & S. F. Portegies Zwart, 2000. *ApJ*, 535:759–775.

- A. Tanikawa & T. Fukushige, 2009. *PASJ*, 61:721–.
- S. Toonen, G. Nelemans, & S. Portegies Zwart, 2012. *A&A*, 546:A70.
- C. A. Trujillo & S. S. Sheppard, 2014. *Nature*, 507:471–474.
- J. A. Valenti & D. A. Fischer, 2005. *ApJS*, 159:141–166.
- J. P. Vallée, 2002. *ApJ*, 566:261–266.
- M. Valtonen, A. T. Bajkova, V. V. Bobylev, et al., 2015. *Celestial Mechanics and Dynamical Astronomy*, 121:107–119.
- J. J. Webb, N. Leigh, A. Sills, et al., 2014a. *MNRAS*, 442:1569–1577.
- J. J. Webb, A. Sills, W. E. Harris, et al., 2014b. *MNRAS*, 445:1048–1055.
- J. L. Weiland, R. G. Arendt, G. B. Berriman, et al., 1994. *ApJ*, 425:L81–L84.
- B. J. Weiner & J. A. Sellwood, 1999. *ApJ*, 524:112–128.
- M. Wenger, F. Ochsenbein, D. Egret, et al., 2000. *A&AS*, 143:9–22.
- R. Wielen, 1977. *A&A*, 60:263–275.
- R. Wielen, B. Fuchs, & C. Dettbarn, 1996. *A&A*, 314:438.
- J. Wisdom & M. Holman, 1991. *AJ*, 102:1528–1538.
- K. Yakut, P. P. Eggleton, B. Kalomeni, et al., 2015. *MNRAS*, 453:2937–2942.
- P. Yoachim, R. Roškar, & V. P. Debattista, 2010. *ApJ*, 716:L4–L8.
- P. Yoachim, R. Roškar, & V. P. Debattista, 2012. *ApJ*, 752:97.
- H. Yoshida, 1990. *PhLA*, 150:262–268.
- H. Zhao, 1996. *MNRAS*, 278:488–496.

NEDERLANDSE SAMENVATTING

Tijdens een heldere nacht kan men een band van wit licht zien die de hele hemel omspant. In vroegere beschavingen dacht men dat deze band een manifestatie van de goden was, of wellicht het pad waarlangs de zielen van de doden reisden. Het was de Griekse astronoom Democritus (460 tot 370 voor Christus) die suggereerde dat deze lichtende band aan de hemel in werkelijkheid bestaat uit talloze sterren die te zwak zijn om direct met het blote oog te zien. Dit idee werd later bevestigd door waarnemingen van Galileo Galilei dankzij zijn gebruik (voor het eerst) van een telescoop. Tegenwoordig weten we dat deze grote verzameling sterren overeenkomt met de Melkweg, het sterrenstelsel (of melkwegstelsel) waarin wij wonen (zie Figuur 1).

Het aantal sterren dat ons sterrenstelsel herbergt wordt geschat op ongeveer 400 miljard. Dankzij astronomische waarnemingen weten we dat ons melkwegstelsel een zogenaamd balk-spiraalstelsel is. Dit betekent dat zich in het midden van het stelsel een langwerpige verdeling van sterren bevindt, ongeveer in de vorm van een balk. Aan de uiteinden van deze balk ontspringen spiraalarmen, gebieden in ons sterrenstelsel van hogere dichtheid waar gas samenkomt en waaruit vervolgens nieuwe sterren gevormd worden. De spiraalarmen bevinden zich in de zogenaamde schijf van ons melkwegstelsel en daar bevindt zich ook de zon. In figuur 1 zien is een artistieke voorstelling te zien van ons melkwegstelsel met daarin aangegeven waar de zon zich bevindt.



FIGUUR 1: Impressie van de Melkweg. De gele cirkel geeft de geschatte locatie van de Zon. Credits: NASA.

Onze ster bevindt zich op een afstand van ongeveer 27 700 lichtjaar van het midden van ons sterrenstelsel³. Echter, het is niet zeker of de zon zich altijd op deze afstand bevond gedurende haar leven. Sommige wetenschappers suggereren dat de zon waarschijnlijk geboren is in een gebied dicht bij het centrum van de Melkweg om daarna naar haar huidige locatie te ‘migreren’. Dit proces wordt ‘radiële migratie’ genoemd (radiëel duidt of het veranderen van de afstand van de zon tot het midden van de Melkweg). Andere studies daarentegen laten zien dat de straal van de baan van de zon om de melkweg niet veel veranderde gedurende haar leven, dat wil zeggen dat de zon dus niet veel radiële migratie ondergaan zou hebben. In hoofdstuk 3 van dit proefschrift gebruik ik numerieke technieken om de baan van de zon in de Melkweg te berekenen en ik laat zien dat onze ster waarschijnlijk niet ver van zijn geboorteplaats gemigreerd is. Slechts onder bepaalde omstandigheden kan het voorkomen dat de zon gemigreerd is, maar deze migratie is niet vanuit de binnendelen van ons melkwegstelsel, zoals eerder onderzoek suggereerde, maar vanuit de buitendelen van de schijf van de Melkweg. Het blijkt dat in een aantal van deze bijzondere gevallen de zon geboren zou kunnen zijn op een afstand van 11 kilo-parsec

³Dit betekent dat als we met de snelheid van het licht zouden kunnen reizen we er 27 700 jaar over zouden doen om in het midden van ons sterrenstelsel aan te komen.

(35 000 lichtjaar) van het Melkwegcentrum.

Het is belangrijk om uit te zoeken waar in ons melkwegstelsel de zon geboren is omdat dit aanwijzingen zou kunnen geven die ons meer inzicht verschaffen in de vorming van ons zonnestelsel. De geboorteplek van de zon vormt daarnaast ook het startpunt voor het bestuderen van de evolutie van de sterrenhoop waar de zon in gevormd is. Een sterrenhoop is een groep sterren van dezelfde leeftijd (ze zijn gelijktijdig gevormd) en dezelfde samenstelling, die door de onderlinge zwaartekracht bij elkaar blijven. In de schijf van onze Melkweg zijn zo'n 1000 sterhopen waargenomen en het is waarschijnlijk dat er veel meer zijn. Deze groepen van sterren worden gevormd in de spiraalarmen en worden 'open' sterhopen genoemd omdat de onderlinge aantrekkingskracht van de sterren niet erg groot is. Daar komt bij dat de getijdenkrachten in het zwaartekrachtsveld van de Melkweg ervoor zorgen dat deze sterhopen in relatief korte tijd (van ongeveer honderden miljoenen jaren) uiteenvallen.

Verscheidene onderzoeken laten zien dat de meeste sterren in de schijf van ons sterrenstelsel in open sterhopen gevormd zijn en het ziet ernaar uit dat de zon geen uitzondering is. Men denkt dat de zon ook in een open sterrenhoop gevormd is vanwege een aantal specifieke eigenschappen van het zonnestelsel, zoals bijvoorbeeld de hoge excentriciteit en inclinatie van de baan van een deel van de kleine hemellichamen in de buitendelen van het zonnestelsel. Het is waarschijnlijk dat de baaneigenschappen ontstaan zijn na de wisselwerking tussen het zonnestelsel en andere sterren in de sterrenhoop waar de zon geboren is.

Als de zon inderdaad in een open sterrenhoop gevormd is zullen de overige sterren die samen met de zon gevormd zijn nu verspreid zijn over de schijf van de Melkweg. Waar bevinden deze sterren zich vandaag? Is het mogelijk om ze te vinden temidden van de overige sterren in de schijf van de Melkweg? Deze vragen kunnen beantwoord worden met behulp van N -deeltjes simulaties. Dit zijn numeriek modellen die de dynamica beschrijven van een systeem van sterren dat zich ontwikkelt onder de invloed van de zwaartekracht tussen de sterren in de groep. In hoofdstuk 4 maak ik gebruik van N -deeltjes simulaties om te bestuderen wat de mogelijke evolutie is geweest van de sterrenhoop waar de zon in geboren is. Daarbij wordt ook de invloed van de getijdenkrachten van de Melkweg meegenomen in de berekeningen. De resultaten wijzen uit dat

er voor de sterren die samen met de zon gevormd zijn (ook wel de broertjes en zusjes van de zon genoemd) geen unieke verdeling in de Melkweg te verwachten is. Echter, hun verdeling hangt sterk af van de aannames die gemaakt worden over de eigenschappen van de Melkweg. Niettemin laat een statistische analyse van de verschillende gesimuleerde verdelingen zien dat het mogelijk is om in de gegevens over de afstanden en snelheden van sterren intervallen aan te wijzen waar het waarschijnlijker is om de familieleden van de zon aan te treffen. Deze voorspellingen zijn van groot belang voor de zoektocht naar de broertjes en zusjes van de zon met toekomstige gegevens.

De kennis van de baan van de zon in de Melkweg is ook nuttig voor het vaststellen van de effecten van de Melkwegomgeving op de vorming en ontwikkeling van het zonnestelsel, en in het bijzonder van de Oort wolk⁴. Als de zon in een gebied met hoge sterdichtheid gevormd is, bijvoorbeeld dicht bij het centrum van de Melkweg, dan is het waarschijnlijk dat verscheidene sterren vlak langs de zon gescheurd zijn. Dit zou de Oort wolk verstoord kunnen hebben en daarmee ‘kometenregens’ veroorzaken. Zulke gebeurtenissen zijn wellicht de oorzaak van sommige van de massasterftes die gedurende de geschiedenis van de aarde hebben plaatsgevonden. In hoofdstuk 5 wordt bestudeerd hoe vaak sterren langs de zon gescheurd zijn in de loop van haar rondgang door de Melkweg. Hierbij wordt bepaald wat de meest ver verwijderde gebieden in het zonnestelsel zijn die niet door langsscherende sterren verstoord zijn in het verleden. Het blijkt dat lichamen in het zonnestelsel die op een afstand van kleiner dan 300 astronomische eenheden van de zon afstaan nooit verstoord zijn door zonne-scheerders⁵. Dit resultaat laat zien dat onafhankelijk van de precieze baan van de zon in de Melkweg de Oort wolk flink verstoord moet zijn in het verleden door het langs elkaar scheren van de zon en andere sterren in de schijf.

Ik heb gebruik gemaakt van nieuw ontwikkelde numerieke methoden en *N*-deeltjes berekeningen om de baanbeweging van de zon en zijn familie in

⁴De Oort wolk is het meest afgelegen gebied van het zonnestelsel, waar men denkt dat de kometen vandaan komen.

⁵Één astronomische eenheid (1 AU, oftewel ‘Astronomical Unit’) komt overeen met de afstand van de aarde tot de zon. De buitenste planeet in het zonnestelsel, Neptunus, bevindt zich op slechts 30 AU van de zon.

de Melkweg te bepalen. Deze numerieke methoden zijn ook geschikt om de processen te bestuderen die een rol hebben gespeeld bij het ontstaan en de verder evolutie van ons melkwegstelsel. De details van de in dit proefschrift gebruikte numerieke technieken staan in hoofdstuk 2 beschreven.

Is het mogelijk om de voorspellingen in dit proefschrift te toetsen aan huidige astronomische waarnemingen? De meest complete stercatalogus op dit moment is door de Hipparcos satelliet geproduceerd. Deze ruimtemissie heeft de kinematische eigenschappen van 120 duizend sterren in de buurt van de zon gemeten. Alhoewel deze gegevens zeer nuttig waren om de vormingsprocessen van onze Melkweg beter te begrijpen, is de zoektocht naar broertjes en zusjes van de zon in deze catalogus niet succesvol geweest. Het is ook niet mogelijk geweest om precies te bepalen hoe vaak sterren langs de zon gescheerd zijn gedurende haar rondgang in de Melkweg. Om deze vragen te beantwoorden is het nodig om van een veel grotere verzameling sterren de kinematische gegevens te bepalen. De Gaia missie, gelanceerd in december 2013, zal ons voorzien van zeer nauwkeurige metingen van de plaats en beweging van 1 miljard sterren, ongeveer 1 procent van de hele populatie sterren in ons sterrenstelsel. De Gaia catalogus zal dus van onschatbare waarde zijn bij de zoektocht naar de familieleden van de zon en om beter te begrijpen hoe vaak sterren in het verleden langs de zon gescheerd zijn. Aanvullende gegevens over de astrofysische eigenschappen van een groot monster van sterren, aangeleverd door waarneemprojecten zoals WEAVE, 4MOST en het Gaia-ESO programma, zullen ook van groot belang zijn bij het zoeken naar de familie van de zon.

RESUMEN EN ESPAÑOL

En una noche completamente despejada puede observarse una banda de luz blanca alrededor de toda la esfera celeste. Las civilizaciones antiguas creían que aquélla mancha era producto de la manifestación de los dioses o caminos que conducían a las almas de los muertos. El astrónomo Demócrito (460 a.C - 370 a.C.) sugirió que aquel haz de luz blanco en el cielo era en realidad un conglomerado de muchísimas estrellas demasiado tenues para ser observadas a simple vista. Esta idea fue posteriormente respaldada por Galileo Galilei mediante el uso del telescopio. Actualmente, sabemos que este gran conglomerado de estrellas corresponde a la Vía Láctea, nuestra Galaxia.

Se estima que nuestra Galaxia alberga alrededor de 400 mil millones de estrellas. Mediante observaciones astronómicas sabemos que la Vía Láctea es una galaxia espiral barrada. Esto es, su centro contiene una distribución alineada de estrellas que van de un extremo a otro en la Galaxia, como en forma de barra. En los extremos de ésta, comienzan los brazos espirales, los cuales son regiones de alta densidad en donde el gas se colapsa para formar nuevas estrellas. El lugar donde residen los brazos espirales se conoce como disco Galáctico y es donde se localiza el Sol. En la Figura 1 vemos una representación artística de la Vía Láctea junto con la ubicación actual del Sol.

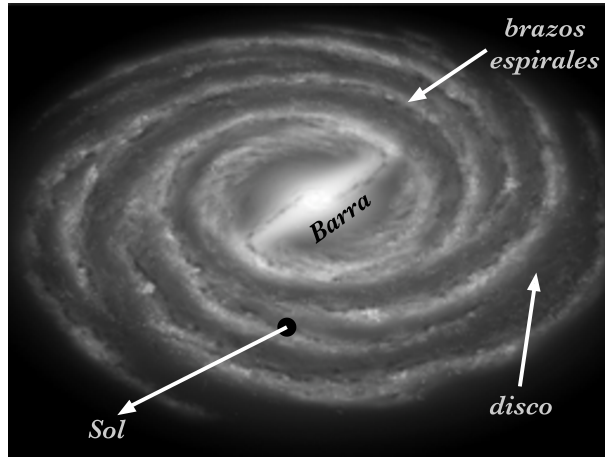


FIGURA 1: Impresión artística de la Vía Láctea. El círculo negro indica la ubicación aproximada del Sol. Créditos: NASA.

Nuestra estrella se encuentra a aproximadamente 27700 años luz del centro de nuestra galaxia⁶. Sin embargo, no es claro si el Sol ha permanecido o no en esta distancia radial durante el tiempo en que se ha movido a través de la Galaxia. Algunos científicos sugieren que el Sol probablemente nació en regiones más cercanas al centro Galáctico y que posteriormente migró a la distancia radial donde actualmente se encuentra. Otros estudios por el contrario, indican que el radio de la órbita del Sol no ha cambiado mucho durante su tiempo de vida; es decir, que el Sol no ha migrado radialmente. En el capítulo 3 hago uso de técnicas numéricas para calcular la órbita del Sol y muestro que nuestra estrella probablemente no migró desde su lugar de nacimiento hasta su posición actual en la Galaxia. Sólo bajo ciertas condiciones galácticas el Sol pudo haber migrado; sin embargo, dicha migración radial no es desde regiones internas de la Galaxia, como estudios anteriores sugieren, sino desde regiones externas del disco de la Vía Láctea. En algunos de estos casos, encuentro que el Sol pudo haber nacido a una distancia de hasta 11 kiloparsecs (35000 años luz) del centro Galáctico.

Es de gran importancia establecer el lugar donde el Sol nació en la Galaxia,

⁶Esto quiere decir que, si pudiéramos viajar a la velocidad de la luz, demoraríamos 27700 años en llegar al centro de la Galaxia.

ya que esto podría aportar pistas que expliquen la formación del Sistema Solar. Además, es el punto de partida para estudiar la evolución del cúmulo estelar donde se formó el Sol. Un cúmulo estelar es un conglomerado de estrellas con la misma edad y composición química que interactúan gravitacionalmente entre sí. En el disco de nuestra Galaxia se han observado alrededor de 1000 cúmulos estelares, aunque se estima que hay muchísimos más. Estos sistemas nacen en los brazos espirales de la Galaxia y son comúnmente llamados cúmulos abiertos porque la interacción gravitacional entre sus estrellas no es tan fuerte. Además, debido a la fuerza de marea producida por la Galaxia, los cúmulos abiertos suelen ser destruidos en cortas escalas de tiempo (de alrededor de cientos de millones de años).

Varios estudios indican que la mayoría de las estrellas pertenecientes al disco Galáctico se formaron en cúmulos abiertos y al parecer, el Sol no fue la excepción. Se cree que el Sol nació en un cúmulo abierto, entre otras cosas, debido a la alta excentricidad e inclinación en la órbita de algunos objetos del Sistema Solar que están localizados en el exterior éste. Algunos estudios señalan que dichas órbitas se originaron a partir de interacciones entre el Sol y otras estrellas pertenecientes al cúmulo abierto donde nuestra estrella nació.

Si el Sol se formó en un cúmulo abierto, las demás estrellas que se formaron junto con el Sol, estarán actualmente dispersas en el disco Galáctico. ¿Dónde se encuentran actualmente estas estrellas? ¿Es posible identificarlas de las demás estrellas del disco Galáctico? Estas preguntas pueden responderse mediante el uso de simulaciones de N -cuerpos, los cuales son modelos computacionales de un sistema dinámico de partículas el cual evoluciona bajo la fuerza de gravedad. En el capítulo 4 hago uso de simulaciones de N -cuerpos para estudiar la evolución en la Galaxia del cúmulo donde nació el Sol. Las simulaciones muestran que las estrellas que se formaron junto con el Sol (en la literatura se les conoce como “hermanos solares”) no tienen una distribución única en la Galaxia. Tal distribución depende de los parámetros que se usen para modelar la Vía Láctea. Sin embargo, al hacer un análisis estadístico sobre todas las posibles distribuciones espaciales de los hermanos solares, yo encuentro la región en el cielo donde es más probable encontrar estas estrellas. Las predicciones mostradas en el capítulo 4 serán de gran importancia para encontrar hermanos solares en el futuro.

Conocer la órbita del Sol alrededor de la Vía Láctea puede también ayudar a establecer el efecto del entorno Galáctico sobre la formación del Sistema Solar; en particular sobre la nube de Oort⁷. Si el Sol se formó en regiones de alta densidad estelar; por ejemplo, más cerca del centro Galáctico, es posible que éste haya sufrido de varios encuentros estelares cercanos que hubieran perturbado la nube de Oort al punto de generar lo que se conoce como una “ducha de cometas”. Es probable que tales eventos hayan sido los responsables de algunas de las extinciones en masa ocurridas en la Tierra. En el capítulo 5 se estudian los encuentros estelares que ha sufrido el Sol a lo largo de su trayectoria por la Galaxia y se determina la región más externa del Sistema Solar en donde tales encuentros no generan ninguna perturbación. Yo encuentro que objetos del Sistema Solar localizados a distancias menores que 300 AU no son perturbados por encuentros estelares⁸. Este resultado indica que, independientemente de la órbita que haya tenido el Sol a lo largo del disco de la Galaxia, la nube de Oort ha sido fuertemente perturbada por encuentros cercanos entre el Sol y otras estrellas del disco.

Para calcular la órbita del Sol y el movimiento de los hermanos solares a lo largo del disco de la Vía Láctea hice uso de técnicas numéricas y simulaciones de N -cuerpos. Estos métodos numéricos son muy útiles para estudiar los procesos que han intervenido en la formación y evolución de nuestra Galaxia. Los detalles de las técnicas numéricas usadas en esta tesis están ampliamente explicadas en el capítulo 2.

¿Es posible comparar las predicciones mostradas en esta tesis con observaciones astronómicas actuales? El catálogo estelar más completo hasta el momento es el que proporcionó el satélite *Hipparcos*. Esta misión midió las propiedades cinemáticas de 120 mil estrellas localizadas en la vecindad del Sol. Aunque estas mediciones han sido útiles para entender un poco más los procesos involucrados en la evolución de nuestra Galaxia, científicos han tratado de buscar hermanos solares en el catálogo estelar de *Hipparcos* sin obtener re-

⁷La nube de Oort es la región más externa del Sistema Solar en donde se cree que se originan los cometas.

⁸1 AU o Unidad Astronómica, por sus siglas en inglés, corresponde a la distancia que hay de la tierra al Sol. El último planeta del Sistema Solar, Neptuno, se encuentra a tan solo 30 AU del Sol.

sultados positivos. Tampoco ha sido posible hacer una indentificación robusta de la probabilidad de encuentros estelares experimentados por el Sol a lo largo de su órbita. Es necesario obtener las propiedades cinemáticas de una amplia muestra de estrellas para lograr estos objetivos. Lanzada en diciembre de 2013, la misión *Gaia* proporcionará con detallada precisión la posición y el desplazamiento de 1000 millones de estrellas, aproximadamente un 1% de la población estelar de la Galaxia. El catálogo de *Gaia* contendrá por lo tanto, información invaluable que será de gran utilidad para identificar hermanos solares y para hacer mejores predicciones de los encuentros estelares experimentados por el Sol. Datos complementarios proporcionados por campañas observaciones como WEAVE, 4MOST y Gaia-ESO serán también de gran utilidad para identificar la familia solar, debido a que éstos instrumentos medirán las propiedades astrofísicas de un amplio conjunto de estrellas en la Galaxia.

CURRICULUM VITÆ

I was born on August 25th, 1984, in Bogotá, the capital of Colombia. My interests in astronomy started when I was six years old. I remember that by accident, I opened one of my mom's books. I was completely stunned with the marvelous pictures that book was showing me. I was intrigued to know how those beautiful objects I was looking at were formed and how people managed to observe them. That day I decided to become an astronomer.

In 2002, following my passion for the universe, I started my career in physics at the National University of Colombia in Bogotá. My thesis was focused on studying the physical properties of the NLR (Narrow line region) of a large sample of Seyfert 2 galaxies. This work, which was done under the supervision of M.Sc. Benjamín Calvo, was the first astronomical research project I did on a professional level. I really enjoyed it and I decided to continue further.

In 2008 I enrolled in the master program of physics at the National University of Colombia. I conducted my thesis with Dr. Rigoberto Casas on the study of the dark matter content of the Sagittarius dwarf galaxy, using non-cosmological N-body simulations. I had the opportunity to present this work at different meetings in Mexico and Brazil. I also published this research in an international journal. Thanks to these achievements, in October of 2011, I received my diploma with honors. Doing my masters was an incredibly experience that brought me many professional and personal achievements. One

CURRICULUM VITÆ

of them was to meet two researchers who were doing their PhDs here, in Leiden. Their fascinating experiences in the Netherlands and in the academia, motivated me to gain a doctoral position at the Observatory of Leiden.

After staying my entire life in Bogotá, I moved to Leiden in November of 2011, to start my PhD under the supervision of Dr. Anthony Brown and Prof. Dr. Simon Portegies Zwart. My research was focused on establishing a kinematical selection criteria to search for solar siblings in large phase-space surveys like *Gaia*. I presented my work in several conferences in Slovenia, Italy, Switzerland and the Netherlands. During my PhD I also attended several schools on Galactic dynamics devoted to prepare the scientific community to exploit the upcoming data of the *Gaia* satellite. Besides my research work I was a teaching assistant for the course *Astrostatistics*, taught by Prof. Richard Gill. In my free time, I enjoy to walk and write poems in spanish.

LIST OF PUBLICATIONS

Refereed publications

1. *The effect of Galactic stellar encounters on the outer edge of the Solar System's parking zone*
Martínez-Barbosa, C.A., Jílková, L., Portegies Zwart, S., Brown, A.G.A., *in prep.* (**Chapter 5**)
2. *Self-consistent High-order Symplectic coupling between gravitational systems*
Pelupessy, F.I., **Martínez Barbosa, C.A.**, Gonçalves Ferrari, G., Portegies Zwart, S.F. *Journal of Computational Astrophysics and Cosmology*, *in revision.* (**Chapter 2**)
3. *The evolution of the Sun's birth cluster and the search for the solar siblings with Gaia*
Martínez-Barbosa, C.A., Brown, A.G.A., Boekholt, T., Portegies Zwart, S., Antiche, E., Antoja, T., 2016, MNRAS, 457, 1062. (**Chapter 4**)
4. *Radial migration of the Sun in the Milky Way: a statistical study*
Martínez-Barbosa, C.A., Brown, A.G.A., Portegies Zwart, S., 2015, MNRAS, 446, 823. (**Chapter 3**)

LIST OF PUBLICATIONS

5. *Quest for finding the lost siblings of the Sun*
C. Liu, G. Ruchti, S. Feltzing, **C. A. Martínez-Barbosa**, T. Bensby,
A. G. A. Brown, S. F. Portegies Zwart., 2015, A&A, 575, 51
6. *Is the Sgr dSph a dark matter dominated system?*
Martínez-Barbosa, C.A., Casas-Miranda, R.A., 2013, NewA, 20, 7

Conference Proceedings

1. *The Solar siblings in the Gaia era*
Martínez-Barbosa, C.A., Brown, A.G.A., Portegies Zwart, S., 2014,
EAS, 67, 123
2. *Origin and evolution of the Sagittarius dwarf galaxy using N-body simulations*
Martínez-Barbosa, C.A., Casas, R.A., 2011, RMxAC, 40, 68
3. *Computation of initial conditions for a thin disk as an extension of the Dehnen algorithm*
Celis-Gil, J.A., **Martínez-Barbosa, C.A.**, Casas, R.A., 2011, RMxAC,
40, 113

Outreach papers

1. *Searching for solar siblings with Gaia*
http://www.cosmos.esa.int/web/gaia/iow_20160204

ACKNOWLEDGEMENTS

*Let us be grateful to the people who make us happy;
they are the charming gardeners who make our souls blossom.*

Marcel Proust

Doing my PhD here in Leiden, has been one of the best things that have happened in my life. I've had the opportunity to grow personally and intellectually and now, after four years of hard work and many beautiful and unforgettable moments, I can say that one of my dreams has become true.

A mi querida familia: mi mamá; mis tíos Agustín, Samuel y Amanda. Ustedes son el motor de mi vida. Gracias por siempre estar ahí, por escucharme, por consolarme y por darme siempre ánimo. Gracias a ustedes soy la persona quien soy ahora y soy muy feliz por tenerlos. Ustedes son la mejor familia del mundo y este triunfo es también de ustedes. Los amo con todo mi corazón. Tías Ilse y Yenith; gracias por sus concejos y por las largas y fructíferas conversaciones sobre la vida. Gabriela y Zulma, ustedes son como mis hermanas. Gracias por escucharme y por ser tan especiales conmigo. This thesis is dedicated to my father, a person who truly had a passion for science. This achievement is to his memory.

During this journey, I met great scientists. Teresa, every time we talk I always learn something new about Galactic dynamics. It was a pleasure to meet you and I wish you many success in your scientific career and in your life

ACKNOWLEDGEMENTS

in general.

My PhD would not have been the same without my previous and current officemates and friends. Michiko, you are such a great person. Thanks for all the nice discussions on star clusters and dynamics of the Galaxy. Also, thanks for the delicious dinners; specially, the one where you prepared the ice tempura. Every time I remember it, I would like to eat it again!. I'm very glad to have you as my friend and I'm looking forward to see you soon. Steven, you were very kind with me. I wish you all the best in Japan and in your future life!. Lucie, thanks for all your advices on how to make nice plots and for the fruitful scientific discussions. I also want to thank you for the nice dinners; but specially, for your support in my wedding. You helped me to choose the dress, you took beautiful pictures and you made the nice decoration on Tjarda's car. Those were a very special details that I will never forget. Edwin, I enjoy talking to you, specially because you are so funny. Thanks for listening to me and for helping me with python. Tjibaria, you are a very nice and kind person. Thank you very much for your friendship!

Noel and Tjarda, you were the first people I met at the observatory. It has been a pleasure for me to share different moments with you guys and I hope we will continue in touch, no matter the places we will be in the future. I wish you many success in your projects and in your lives. Susanita (y Noel), gracias por haber sido mis padrinos de boda. Espero que ese amor tan bonito que hay entre ustedes, nunca termine.

Jeanette, Ainil, Guilherme, Margot, Vivianni, Paula, Silvia, Gráinne, Luis, Paola, Berenice, Mattia, Marco, Heather, Evelijn: Thanks to all of you for the lunches and the nice chats during the borrels and the coffee breaks.

The AMUSE team was also very important during this process. I want to thank Inti, Natan and Arjen for their help (and patience) when I was having troubles at implementing the Galaxy model in AMUSE. I wish to all of you success!

To my friends outside astronomy who are in Colombia and The Netherlands: Alexa, Clau, Jean Paul, Edwin, Juan Carlos, Carlos Augusto, John Jairo, Franz and Yolanda. Thank you for your teachings. All of you have helped me to be a better person.

Last but not least, I want to thank my husband. Josein, tú eres mi polo

ACKNOWLEDGEMENTS

a tierra, mi complemento y mi amor. Gracias por haberme esperado y por haber decidido venir a Holanda. Tu soporte y paciencia me ayudaron mucho, especialmente durante el último año de doctorado; por ello, este logro también es tuyo. Espero poder estar siempre a tu lado, para que sigamos haciendo realidad nuestros sueños.